Diode Laser Processing of PMMA and LCP Materials for Microsystem Packaging

Xin Jiang

Submitted for the degree of Doctor of Philosophy

Heriot-Watt University

School of Engineering and Physical Sciences

March 2015

Abstract

The thesis describes the development of laser-assisted bonding methods for assembly of microfluidic devices and MEMS packaging. A laser microwelding technique for assembly of transparent polymer substrates for fabrication of microfluidic devices was studied. The transparent PMMA substrates were bonded together using a high power diode laser system with a broad top-hat beam profile and an intermediate titanium thin film consisting of 0.7 mm diameter spots. A tensile strength of 6 MPa was achieved for this novel method which is comparable to that of the previous work in laser welding of polymers. It has been demonstrated that the method is capable of leak free encapsulation of a microfluidic channel. Furthermore, a novel laser-based method using an LCP film for packaging of MEMS, sensors and other microelectronic devices has been investigated. The results show that it is possible to use a laser based method with an LCP polymer for high quality substrate bonding applications. Glass-glass based cavities allow optical transmission and have potential applications for optical sensors and other photonic devices. For glass-glass bonding, it was shown that thin film titanium material can be used as an effective optical absorber in the laser based LCP bonding technique. Laser bonding of glass and silicon using an LCP film has also been achieved but in this case the silicon substrate acted as the absorber to capture the laser power. Laser bonding of a silicon cap to a molded LCP package has also been demonstrated successfully. The results of temperature monitoring using embedded sensors show that the temperature at the base of the LCP package (~130°C) is substantially lower than the bonding temperature (> 280°C). The results of shear and leak test show good reliability and hermeticity of the laser bonded microcavities. Both two-dimensional and three-dimensional models of heat transfer are developed and studied using the COMSOL Multiphysics software tool to understand the localised laser heating effects. The results are in good agreement with those of the practical work.

Acknowledgement

Firstly, I would like to express my gratitude to my supervisor Professor Changhai Wang for giving me the opportunity to study within the MISEC research group and supervising me throughout the past five years. Without him, this work would not have been possible.

I would like to thank my second supervisor Professor Marc Desmulliez and PhD progress reviewer Professor Resh Dhariwal in Heriot-Watt University. In particular, I would like to thank Mr. Mark Leonard for his assistance in the cleanroom. I would also like to thank all the staff at Heriot-Watt University.

I am glad that I made such great friends during my time at the MISEC group, especially Dave, Yves, Suzanne, Soni, Komsan, Sumanth, Iqy, Stefan, Jack, Jun, Jia, Wei, Yu, Xinghui, Jianyong, Yi, Shilong, Wenxing, Ross, Julia, Maria, Curro. Thank you all for the conversations, fabrication suggestions and measurement help. I will miss you all.

Most importantly, I would like to thank my Mum, Dad and wife Qixi Huang for their continuous support, encouragement, quiet patience and assistance. I love you always forever.

ACADEMIC REGISTRY
Research Thesis Submission

Name*:*	XIN JIANG		
School/PGI:	School of Engineering and Physical Sciences		
Version: *(i.e. First, Resubmission, Final)*	Final	Degree Sought (Award **and** Subject area)	Doctor of Philosophy

Declaration

In accordance with the appropriate regulations I hereby submit my thesis and I declare that:

1) the thesis embodies the results of my own work and has been composed by myself
2) where appropriate, I have made acknowledgement of the work of others and have made reference to work carried out in collaboration with other persons
3) the thesis is the correct version of the thesis for submission and is the same version as any electronic versions submitted*.
4) my thesis for the award referred to, deposited in the Heriot-Watt University Library, should be made available for loan or photocopying and be available via the Institutional Repository, subject to such conditions as the Librarian may require
5) I understand that as a student of the University I am required to abide by the Regulations of the University and to conform to its discipline.

* *Please note that it is the responsibility of the candidate to ensure that the correct version of the thesis is submitted.*

Signature of Candidate*:*		Date:	

Submission

Submitted By *(name in capitals):*	
Signature of Individual Submitting:	
Date Submitted:	

For Completion in the Student Service Centre (SSC)

Received in the SSC by *(name in capitals):*			
Method of Submission *(Handed in to SSC; posted through internal/external mail):*			
*E-thesis Submitted (**mandatory for final theses)***			
Signature:		Date:	

Table of Contents

List of Tables

List of Figures

List of Publications

Jiang, X., Chandrasekar, S., and Wang, C., *A laser microwelding method for assembly of polymer based microfluidic devices*. Optics and Lasers in Engineering, 2015. *66*: p. 98-104.

Jiang, X., Changhai Wang, and Wei Liu, *A laser assisted bonding method using a liquid crystal polymer (LCP) film for MEMS and sensor packaging*. IEEE Transactions on Components, Packaging and Manufacturing Technology. Accepted.

Chapter 1 Introduction

1.1 Introduction

MEMS is acronym for Micro-electromechanical systems that originated in the United States and are also referred to as Micro System Technology (MST) in Europe and Micromachining in Japan. MEMS devices are very small and their components are usually microscopic [1]. Pumps, sensors, values, gears, actuators and even steam engines have been successfully fabricated by MEMS. Since early 1950's, MEMS has gradually made its way out of research laboratories and into industrial products. In the mid-1990's, MEMS elements started coming out in larger number of commercial products and applications including pressure sensors for medical applications, inkjet printer heads and accelerometers used to control airbag deployment in vehicles. Later, other products were developed such as lab on chip, MOEMS, RF-MEMS and microphones.

Micro-electromechanical systems (MEMS) are technologies used to achieve small integrated devices and systems that associate electrical and mechanical components. They have characteristic sizes ranging from micrometers to millimeters and the size also make them possible to be integrated into a wide range of systems. Generally, mechanical microstructures, microsensors, microactuators and microelectronics are constituents of MEMS and all of them are integrated onto a silicon chip which is shown schematically in Figure 1.1 [1].

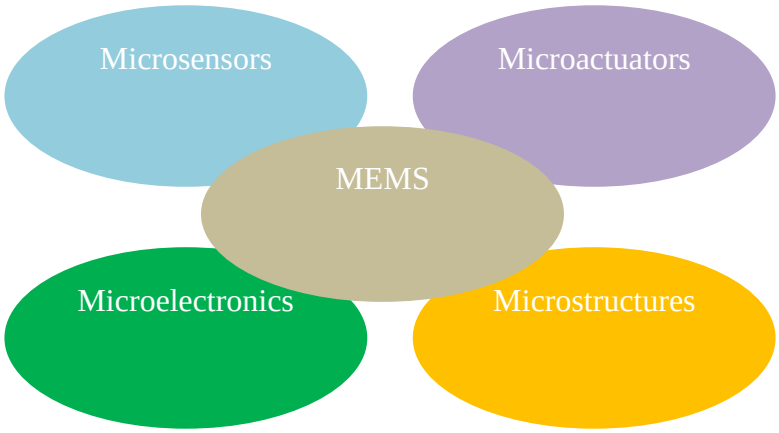

Figure 1.1: Schematic diagram of MEMS components [1].

Since MEMS have small size and weight features, they are attractive and widely used in

many applications which allow devices to be miniaturized. Moreover, parallel fabrication of thousands of systems can be processed with many MEMS fabrication technologies in the integrated circuit industry that may economize the manufacturing cost and enhance the reliability. Similar to other technologies, MEMS present some challenges. Due to most of the microsystems operating at a size scale far below normal mechanical devices, it is extremely difficult to control the surface forces which means a little bit over-force may lead to the device being damaged. Besides for MEMS components, every part presents a challenge which is why the surface must be kept clean and free of contamination to achieve the optimal application. Finally, the processing temperature acts as an important factor and is difficult to control on both inner and exterior MEMS devices.

The area of microfluidics, also referred to as lab-on-a-chip, has become a growing field in the last decade and offers significant potential in future applications. The original concept of microfluidics is the operation and analysis of fluids in micro-channels which are fabricated by micro-engineering techniques. Microfluidics devices offer effective benefits in fluid delivery, drug synthesis, inkjet printing, bioarrays, and biomedical engineering (BioMEMS). Originally, silicon and glass were primary used in the fabrication of microfluidic channels by micromachining methods. Then, several other types of polymers have been applied for creating microfluidic channels, such as SU-8, polymethyl methacrylate (PMMA) and polydimethyl dimethylsiloxane (PDMS). The main reason for interest in polymers is because of their low cost, fast processing time, ease of processing, and potentials of achieving flexible transmutable modules. The bonding and sealing of polymer based microfluidic devices without any deformation or damage of fabricated microstructures is a considerable problem. Several bonding methods of microfluidics devices have been studied such as indirect bonding methods (adhesive bonding) and direct bonding approaches based on thermal fusion bonding, solvent bonding, and localized bonding techniques.

1.2 Aims and Objectives of the Thesis Work

The main aim of this study is the development of fabrication processes for sealing of microfluidic devices and packaging of MEMS devices based on laser welding technology. The main objectives can be briefly described as follow:

- Developing and designing several masks which could be suited for PMMA and

LCP manufacturing.

- Fabricating microchannel for testing the sealing of microfluidic application based on laser bonding technology.
- Developing and fabricating near-hermetic MEMS packages by using an intermediate LCP film.
- Creating development of monitoring approximate temperature during the laser bonding MEMS packages process.
- Understanding and optimizing the parameters of the thermal transfer in term of laser bonding process based on COMSOL simulation.

1.3 Layout of Thesis

Chapter 2 provides a comprehensive overview of traditional bonding methods for microfluidic devices and MEMS package. The fabrication processes to create microfluidic devices and bonding approaches of microfluidic systems based on thermoplastics are reviewed. Then the reviews of MEMS package using global heating method are presented. In addition, laser bonding technology for microfluidic devices and MEMS packaging are discussed.

Chapter 3 reports the material preparation, theoretical investigations and experimental results of laser bonding PMMA substrates. Different bonding parameters are analyzed such as laser output power, bonding time and bonding force. At the beginning, the theory of the laser system used in this study is presented. Then the material preparation in terms of PMMA mask designing by CO_2 laser micro-machining and PMMA substrate cleaning and metal film deposition are demonstrated. After that, numeric models with several process parameters of laser bonding PMMA substrates are analyzed to achieve the optimal bonding conditions including the analysis of bonding melt zone and heat affected zone. Based on the best bonding parameters, more designs of metal film patterns are applied on PMMA substrates to test the bonding strength and to achieve the optimal PMMA joining effects that could be used in practical microfluidic devices. Finally, a simple microfluidic system is bonded to test this bonding method.

In chapter 4, the method of laser bonding MEMS devices using an LCP film as the adhesive layer is studied. As an important adhesive material, the properties of LCP are discussed in details. Then the method of micromachining LCP by using a CO_2 laser system is described. Following that, several LCP packaging design configurations are

presented including the bonding parameters and temperature monitoring during the bonding process. After this, quality tests such as shear force testing and leak testing are presented within several approaches. Finally, SEM images of cross-sectional of different configurations are viewed and analyzed.

In chapter 5, the temperature distribution during laser processing of microfluidic devices and MEMS packaging is simulated by COMSOL. Two-dimensional and three-dimensional time-dependent models of heat transfer are developed including different process parameters such as laser power and heating times. And the material properties and heat transfer equation are described. Compared with the practical experiments, the temperature distributions of several configurations in term of microfluidic devices bonding and MEMS packaging are simulated.

Chapter 6 provides all the conclusions of the study presented in this project. Suggestions for future work are also discussed at the end.

Chapter 2 Literature Review

This chapter presents a review of the previous techniques for sealing of microfluidic devices and packaging of microelectronic and microelectromechanical systems. First, the development and challenges in packaging of micro-devices are discussed. Then several bonding methods for packaging of micro-devices are reviewed including microfluidic system sealing methods and MEMS packaging approaches. Furthermore, laser bonding techniques such as for thermoplastics and laser bonding for packaging of MEMS devices are described.

2.1 Sealing of Microfluidic System

The area of microfluidic systems has had considerable attention over the past two decades. This is because these devices are able to manipulate liquid through a series of micro-channels, pumps and filters at the submillimeter level in order to process DNA, proteins and other cells in nano volumes [2]. Over the years, a number of applications of microfluidic systems have been demonstrated. Development of bonding techniques has been one of the major fields of research in microfluidic systems.

Several materials have been used to produce the structures of microfabricated devices such as silicon, glass, polymers, metals and ceramic materials. Silicon has been widely used since the material and the fabrication processes were available in the early days of the field. Glass was also vastly used in microfluidic system, in particular for biological applications, because most of the biochemical behaviors can be monitored through glass [2]. Compared to silicon and glass, thermoplastics as substrate materials for microfluidic systems have significant industrial advantages such as low raw material cost, low manufacturing cost and simple to process [3]. In the early development of thermoplastic microfluidic systems, polycarbonate (PC) and poly(methyl methacrylate) (PMMA) were largely studied because of their useful properties, for example, good optical transmission at both visible and UV wavelengths, good solvent and chemical compatibility and good molding ability. Recently, cyclic olefins polymer (COC and COP) have widely appeared as microfluidic materials because of their attractive properties which are low water absorption and high optical transparency into the UV range [4]. Some of other engineering thermoplastics have also been used for microfluidic systems including polystyrene (PS), polyethylene terephthalate (PET), polyetheretherketone (PEEK), parylene and fluoropolymers such as

polytetrafluoroethylene (PTFE) and fluorinated ethylene propylene (FEP). Since microfluidic systems often required optical detection, most thermoplastics are amorphous materials and offer wide wavelength range of transmission in lab-on- a-chip systems. However for PET, it is either transparent or opaque depending on the grade and processing conditions [5]. Several important properties of thermoplastics materials for microfluidic devices are summarized in Table 2.1 [3].

Table 2.1: Properties of common thermoplastic materials [3].

Polymer	T_g(℃)	T_m(℃)	***CTE*** (10^{-6}/℃)	**Water Absorption (%)**	**Solvent Resistance**	**Optical transmissivity**	
						Visible	**UV**
COC/COP	70-155	190-320	60-80	0.01	Excellent	Excellent	Excellent
PMMA	100-122	250-260	70-150	0.3-0.6	Good	Excellent	Good
PC	145-148	260-270	60-70	0.12-0.34	Good	Excellent	Poor
PS	92-100	240-260	10-150	0.02-0.15	Poor	Excellent	Poor
PP	-20	160	18-185	0.10	Good	Good	Fair
PEEK	147-158	340-350	47-54	0.1-0.5	Excellent	Poor	Poor
PET	69-78	248-260	48-78	0.1-0.3	Excellent	Good	Good
PE	-30	120-130	180-230	0.01	Excellent	Fair	Fair
PVDC	0	76	190	0.10	Good	Good	Poor
PVC	80	180-210	50	0.04-0.4	Good	Good	Poor
PSU	170-187	180-190	55-60	0.3-0.4	Fair	Fair	Poor

$\boldsymbol{T_g}$-glass transition temperature ($\boldsymbol{T_g}$ characterizes the transition from true solid to very viscous liquid), $\boldsymbol{T_m}$-melting temperature ($\boldsymbol{T_m}$ of a solid is the temperature at which it changes state from solid to liquid at atmospheric pressure), ***CTE***-coefficient of thermal expansion.

Normally, microfluidic bonding methods can be categorized into two main types that are indirect bonding and direct bonding. In the indirect bonding technique, an additional glue or epoxy layer is applied to bond one substrate to another one. However, in the direct bonding technique two substrates are bonded together without any additional intermediate materials. Here some typical bonding techniques that have been used for bonding microfluidic systems are discussed, and several issues which affected the development of the field are also described.

2.1.1 Adhesive Bonding

Adhesive bonding has been extensively used for bonding polymer microfluidic systems since this technique is relatively simple and is easy to use [6-10]. The simplest adhesive

bonding method is to use a glue to bond the substrates, for example, using liquid adhesives through the evaporation of solvent or epoxies and acrylates which can be cured using catalyzing agent [11-12], but the main challenge of this method is channel clogging. Generally, adhesive bonding is processed by using a thin layer such as a high viscosity liquid adhesive to form a bond after curing by UV light irradiation. In order to prevent the adhesive from clogging the microchannels, various approaches have been studied. Figure 2.1 shows a contact printing process has been developed in which a stainless steel plate and a sacrificial channel network design were used to produce a thin adhesive layer in a rubber pad for printing onto a microfluidic substrate for bonding [8].

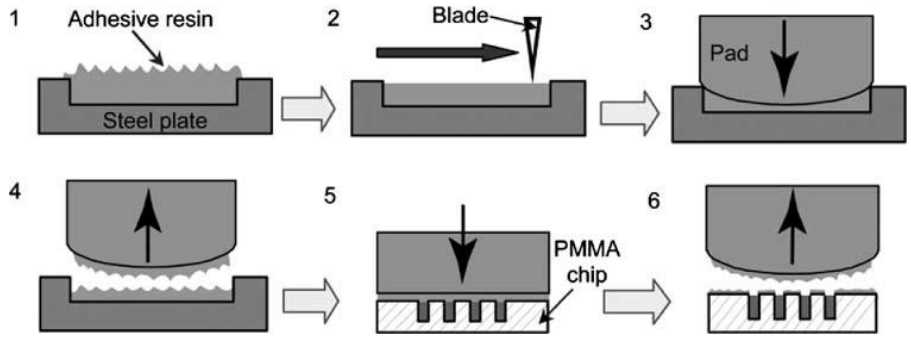

Figure 2.1: Adhesive application using a contact printing process. (1) Adhesive was poured on a steel plate with a hollow. (2) Adhesive was spread over the plate using a blade. (3) Adhesive was applied on a silicon rubber pad. (4) The silicon pad was removed with adhesive. (5) The silicon pad with adhesive was deposited on the PMMA chip. (6) The excessive adhesive was removed by sacrificial channels [8].

Another attractive approach for adhesive bonding is based on a laminated film because the commercial laminators are inexpensive and easy to use. A range of laminate films are available with thickness as low as 40 μm. For thermal lamination, they consist of a polymer layer coated with an adhesive resin which is activated at promoted temperatures between 100 ℃ and 150 ℃. A range of basic lamination processes have been reported such as using a thin COC sheet within an intermediate solvent mixture as an adhesive lamination film [13], or using dry lamination films to form an uncrosslinked photopatternable resin (SU-8) spun onto a polyethylene terephthalate (PET) backing sheet in opposition to another crosslinked SU-8 layer [14].

2.1.2 Thermal Fusion Bonding

In direct thermal fusion bonding, two substrates are pressed together under a pressure and are heated up to a temperature above the glass transition temperature (T_g) of one or both of the substrate materials. In this case, the interface between the two substrates can be in close contact and strong bonding can be obtained since the combined temperature

and pressure can generate sufficient flow of polymer materials. One of the most important advantages of direct thermal fusion bonding is the homogeneous surface properties of the microchannels when the same materials are used for both the lid and the substrate of the microchannels. Due to the two advantages that are high bonding strength and simple approach to process, the thermal fusion bonding method is one of the most common methods for bonding microfluidic systems. Several thermoplastic materials have been widely used in thermal fusion bonding such as PC [15-19], PMMA [20-25] and COC [26-30]. A number of other polymers have also been explored for direct thermal bonding including polystyrene and polysulfone [31], polystyrene and copolyester [32].

One of the main challenges of thermal fusion bonding is channel distortion because of the high temperature or pressure. In order to prevent excessive polymer flow and restrict deformation of the embedded microchannels, precisely controlled temperature, pressure and time are crucial to achieving strong strength. In this situation, the use of a specially devised hot press [33-35] and high throughput roller laminator [27, 30] methods is generally preferred. There are some methodologies explored to reduce the degree of broken microchannel during thermal bonding. An interesting approach relies on the use of a high bond temperature of 165 ℃ which is above the substrate T_g, while carrying out at low pressure to limit deformation of the substrates [22]. Excellent channel cross sections can be obtained using this method as shown in Figure 2.2.

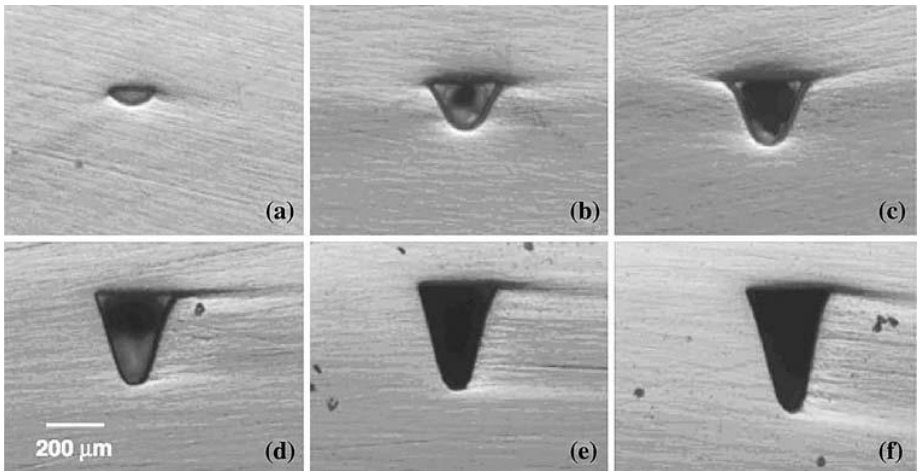

Figure 2.2: Cross-sectional images of laser micromachined PMMA channels with thermally bonding at 180 ℃ and a low bonding pressure below 20 kPa [22].

2.1.3 Solvent Bonding

In solvent bonding, a solvent is used which can dissolve the polymer at room

temperature. When this happens, the chains of the polymer are moving in the liquid and mixing with some dissolved chains of the other substrate. Solvent bonding of thermoplastics makes use of polymer solubility in selected solvent systems to achieve interaction of polymer chains across the interface. When the surface of a thermoplastic is solvated, the polymer chains become unstable and can easily spread on top of the solvated layer resulting in a strong bond between the thermoplastic and the material it is being adhered to. According to the method, it is easy to achieve a high quality product whether fabricating prototypes or in mass production. Besides, polymer substrates are used solvent method can be applied either liquid or vapor phase. In conclusion, liquid phase applications are carried out using solvent and polymer systems with appropriate solvability parameters in order to prevent residual solvent within the polymer model to avoid deformations of channels during processing. The residual solvent absorption can also be blocked by using fast solvent exposure times.

PMMA as a polymer material for solvent bonding for microfluidic applications has been widely reported. Before attaching PMMA substrates together under pressure of solvent bonding, they were immersed in ethanol for 10 min. Because the solvability parameters of PMMA and ethanol are different, the immersion processing could be carried out without channel deformation [36]. The PMMA based solvent bonding method has also been studied using methanol and isopropanol which applied solvent to the covered layer by fast bucking the polymer chip into a solvent bath. Under different pressures, temperatures and times to identify best process conditions, these chips were immediately removed and bonded to the microchannel plates [37]. Based on the results of the tensile test, the bonding strength can be as high as 23.5 MPa. In order to prevent microchannel deformation the solvent composition, exposure time and temperature must be under precise control. One solution was to use a sacrificial phase change material. In this method, the microchannels filled with liquid wax [38] or water [39] are cooled to solidify the sacrificial material. Once the ethelyene dichloride applied on the surfaces of the chips, the channel distortion can be actually eliminated since the sacrificial materials prevent solvation of the channels walls. The microfabrication process is described in Figure 2.3 [39].

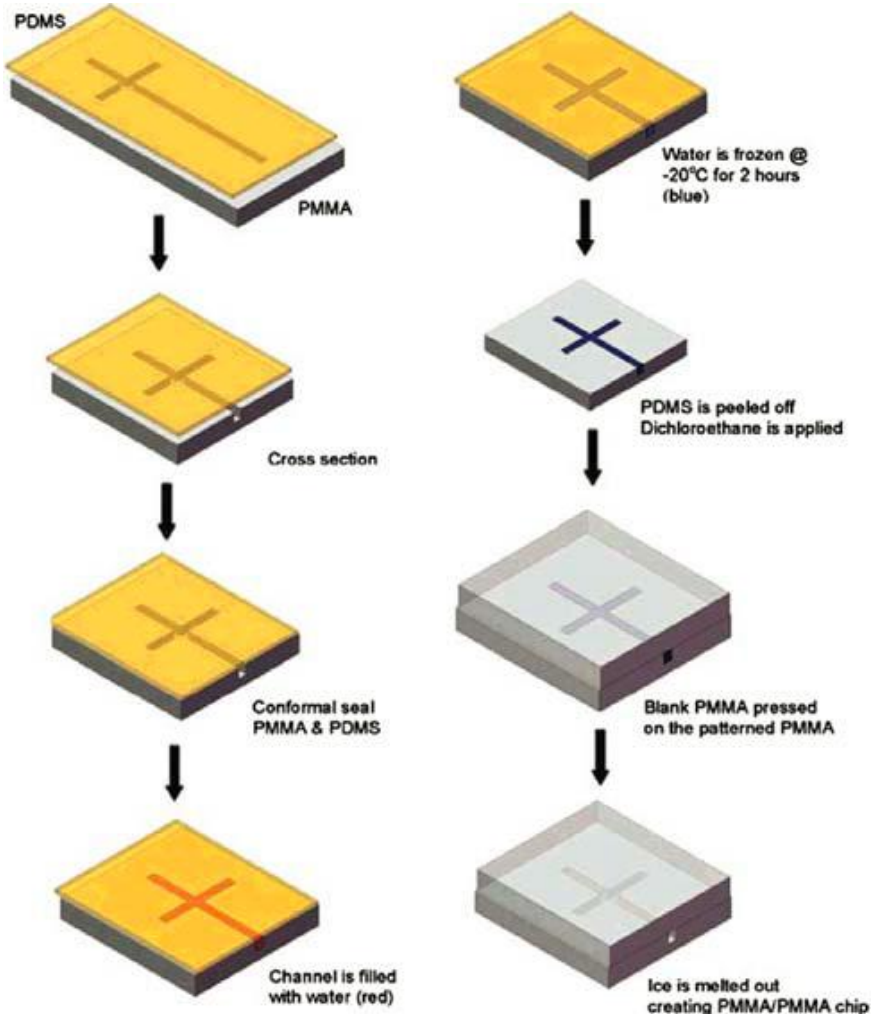

Figure 2.3: Frozen water as a sacrificial layer was employed in solvent bonding process to protect the enclosed microchannels stability [39].

2.1.4 Localized Bonding

An interesting method unlike the adhesive and fusion based approaches for bonding thermoplastic substrates is to use ultrasonic energy to soften the interface between the bonding parts to produce a strong bond. The advantage of this method is that the ultrasonic energy can be applied locally to particular areas for bonding or to the entire interface [5]. An ultrasonic welding method for PMMA and PEEK microfluidic devices has been reported [40]. In this method, the microchannel chip and the cover plate were machined to contain energy directors and structures to generate the melt flow during welding process, and good bonding results were achieved by optimizing the bonding pressure, power and time as shown in Figure 2.4.

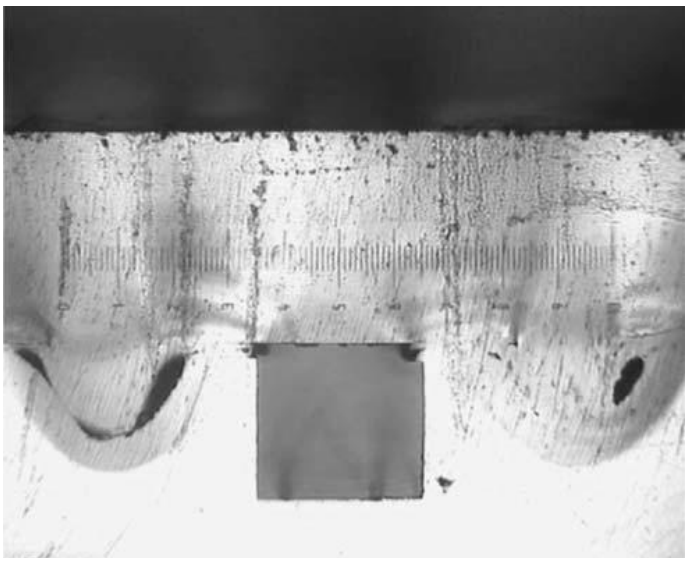

Figure 2.4: Cross-section microphotograph of PMMA microchannel with 500 μm square and sealed by ultrasonic bonding [40].

Another method of localized welding of thermoplastics is to use microwave energy to heat metal films placed between the bonding surfaces. In this technique a 100 nm thick layer of chromium/gold was coated onto an embossed PMMA substrate, and the cover plate was also deposited with a 100 nm metal film. Then the two substrates were clamped together and placed into a microwave chamber. The frequency of the microwave source was 2.4 GHz. When the microwave energy was applied, the PMMA was transparent and the metal films absorbed the microwave energy efficiently to melt the surrounding polymer materials resulting in localized bonding. The successful bonding was achieved with 10 W microwave power and 120 s of heating time [41].

A method of employing nickel as an intermediate layer was also studied in low frequency induction heating of two PMMA substrates. The intermediate 50-100 nm thick nickel layer was deposited onto a PMMA substrate and was heated using different coils and frequencies [42]. The details of results are shown on Figure 2.5.

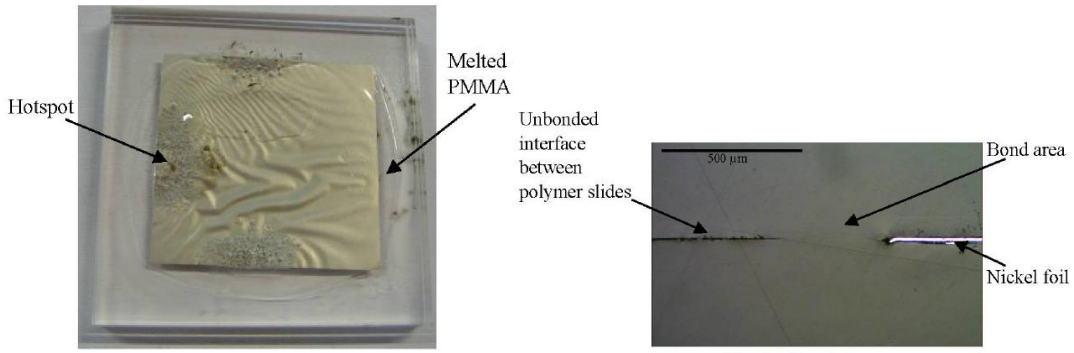

(a) (b)

Figure 2.5: The results of PMMA bonding in low frequency induction heating method: (a) bonded PMMA substrates with 7.5 µm thick nickel foil, and (b) cross-section microphotograph of bonded area [42].

2.2 Review of MEMS Packaging Methods

For the commercialization of Micro-Electro-Mechanical-Systems (MEMS) products, one of the most crucial challenges is packaging. A suitable surrounding is provided by packaging of MEMS devices to improve their reliability. Packaging is often one of the most expensive steps in MEMS manufacturing, and it is also the main factor to determine the final response of MEMS devices. It often has an influencing effect on the microsystem performance. A number of technologies of MEMS and microsystems are required to achieve successful development, such as their packaging, assembly and low-cost fabrication. The long term stability and the cost of several MEMS devices are usually determined by packaging. Several techniques are required in many MEMS, for example, wafer level fabrication, temperature control, vacuum and hermetic encapsulation. In the previous studies, wafer bonding has been investigated and thin film approaches have attracted recent attention. For most of MEMS devices, bonding techniques are the most important requirements. A number of bonding methods have been studied so far, including anodic and eutectic bonding, adhesive, solder and laser joining using thin films such as glass frit and benzocyclobutene (BCB).

2.2.1 Anodic Bonding

Anodic bonding which is also known as electrostatic bonding, field assisted bonding or Mallory bonding, was first reported in 1969 [43]. Originally anodic bonding was used for glass to metal sealing, but nowadays it is used for bonding of silicon to glass applications in the production of microsystems and MEMS, for instance, encapsulation of sensors [44-46]. The classic configuration of the bonding process is shown in Figure 2.6. For silicon wafer to glass wafer bonding, the two polished surfaces are kept clean,

then clamped to ensure intimate contact and at 400 ℃ to 450 ℃ of representative temperature and a voltage between 400 V and 1200 V is applied across the wafers to realize bonding at the interface. And the glass wafer acts as cathode and the silicon wafer as anode. Because of the increased temperature the movement of the sodium ions (Na^+) is improved within the glass wafer. The positively charged Na^+ move to the cathode and generating a depletion area in the glass side between the glass and silicon interface. The negatively charged and relatively constant oxygen anions are left behind creating a space charge region. And in the silicon side between the glass and silicon interface, an equivalent positive charge is generated. This leads to a strong electrostatic attraction of the bond interfaces driving them into close-contact. The oxygen anions are pulled to this interface induced by the high electric field and react with the silicon because of the increased bonding temperature. Bonding strengths ranging from 15 to 25 MPa have been achieved between the two surfaces in an electrochemical reaction [44, 46-48]. During anodic bonding, sodium rich glass wafers are needed such as Corning #7740, Corning #7070, soda lime #0080 and K_4 glass [45, 46, 49-51].

The main anodic bonding process include four steps: firstly, the polished and cleaned bonding surfaces are prepared in order to ensure a particle-free interface, then the polished surfaces of the wafers are clamped to make intimate contact and heated in an oven or on a hot plate to the required temperature, after that the bonding process is carried out by application of an electrostatic field, and lastly the wafer stack is cooled down after normally 5 to 10 min. For successful bonding, one of the key factors is the coefficient of thermal expansion (CET) of the bonding partners has a good match over the temperature range of the bonding process. Otherwise the bond can fail due to the mechanical stress at the interface after cooling to room temperature, or causing a wafer warping effect which might influenc the stability of the MEMS devices [43, 46, 49, 51].

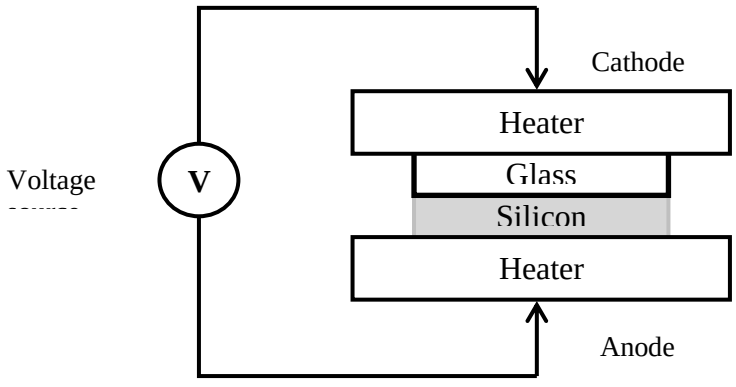

Figure 2.6: The schematic of anodic bonding [46].

In comparison to silicon fusion bonding, anodic bonding has an important advantage which is less stringent requirement on the surface flatness although it still requires clean, smooth and polished interface with less than 1 μm of surface roughness. The similar challenge of silicon fusion bonding and anodic bonding is that there might be non-bonded areas if the bonding surfaces are not free of dust particles [43, 50, 51]. For anodic bonding, the most important processing parameters are the bonding temperature and the voltage. Generally, stronger bonding can be achieved at higher bonding temperature (restricted to a maximum 450 ℃) and at stronger electric fields. If the temperature is higher than 450 ℃, the difference in the CTE of glass and silicon might cause excessive mechanical stress between the wafers and hence bond failure.

Although anodic bonding is reliable and widely used in the MEMS industry, it has several limitations. The successful bonding requires particle-free and less than 1 μm of surface roughness which can only be guaranteed in controlled environments and also requires complex preparation of the bonding interface before bonding. In contrast to the other bonding methods it is restricted to bonding of materials with closely matched CTE. Moreover, during the anodic bonding process, the strong electric field requirement prevents the technique from being applied to packaging of sensitive electronics and other prefabricated devices like RF-MEMS [51].

2.2.2 Eutectic Bonding

Eutectic bonding, which is also known as eutectic soldering, is a bonding method using intermediate metallic layers as the joining layer to form an eutectic alloy. There are several advantages in this technique, one of which is that the melting point of the eutectic alloy that is formed during bonding process is much lower than the melting temperature of the original materials. Usually, one of the main materials for eutectic bonding is the eutectic solder. For chip packaging, eutectic bonding has been a well-established method in the industry since the early 1990's, the first application of wafer to wafer bonding for packaging of silicon microsystems was studied by Woffenbuttel in 1994 [52, 53]. For eutectic bonding, it is easier to achieve strong bonding in hermetic packaging with considerably lower temperatures than in the direct bonding approaches. In silicon eutectic bonding, gold as an important material, has been widely used in MEMS packaging [52, 54, 55]. At the temperature of 363 ℃, an eutectic alloy is formed with silicon at an eutectic composition of 19% Si and 81% Au. The

important thing is the melting point of 363 ℃ is below the melting point of gold which is 1064 ℃ and silicon which is 1414 ℃. The phase diagram is shown in Figure 2.7 [53].

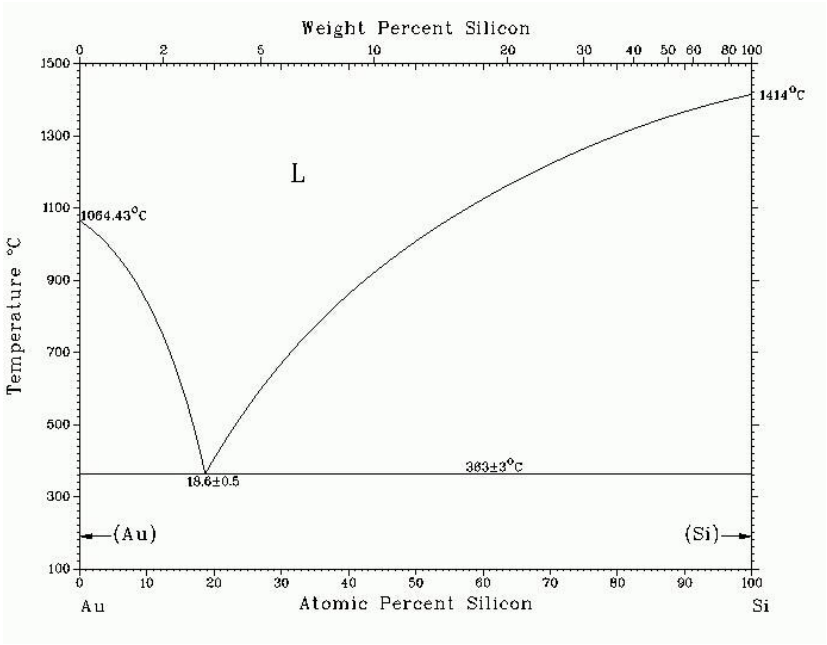

Figure 2.7: The phase diagram of silicon and gold [53].

During the eutectic bonding process, a liquid phase is directly formed while the compound is heated above the eutectic temperature of 363 ℃. The compound will keep fluid unless the temperature falls below the eutectic temperature or the concentration of the composition changes below the liquid line [52]. In order to achieve two wafers to bond together, silicon and gold must be applied to the bond interfaces to form the eutectic alloy. Generally, gold is evaporated onto either one wafer and silicon is provided from the silicon wafer itself. Compared with direct bonding, the atomic contact of the gold and silicon starts with a diffusion process and then accelerated along with the increasing temperature. Above the eutectic bonding temperature, the eutectic compound can be melted as a liquid phase and then mixed and diffused to act as intermediate bonding layer. Because the silicon comes from the substrate directly with unlimited supply, the solidification starts when the silicon has reached the certain concentration in the mixture and the temperature falls below the liquid line as shown in Figure 2.7. After cooling, a strong eutectic bond is formed that consists of a gold silicon hypereutectic phase [52-54].

The advantages of eutectic bonding are low bonding temperature, lower pressure and no out-gassing during bonding [52, 54, 56]. The most important reason of its wide use in

commercial applications is that hermetic packaging and chip interconnect sensor can be operated in the same processing [52, 56]. There are three steps in the eutectic bonding process, including substrate preparation, bonding process and cooling down to form the bond. For substrate preparation, this step is extremely important. The main problem of this step is the poor wettability and adhesion of gold on an oxide surface, even the native oxide layer absorbed on the silicon substrate can also affect successful bonding. In order to overcome this problem, two approaches have been developed to remove the oxide layer prior to bonding and depositing of additional adhesion layers on the top of the oxide [52, 54, 56]. Mechanically, the oxide layer can be removed by rubbing the surface against each other to break up the oxide or by using ultrasound vibration. Commonly, the method to remove an oxide layer is based on wet chemical etching or plasma cleaning.

Although good bonding of gold and silicon can be achieved after removing the oxide, the second technique is to apply adhesive layers as normally preferred in applications. However the native oxide on the silicon substrate is needed as a passivation layer for integrated circuits. The intermediate metal films are deposited on the top of oxide surface followed by the gold layer deposition. Usually titanium and chromium or combinations of them are the suitable materials. A Au-Sn medium with eutectiv composition Au:Sn nearly 80:20 wt.% was used since this melts at the temperature to ensure a sufficient thermal conductivity through the solder and provide mechanical flexibility. A typical illustration of this processing is shown in Figure 2.8 [55].

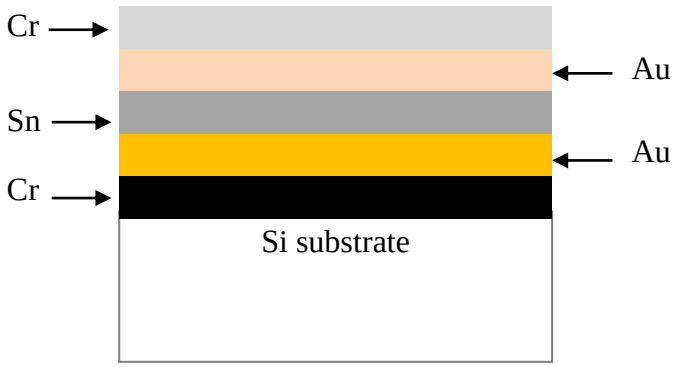

Figure 2.8: The schematic of Eutectic bonding [55].

In silicon-gold eutectic bonding, the bonding process must be carried out as soon as possible because fast processing can prevent re-oxidation of the silicon surface. To achieve a strong bond, these surfaces should be kept free of dust particles and therefore

it is better to process in an inert gas atmosphere or vacuum to avoid oxidation at high temperature. The materials of eutectic bonding should have several microns of thickness to compensate the roughness of non-planar surfaces [54]. After preparation, the wafers which needed to be bonded are placed on the top of each other, and these wafers are heated above the eutectic temperature during the bonding process. Like most of the bonding methods, to achieve intimate contact between the bonding interfaces, a suitable pressure or force must be used throughout the process. The most important bonding parameters of eutectic bonding are the bonding temperature, time and pressure. For the silicon to gold eutectic bonding, the process is typically carried out at the temperature of 390 ℃ to 400 ℃ for roughly 15 minutes and the pressure usually from 100 kPa to 500 kPa [52].

For eutectic bonding of silicon to gold, a bond strength of up to 148 MPa has been reported. But the processing temperature is up to 500 ℃ for reliable bonding which is considerably higher than the eutectic bonding temperature of 363 ℃ [56, 60]. So in this case several problems can occur, for instance, regression of performance, excessive stress at the interface or even totally deformed devices. An interesting example is RF-MEMS which usually can only be packaged below 350 ℃ of temperature protecting the inner sensors. Therefore for reducing the bonding temperature, different eutectic alloys have been investigated [57, 58, 60-62]. For example successful wafer level packaging of RF-MEMS has been obtained using a gold and tin based eutectic alloy [57, 58, 61]. In the study, hermetic packaging with average bonding strengths of up to 71.5 MPa was achieved in a bonding process at a temperature below 300 ℃. Further bonding temperature has to be raised to 180 ℃ to 210 ℃ on reported by using gold and indium based eutectic system [62]. For glass to glass and glass to silicon bonding, average bond strengths of 20 MPa to 40 MPa have been reported. A hermetic seal with bonding strength up to 20 MPa in silicon to silicon bonding has been demonstrated and the bonding temperature was reduced even further below 160 ℃ by using indium-tin alloys.

2.2.3 Glass Frit Bonding

Glass frit bonding is a packaging method using glass frit as the intermediate bonding layer. This approach is widely used in the industry field, such as gyroscopes, micro relays, acceleration sensors, IR-bolometers and many other devices [63-70]. In these applications, it is necessary to make sure the devices are hermetically sealed with long term reliability and functionality. In the past several years, glass frit bonding has been

studied and reported to be a suitable sealing method [71-73]. The main advantage of glass frit packaging is high bonding strength, high process yield and good process repeatability. It does not require a very flat surface due to its high wetting abilities. It is also possible to directly bond the sealing ring without deforming the inner sensors. Glass frit as the adhesive layer can be used for most materials in microsystem technologies. An important factor in packaging is temperature, the temperature in glass frit bonding ranges from 300 ℃ to 450 ℃ which limit the use of the method for temperature sensitive materials and structures within the package. The outgassing of the glass frit material during bonding could affect the encapsulated structures.

As an important bonding material, glass frit is processed as paste and it is available from different companies such as Corning, Diemat, Schott and Asahi Glass Company (AGC). In order to ensure the glass frit bonding method is compatible with IC packaging and suitable for most MEMS applications, glass frit materials are usually designed to enable the processing temperature below 450 ℃ [64, 65, 67-69]. Glass frit materials with a processing temperature below 400 ℃ can also be used for CMOS packaging [74]. Low bonding temperature is usually achieved by using lead or lead silicate glass with high lead oxide content [67, 469, 74]. The glass is made into many small particles such as frits and the sizes of these frits range from 1 μm to 15 μm. The glass powder is compounded with organic binder and solvents to generate a printable paste which can be printed onto the bonding surface. Like silicon bonding, inorganic fillers are added to the paste to match the coefficient of thermal expansion of the materials to be bonded [64, 65, 67-69, 74].

In glass frit bonding, the glass frit paste can be screen-printed, stencil-printed or dispensed onto one of the surfaces to be bonded. When screen-printing is used, the mesh size of roughly 190 μm with a minimum spacing of 100 μm can be achieved. Roughly a height of 30 μm for glass frit paste is recommended to ensure sufficient material for reflow [67, 68]. These deposition techniques have the disadvantages that the rough frit quantity is different to control and the deposition accuracy is marginal. After deposition of the glass frit paste onto the substrate, the paste is heated at elevated temperatures to drive out solvents and burn out the organic binder before bonding. The temperature profile of the thermal conditioning process of the glass frit is shown in Figure 2.9.

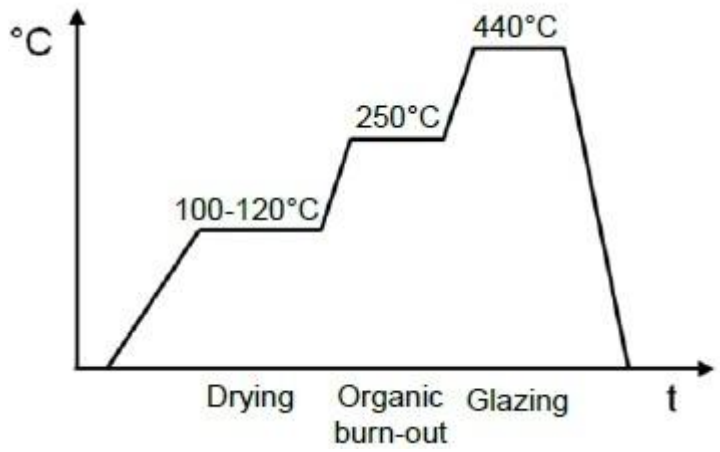

Figure 2.9: Profile of thermal conditioning temperature of glass frit material [67].

At the beginning, the frit paste is first heated to a temperature of 100 ℃ to 120 ℃ for usually 10 minutes to 30 minutes to dry the paste and remove any remaining solvents. After that, the temperature is increased to around 250 ℃ for 30 minutes to 60 minutes until the organic elements are totally burnt out. The precise temperature depends on the mixture of the paste. The paste is then heated to the bonding temperature at around 440 ℃ and a compact glass without any gap is formed. After glazing, it is easy to observe that the thickness of the glass frit layer is reduced. The inorganic fillers applied to match the coefficient of thermal expansion of the substrates are melted in the glazing process. Then the final properties of the layer are achieved.

Glass frit packaging is a thermo-compression bonding method. The materials can be bonded and the glass frit is heated to the bonding temperature with a suitable pressure that results in reduction of the thickness of the glass frit layer to enhance the wetting of the bonding interface. The increased temperature reduces the viscosity of the glass frit to such a degree which even for rough and non-planar surfaces, a total wetting of the bonding area can be achieved. During the glass frit bonding process, the critical parameter is the temperature rather than the applied pressure. The temperature must be high enough to make proper wetting, however, too high temperature will cause flow of the glass frit material into the microstructures which would damage the inner devices. In the case of silicon and glass bonding, a thin glass mixture is additionally formed between the silicon and glass interface which enhances the bond strength. Cooling stress can occur because of the mismatch of coefficient of thermal expansion of the materials, however, this is only crucial at temperatures above 200 ℃ [64, 65, 67-69]. A cross-sectional monograph of a bonded silicon to silicon substrate is shown in Figure

2.10 [67].

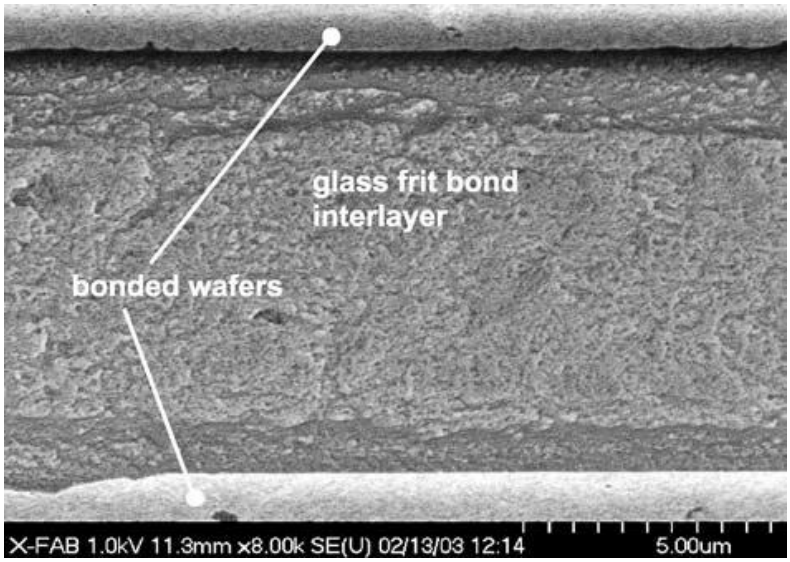

Figure 2.10: Cross-sectional image of wafer level encapsulation and packaging with glass frit layer [67].

Glass frit bonding is a simple and successful process without the requirements for careful preparation of the surface of the bonding substrates. Comparing with anodic and eutectic bonding, glass frit bonding can produce hermetic sealing with up to 20 MPa of shear strength [67, 68]. In contrast to the other bonding methods, glass frit bonding has high viscosity during bonding and it is suitable for rough surfaces and non-planar surfaces. No additional passivation is needed when the glass frit is heated up to temperature of 150 ℃ to prevent leakage of currents since glass frit is a dielectric material [63, 67, 68]. After processing, the thickness of the glass frit layer ranges from 5 μm to 10μm which can be used as a spacer between the sealed surfaces to create an inner cavity for MEMS applications as shown in Figure 2.11.

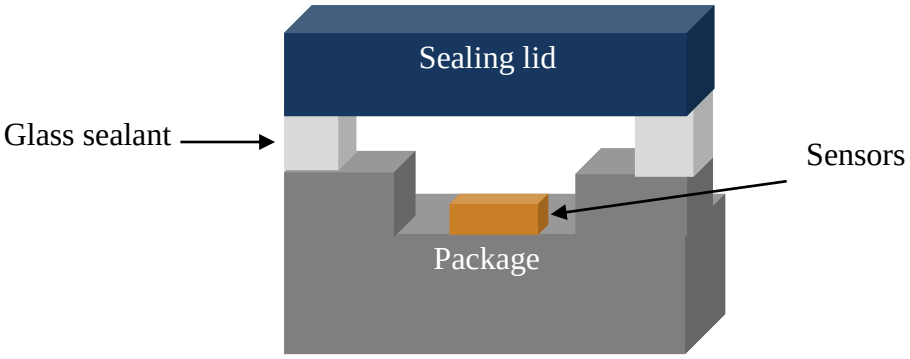

Figure 2.11: A schematic diagram of bonded MEMS device intermediate glass frit [68].

For the glass frit bonding, almost all the materials that are used in MEMS technologies

are suitable for successful joining, for example silicon, metals, glass, insulators and passivation layers [63, 67, 68, 76]. For glass frit to silicon oxide bonding, it is not possible to use eutectic bonding but it can be achieved using glass frit bonding with good bond strength. Moreover, electric fields are not needed in glass frit bonding and bonding temperatures below 400 ℃ enable glass frit packaging to be compatible with the IC and CMOS chips. Glass frit bonding has been successfully used for vacuum packaging of silicon resonators [71-73, 77]. In order to solve the problem of outgassing of moisture and carbon from the glass frit, lower cavity pressure of less than 1.13×10^{-3} mbar can be obtained by using getters. From these studies, glass frit as a sealant achieved useful properties for packages of hermeticity and long-term stability. Even after the samples were stored at a high temperature of 95 ℃ for three years, there was no loss of vacuum in the packages.

The main disadvantage of glass frit bonding is the relatively high temperature up to 450 ℃ and normally the whole packages are heated. This bonding method is not suitable for hermetic packaging of temperature sensitive devices [78].

2.2.4 Polymer Based Bonding Methods

Polymer based bonding is a technique that uses a polymer film as an intermediate bonding layer and it is also referred to as adhesive layer bonding. Several polymers, such as PMMA, SU-8, parylene, benzocyclobutene (BCB) and liquid crystal polymer (LCP), have been widely used for MEMS devices, wafer bonding and packaging of IC [80-102].

For polymer layer bonding, it is possible to carry out the bonding process below 100 ℃ and hence without any effect on the substrate materials. In this method, strong bond strengths and good adhesion can be achieved for most packaging materials. Since it does not need electrical fields during the bonding process, the approach can be used for IC packaging. This bonding process is a simple and favorable method which is less sensitive to particles, surface roughness and non-planar bond surfaces. This makes the bonding process easy and cost effective. Low pressure bonding is possible since the intermediate polymer film is a flexible material and sometimes has liquid behaviour during the bonding process. After bonding, the thickness of the polymer film layer can range from tens to hundreds of microns, so that the layer can also be used as a spacer for cavity packages. Some limitations should be considered, for example, lack of

hermeticity, limited temperature stability and limited long-term stability of the bonds in harsh environments such as moisture, temperature and radiation [79, 80, 88, 92, 95, 102].

Generally, there are three main process steps in polymer layer bonding. First, the polymer film is placed onto one or both surfaces of the substrates. Then, the two substrates are aligned to each other. Last, a pressure or force is applied to the substrate. The polymer layer has intimate contact with the surfaces of the substrates. During the bonding process, the polymer film is transformed from a solid to a viscous liquid by heat in thermal bonding and then become a solid again after cooling. The principle of the polymer film bonding is that the surfaces of both substrates are bonded to each other using an intermediate polymer layer. In order to make sure the surfaces of both substrates have enough contact without any gaps, the polymer film should have low viscosity. When the polymer film is melted and flowed to cover the uneven surface, the bonding areas are all covered with the polymer and a complete bond is formed after cooling. In this case, a strong bond is generated between the substrates [80]. Polymer materials are divided into four main types, namely thermoplastics, thermosetting polymers, elastomers and hybrid polymers. All of these four polymer materials can be used for polymer layer based bonding. In these four types of polymers, thermosetting polymers are more suitable for polymer bonding because of their special material characteristics. The glass transition temperature of thermosetting polymers can be from 300 ℃ to 450 ℃ with a fairly high chemical resistance. Actually the polymer layer bonding is an originally heat activated polymerization process which is also called curing. Because of the chemical reaction, the small side chains of the polymer molecules are cross-linked to generate a reliable three-dimensional network. After generating a solid polymer, sufficient curing is pre-condition for a strong bond. As discussed before, the polymer requires a liquid phase at some status during the bonding process to make sure enough wetting of the bonding surfaces. This can be achieved during the preheating step before starting the cross-linking process [80, 102].

For thermosetting polymer based bonding, the process steps are as follow: first, the bonding substrates must be cleaned, then the intermediate layers are deposited and structured, at the last step, the actual curing process is carried out. Before the deposition of the polymer, the wafers must be cleaned to remove the dust and dried on a hotplate or an oven at a suitable temperature to remove moisture. After this, an adhesion promoter

is deposited onto the substrate surface to enhance the adhesion between the polymer film and the substrate surface. Then the adhesive polymer is deposited after drying the promoter. In order to achieve a precise thickness, the polymer is spin-coated over the whole wafer substrate under controlled conditions. A baking process must be performed to allow any solvent to evaporate. This step is extremely important because the remaining solvent on the bonding layer could be the source of bubbles in the film after bonding. The polymer layer can be patterned to form sealing rings by photolithography or reactive ion etching depending on the type of the polymer material. The structured adhesive layer is usually followed by a baking step to partly solidify the polymer. In this case, the polymer should be hard enough to ensure the patterned structures do not deform but also soft enough to be conformal to the bonding interfaces in the bonding process. Normally, the polymer is cured at a temperature between 200 ℃ and 300 ℃ until it is completely bonded and the bonding time depends on the bonding temperature. Better bonding can be achieved in a vacuum to prevent formation of voids due to trapped air bubbles in the polymer [80, 88]. The main processing parameters of this bonding method are bonding time, bonding temperature and the pressure that is applied to the substrates [90, 102]. Figure 2.12 shows a schematic illustration of bonding rough surfaces [80].

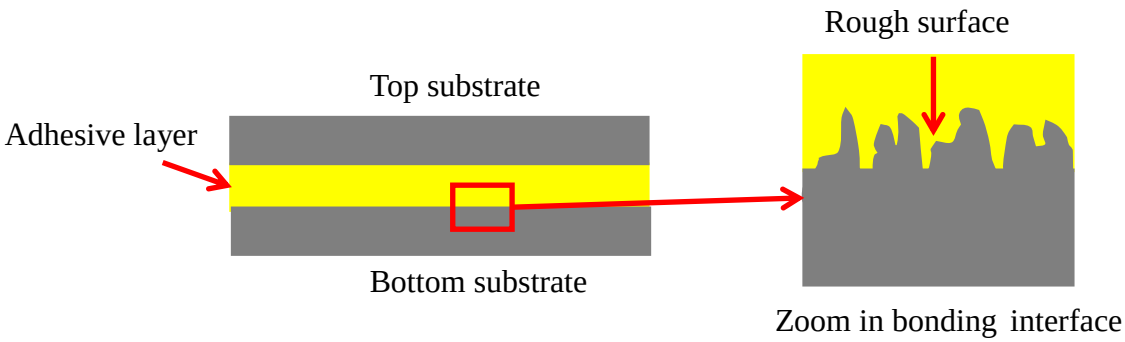

Figure 2.12: The schematic of bonded rough surface [80].

BCB and SU-8 as two important polymers have been widely used in industry for bonding applications in MEMS, RF-packaging, microsystems technologies [79-83, 85, 87, 90-92, 93, 95-98, 101, 102]. Both of the BCB and SU-8 polymers have been regarded as the most useful materials for adhesive bonding. SU-8 is a negative tone photoresist because of its low curing temperature which is from 100 ℃ to 200 ℃. The negative resist remains on the surface wherever it is exposed and the developer solution removes only the unexposed portions, and the positive resists behave in the opposite

manner. Since the bonding temperature is low, the stress generated in the bonding process is small resulting in high yield processes. The thickness of the polymer layers can range from a few microns up to hundreds of microns and these layers can be coated in a single spin coating process [85, 87, 100]. Aspect ratios as high as 17:1 can be accomplished, so that the intermediate layer could also be used as the spacer for most cavity packages [87]. Because of the high tolerance to the surface quality of the bond interface, it is more suitable for low cost and high volume production [85, 87, 100]. Figure 2.13 presents an example of the main steps of a contact imprinting based bonding process [85].

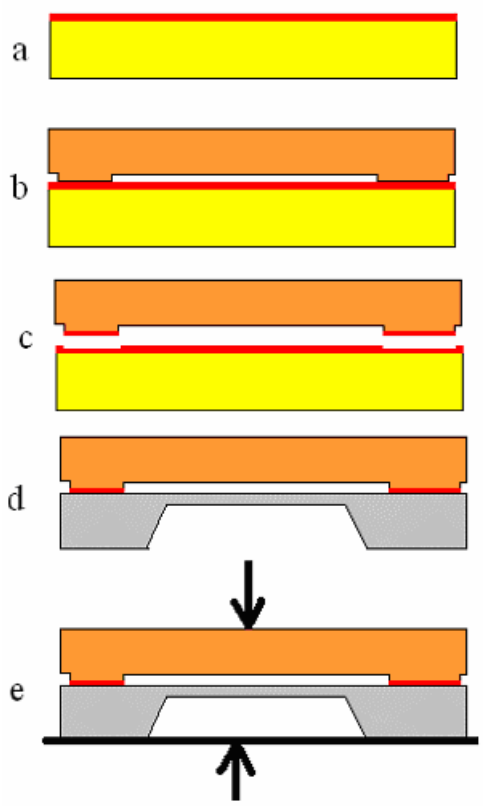

Figure 2.13: (a) SU8-5 photoresist was spun on a dummy wafer, (b) SU8-5 photoresist was contact imprinted by a cover wafer on the dummy wafer, (c) take apart of cover wafer, (d) alignment and contact, and (e) wafer to wafer bonding [85].

Silicon to silicon bonding using an intermediate SU-8 layer has been successfully achieved and reported which has a high bonding strength up to 20.6 MPa at the temperature of 90 ℃ [93, 94]. For silicon to glass bonding, the maximum bonding strength can be up to 20.9 MPa while keeping the bonding temperature below 105 ℃. In comparison with the other materials used in microsystems, the main disadvantage of SU-8 is its high coefficient of thermal expansion (CET) of 50 x 10^{-6} K^{-1}. The high CTE can cause cracks and deformation in the SU-8 bonding ring resulting in package failure

[100].

BCB as a potential polymer is suitable for adhesive bonding [79-83, 90-92, 95-98, 101]. In the thermal curing process of BCB, it does not need any catalyst that can cause outgassing and the solvent has already been evaporated fully during wafer preparation. Moreover, BCB has such advantages as high mechanical strength, low residual stress, high chemical resistance, bio-compatibility and low residual stress level. Due to its excellent electrical properties of high resistivity (1 x 10^{19} $\Omega \cdot cm$), low permittivity (2.65) and low loss tangent (1 MHz to 1.5 THz), BCB is a very suitable material for packaging of RF-devices. Because of the liquid behavior of the BCB, it could be bonded to rough or non-planar surfaces and it is less sensitive to particles than the direct bonding methods. Actually the BCB material can be used as insulating layers in electrical interconnects due to the low bonding temperature [81-83, 89, 90, 92, 95, 11]. For MEMS packaging, a 0-level glass-lid encapsulation technique using BCB and a contact printing method has been studied as shown in Figure 2.14 [92].

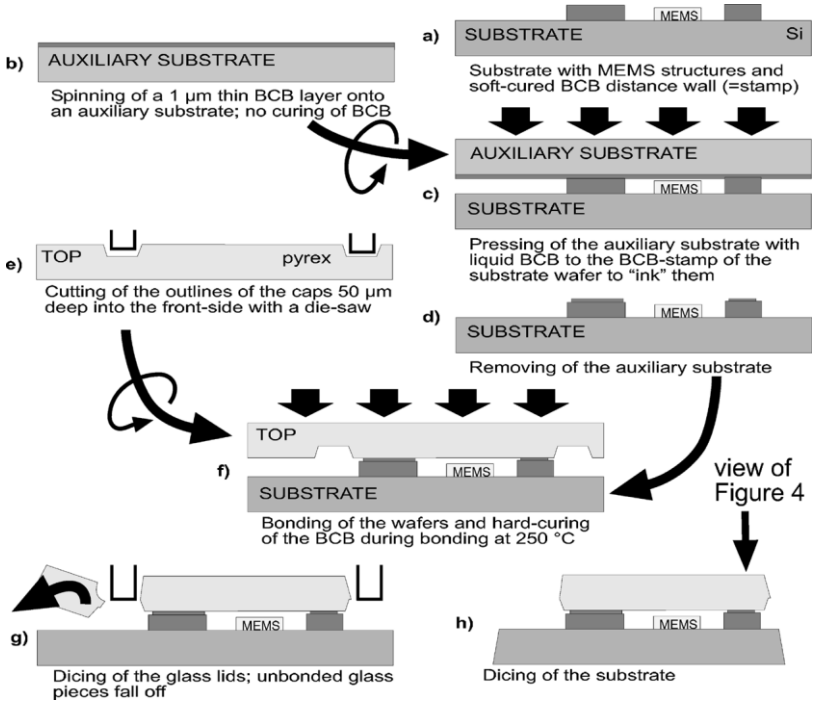

Figure 2.14: Fabrication sequence of 0-level glass-lid encapsulation technique by using BCB contact printing approach [92].

Several papers have reported silicon to glass bonding using BCB as the adhesive layer for packaging of RF-MEMS [81-83, 101]. After processing of the BCB polymer at round 250 ℃, shear strength of up to 37 MPa was accomplished that is even stronger than the value of 15 to 25 MPa in anodic bonding. It has also been demonstrated that the

BCB is not only used as an adhesive layer for the packaging of RF-MEMS but it can also acts as a capping material. A novel encapsulation process was studied to use a thin BCB polymer film for packaging. In comparison with the glass based lid, BCB as the lid material for packaging RF-MEMS has better performance because of its good electrical properties. Like most of the polymers, BCB as the adhesive layer also has a disadvantage which is that it is not incapable of hermetic sealing. In leak test, leak rates of 1.4×10^{-7} and 4.8×10^{-7} *mbar l* s^{-1} can be accomplished which is 3 to 10 times higher than the limits of MIL-STD-883G. In order to enhance hermeticity, an additional diffusion barrier of silicon nitride around the polymer seal has to be deposited although the enhancement is just near-hermetic [90, 92]. Another disadvantage of the BCB polymer for bonding is the thermal stability. The mechanical stability of the bond decreases quickly after bonding at the temperature of 350 ℃ due to the dissolution of the polymer [79].

It has been shown that the polymer layer bonding is simple and robust. This bonding method does not need highly smooth bonding surface. It is insensitive to dust contamination and the substrates could be bonded in a normal environment without any special preparation of the bonding surfaces [102]. The bonding strength can be the same as the method of eutectic and anodic bonding without any careful wafer preparation. But for this technology, the limited long time reliability of the bond in harsh environments and the lack of completely hermetic seals are the main disadvantages. Although the BCB layer bonding process can be achieved at low temperature as compared with the other intermediate layer bonding process, it is a disadvantage to heat the whole package at 250 ℃ since some temperature sensitive devices and materials have low temperature tolerance such as the functional polymers used in organic light-emitting diodes (OLEDs) with the maximum temperature of limit below 100 ℃ [78].

Liquid crystal polymer (LCP) has gained much attention due to its excellent properties for microsystem packaging. It is extremely stable and exhibits near-hermetic properties. As an important polymer, LCP has the potential to be a cheaper option than the other materials such as ceramics materials. Due to its low cost and favorable packaging characteristics, LCP has been widely applied as a dielectric substrate and packaging material for RF applications. Several advantages of LCP are described as quasi-hermetic (water absorption < 0.04%) performance, low cost, flexible for conformal application, flexible circuit substrates and excellent high-frequency electrical properties [103-106].

The lamination process of LCP requires several different hot press steps and many parameters such as bonding time, pressure, temperature and vacuum settings [107]. The main difficulties with the lamination process are the rigorous temperature uniformity and precise control needed for proper adhesion. The rigorous temperature tolerance during the LCP lamination process is because LCP has a steep change in the modulus of elasticity which is shown in Figure 2.15 [107]. Initially, the LCP modulus of elasticity is stable to the melting temperature, then it decreases dramatically. Because in the solid state, molecules are strongly ordered and have little translational freedom. However the characteristic original order of the liquid crystal state is between the traditional solid and liquid phases and this is the origin of term mesogenic state, used synonymously with liquid crystal state. Therefore the process temperature must be monitored and controlled precisely.

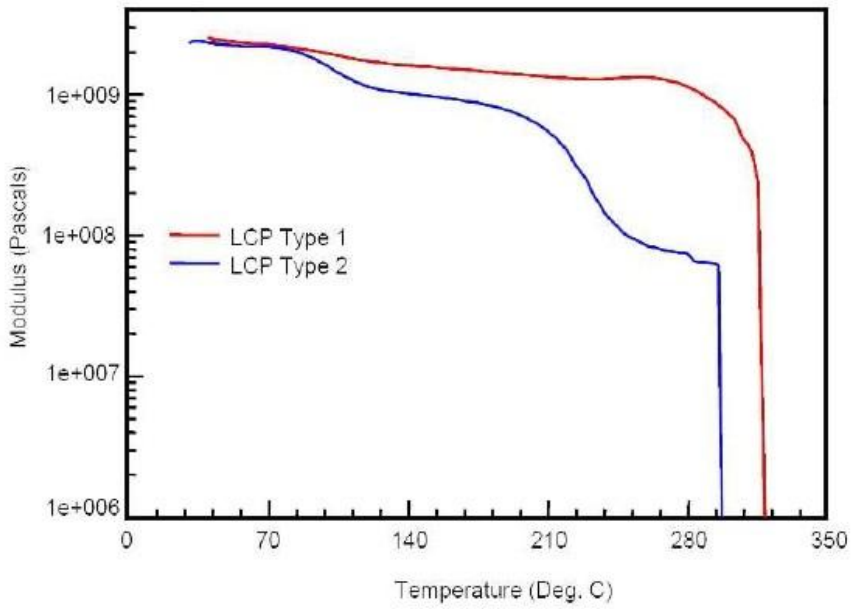

Figure 2.15: The relationship between elastic modulus and temperature for LCP [107].

A temperature profile for successful LCP bond processing from Rogers Corporation is shown in Figure 2.16. After several tests and experimental runs, these parameters have been widely used in commercial applications especially in RF-MEMS.

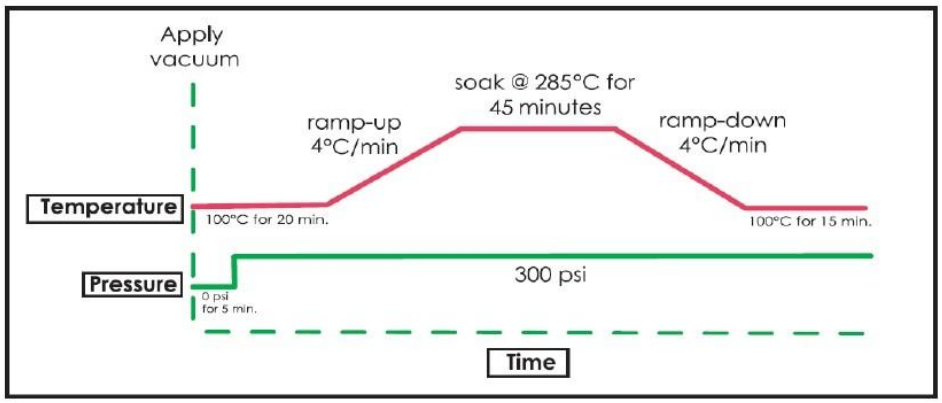

Figure 2.16: A typical LCP bonding process from Rogers Corporation [108].

Liquid crystal polymer as a thermoplastic material has been largely used in electronic packages because of its distinct structural and excellent moisture and oxygen barrier properties. In 2002, Wang et al. [109] described a technique of lamination based bonding of LCP to various materials including glass, copper, gold and silicon surface. In order to achieve successful bonding, a reactive ion etching recipe for LCP using oxygen plasma was developed. From this study, the maximum bonding strength of 29.94 psi (206.4 kPa) was achieved, measured by blister test. The schematic diagram of the blister test for LCP to glass bonding is shown in Figure 2.17.

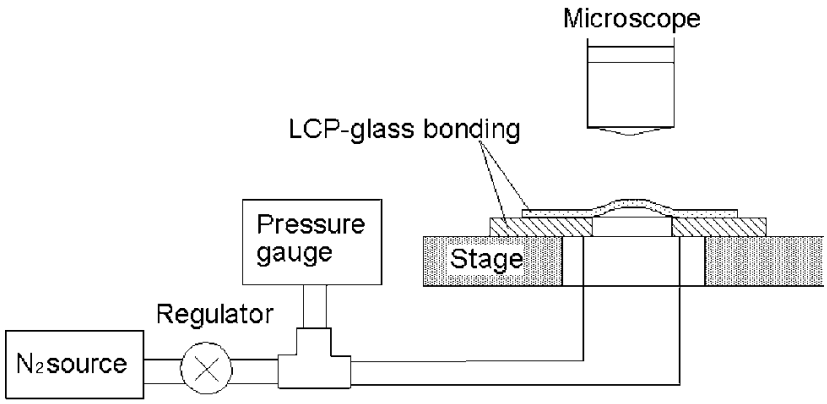

Figure 2.17: A schematic of the bonding strength test at the interface between LCP and glass using blister method [109].

LCP as a structural material offers greater sensitivity than many other materials due to its much lower Young's modulus. Therefore, LCP membrane-based flow sensors have been investigated by Kottapalli et al [110, 111]. They described two methods of bonding LCP film to Si substrates. In the first method, the bottom Si substrate and the top LCP film were coated with a thin layer SU-8 and then placed on a hotplate, enhancing bond strength between the two substrates. However, the wafer-pair buckled after bonding. This occurred due to the CTE mismatch between the silicon (3.2 ppm/^{o}C)

and LCP (18 ppm/^{o}C) resulting in the silicon wafer breaking into pieces during the dicing process. Therefore, the subsequent silicon and LCP bonding using an intermediate SU-8 layer was carried out at a lower temperature. Before bonding, the silicon substrate and LCP film were prepared carefully and the wafer-pair was bonded at the low temperature and for a longer time to prevent the heat generated stress and trapped air bubbles at the interface. The wafer-pair was heated at 40 ℃ for 20 minutes then increased to 80 ℃ for 10 minutes followed by 120 ℃ for 20 minutes. It was found the bond strength between the silicon wafer and LCP film was enhanced. The main fabrication process steps are shown in Figure 2.18.

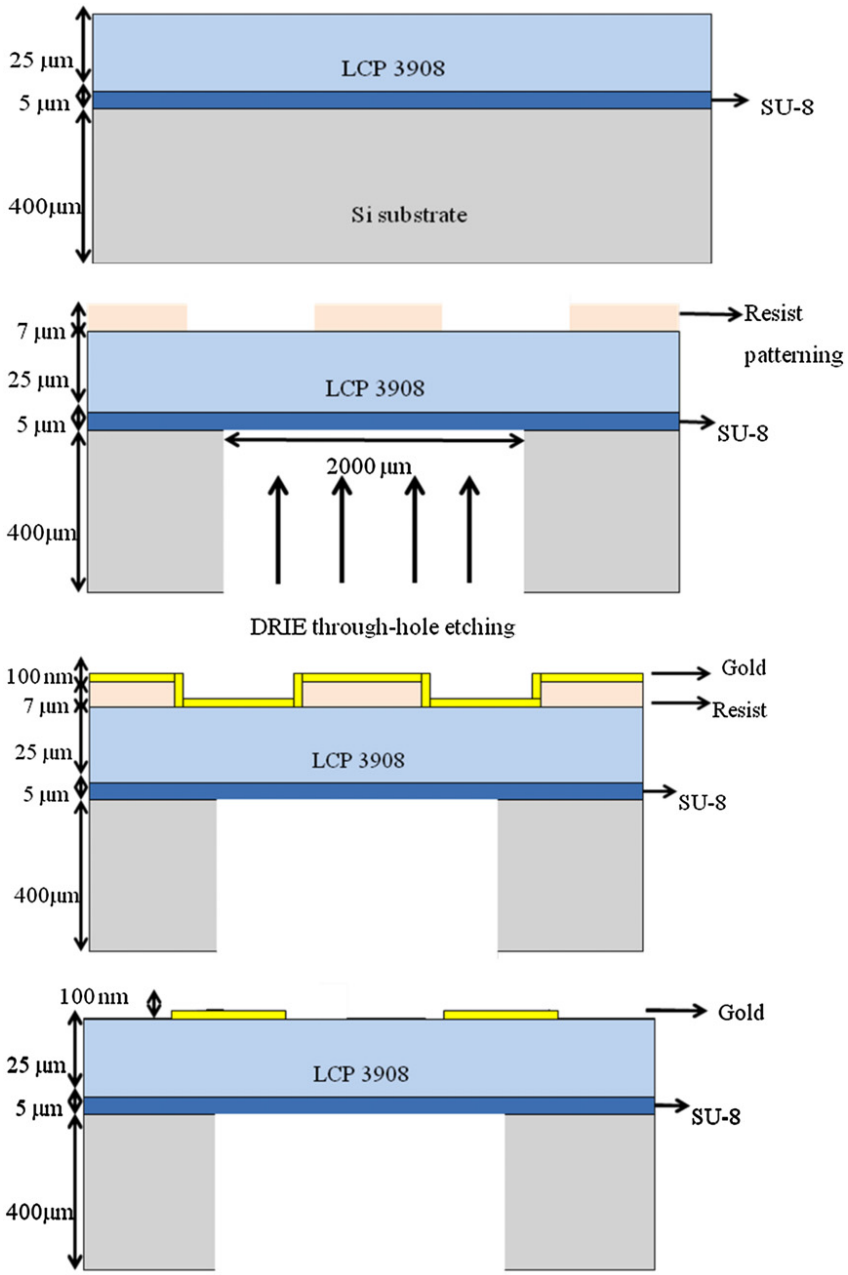

Figure 2.18: The fabrication processing steps for flow sensor: (a) LCP to silicon bonding with intermediate SU-8 layer, (b) resist patterning and DRIE through-hole etching, (c) 100 nm gold sputter deposition, and (d) gold separation [110].

In addition, LCP as a near-hermetic material has been applied in packaging of MEMS for microwave applications achieving excellent bonding strength and near hermetic sealing [111 - 116]. For lamination of LCP as the bonding layer, most of the methods in RF-MEMS applications are based on the traditional hot plate configuration as shown in Figure 2.19 [116]. In the lamination process, the two heating plates were placed above and below the bonding area then the pressure of the press was increased up to 300 PSI. A vacuum plate with a size of 6 inches by 6 inches was located above the bottom heating plate. Another plate, also measuring the same size, is located below the top heating plate with a drilled cavity in the middle and air pressure capability. The MEMS package was then inserted into the vacuum plates for processing based on the recommended lamination temperature and pressure profile which have been shown in Figure 2.16. After several hours, an excellent bond at the interface of the package is achieved. Although the lamination press method can provide good bonding strength of the LCP package, it takes nearly half a day to achieve the final bonding including material preparation and pre-heating of the heating plate.

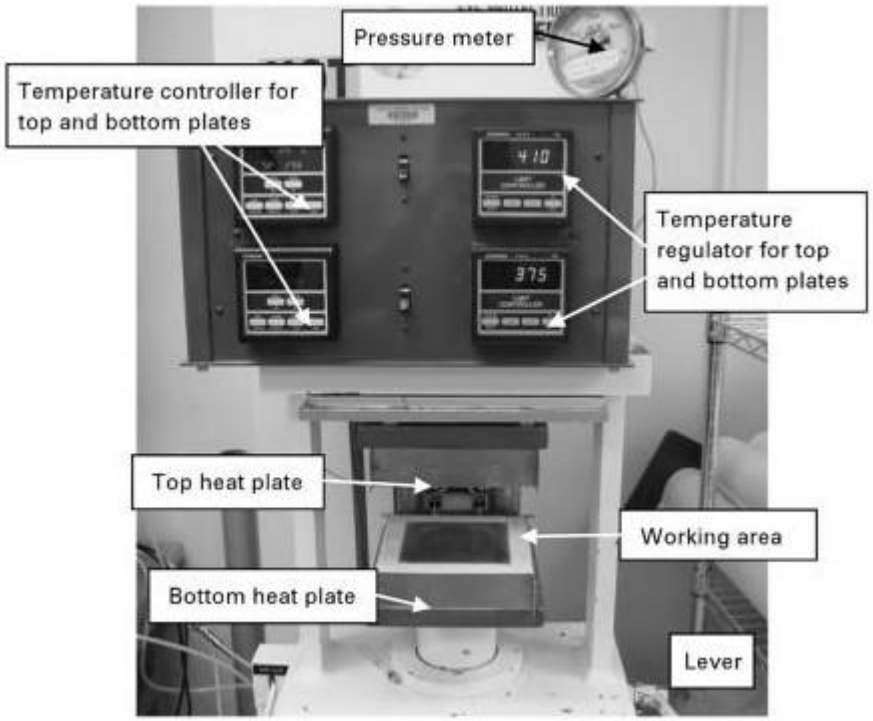

Figure 2.19: A developed press for LCP lamination [116].

An improved study by Aihara et el. [112-113] demonstrated bonding of a molded high temperature LCP lid to a RF-MEMS package using a low temperature LCP film.

During this process, a metal tube was used to heat and press the edge of the lid to melt the LCP bonding film to create a seal between the lid and the substrate, at roughly 280℃ for 1 hour. The melting temperatures of the high temperature LCP lid, the low temperature LCP and the RF-substrate were 355 ℃, 280 ℃ and 315 ℃ respectively. The setup of the LCP lid lamination onto the package is shown in Figure 2.20.

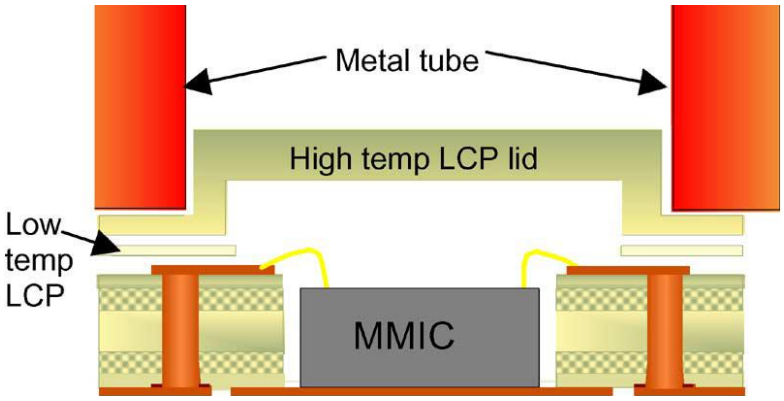

Figure 2.20: Cross section of an assembled package mounted on a PC board using a metal tube [112,113].

2.3 Laser Welding Methods

2.3.1 Laser Transmission Welding of Thermoplastics

The first activities related to laser welding of thermoplastics polymers were carried out in the early 1970's [117]. A 100μm thick polyethylene film in an overlap joint was welded using a CO_2 laser. However, the perception for laser welding of thermoplastics only began to occur in the mid 1990's when stable diode lasers were developed in the wavelength range of 800 to 1100nm and with up to 200 W of output power, more than enough for the typical power requirements of 10 W to 50 W. A typical diode laser is integrated with a mirror based beam scanning system or a flexible production system with the laser beam delivered directly from the output of the laser source or through a fiber optic cable. Nowdays, there are a great number of diode laser system providers on the market supplying equipment mainly for thermoplastic welding. Also other types of lasers such as Nd-YAG lasers, disc-lasers and fiber lasers are being employed in the manufacturing industry. One of the main challenges of laser welding of thermoplastic polymers is the control of the laser power absorption at the joining interface. Most polymers are usually transparent or translucent in the visible and near infrared wavelength range as shown in Figure 2.21 [118].

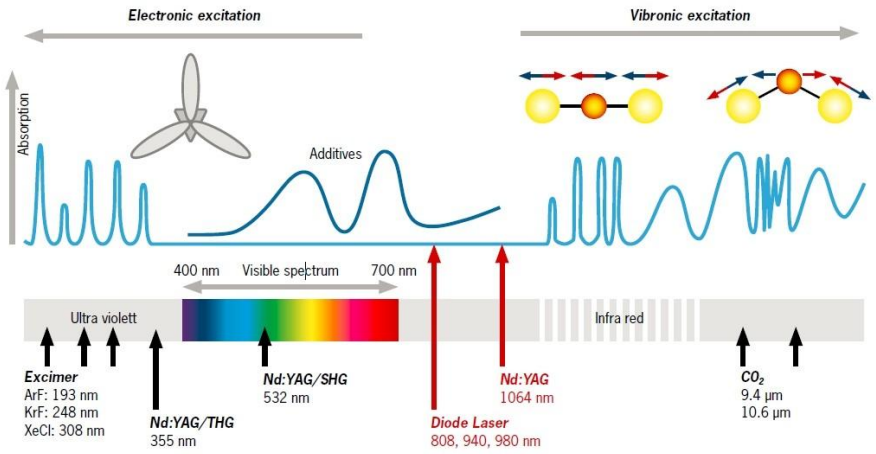

Figure 2.21: The wavelengths of various laser types [118].

An important localised welding approach is based on the laser heating effect since laser based systems have become primary tools for metal processing and have been growing in prevalence in processing thermoplastic materials including marking, cutting and drilling [119]. The emitted laser light which has highly precise geometry, control and consistency allows for its use in high precision and microfluidics applications. Over the past decade, laser bonding has become important as a supplementary joining process for thermoplastics and has been widely used in many industrial application fields [119]. Because the traditional approaches have reached their limits, laser transmission welding offers attractive advantages in microfluidic applications including its cost-effectiveness, controllable local transfer of energy and low mechanical pressure applied on the materials.

The basic principle of laser transmission welding is that one of the joining polymers must be optically transparent at the wavelength of the laser radiation, while another joining polymer absorbs the laser radiation. Before bonding, the two polymer plates are pressed together with a mechanical pressure to ensure close contact at the interface to achieve a strong bond. In the bonding process, the laser beam passes through the transparent polymer and is absorbed by the absorbing polymer. The resulting heat softens both layers at the interface, then one or both molten polymer surfaces are bonded together at the interface. The principle of laser transmission welding of thermoplastics is shown in Figure 2.22.

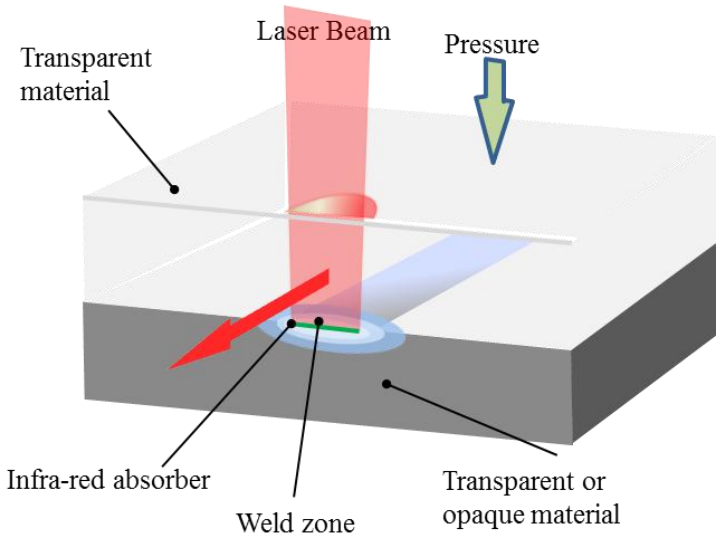

Figure 2.22: The principle of laser beam welding thermoplastics.

Since most polymers are transparent to the laser wavelengths used, thus additives are usually added to change the property of the material to ensure the material absorbs the laser beam. Several colorants are also available that allow the color of the transparent material to match the color of the absorbing material. The degree of complexity of laser joining coloured plastics is shown in Figure 2.23.

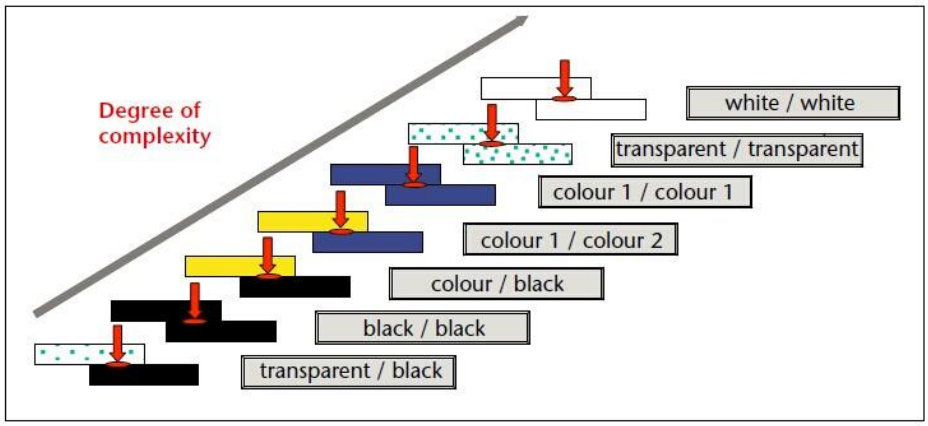

Figure 2.23: The degree of complexity of laser welding thermoplastics [120].

When the laser beam passes through the surface of a transparent part, a small portion of the incident light is reflected and the remaining laser beam goes through the material. The transmitted laser light is then absorbed by the non-transparent substrate. From the Beer's law, the light absorption within a solid can be described by [121]:

$$I(z) = I_0 e^{-\alpha z} \tag{2.1}$$

where $I(z)$ is the optical intensity as a function of material depth; I_o is the optical intensity at z =0; α is the absorption coefficient; and z is the material depth from the surface.

The near-infrared spectrum of the laser energy is absorbed in a thermoplastic material causing vibration of electronic bonds [122]. This vibration leads to localised heating of the material. Based on the law of heat transfer, this heat is conducted from the absorbent part to transparent material at the interface. If the resultant temperature is above the melting point of the material, the surface of the thermoplastic material changes to a liquid state allowing a joint to be produced through the welding effect. Assuming there is no displacement between the two materials, local heating of the material also enhances the interfacial pressure because of thermal expansion.

In the contour welding method the relative motion between the laser beam and the thermoplastic materials is in a direction perpendicular to the laser beam [122]. Either the thermoplastic part or the laser beam is moved, while the other part is kept stable. For example, a step motor based control system can be used to move the thermoplastic materials, or a laser scanner can be used to move the laser beam. The contour welding technique also has many advantages including simplicity, easy controllability, flexibility and cost efficiency. Different laser welding routes can be made by simply changing the program of the control system or the scanner. However, the disadvantage of this approach is that the welding speed is slow for many large-scale industrial production applications.

The main parameters of laser transmission welding that influence the bonding results are laser power, bonding time, absorption properties of the material at the interface, scan speed and the pressure [123]. Usually laser welding is a high speed process and the joint can be generated instantaneously to achieve strong bonding strength at the interface. With laser transmission welding, it provides smaller heat affected zone (HAZ) than other techniques [124]. The HAZ in polymer welding is the area near to the joint where the material is affected by thermal conduction of the laser generated heat. The HAZ is an effect in all of the welding methods [124, 125]. A method of localised sealing of microfluidic chips was successfully reported based on an infrared laser [126]. In this approach, two thermoplastic substrates were assembled together in which the IR-transparent thermoplastic layer was placed on the top of the opaque one. A laser

beam at the wavelength of 1100nm was incident through the transparent substrate and absorbed by the interface of the opaque layer producing a strong bond. A study of PEEK to PEEK welding based on a quasi-simultaneous laser transmission welding method has been also been presented [127]. In order to absorb the laser beam, one of the two PEEK substrates was pigmented with various concentrations of carbon black and it was placed as the bottom layer. The moving speed of motion control system was from 0.1 to 10 m/s with the corresponding laser intensity ranging from 3 to 13 W/cm^2. After several trials, it was found that the weld strength was improved with the increasing laser intensity at slow moving speed. Compared with 3 W/cm^2 laser intensity and 10 m/s of scanning speed with 13 W/cm^2 of laser intensity and 0.1 m/s of scanning speed, an increase in bonding strength by 33% was achieved. A method of laser transmission welding of PMMA material was investigated [128]. The influences of the process parameters on the weld strength and weld seam width were studied. In this method, carbon black (0.2 wt%) in a PMMA substrate was used as an absorbed layer. From the results, a bonding strength of up to 50 MPa was achieved. The bonding strength and welding width increased as the laser power was increased, but the bonding strength and welding width decreased as the scanning speed decreased. For instance, the bonding strength was 35 MPa for the laser power of 19 W and scanning speed of 420 mm/min, but at 25 W of laser power and 300 mm/min of scanning speed, the strength was increased to 56.35 MPa. A study of FEP (fluorinated ethylene propylene) polymer bonding to Ti foil based on a laser joining technique has been reported [129]. Auger electron spectroscopy and scanning electron microscopy coupled with energy dispersive spectroscopy were applied to analyse both the heat affected zone and the actual bond area of the laser welding method. Because titanium and titanium alloys have several advantages such as optimum strength-weight ratio, high corrosion resistance and a good biocompatibility, this material is often used for specific applications in the chemical industry, aerospace engineering and medical device manufacturing. According to the results from these experiments, it was shown that there was presence of Ti to FEP chemical bond formation existing only in the actual bond area and no chemical bond formation was found in the heat affected zone (Figure 2.24).

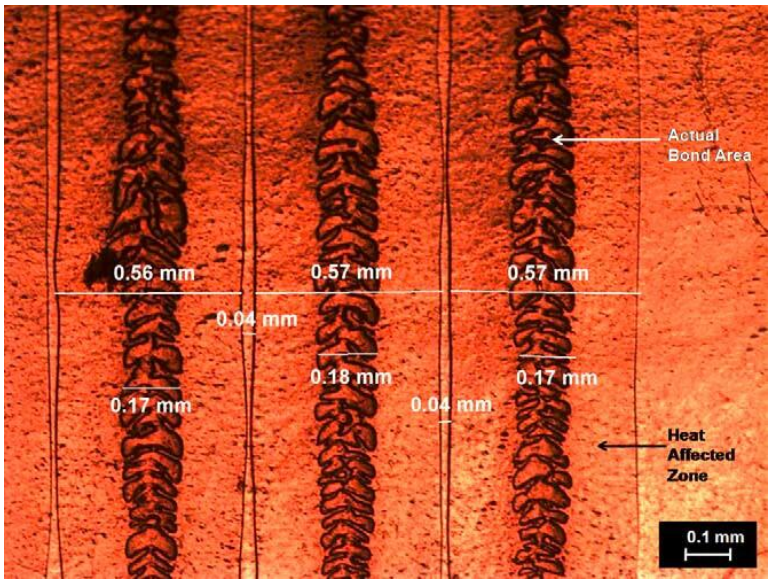

Figure 2.24: The micrograph of FEP to Ti bonding with parallel joint lines based on laser welding techniques [129].

Laser transmission welding methods have been developed for sealing of microfluidic devices due to the advantages of the localised heating effect and therefore minimizing the heat affected zone, fast processing time and good bond strength [126]. This method is a one step process in which heating and welding of the polymer substrates occur concurrently. In this process usually one polymer substrate has high transmittance at the laser wavelength and another one has high absorptance. The latter absorbs the laser radiation to produce the necessary temperature increase at the interface to cause one or both substrates to melt to produce a resultant bond between the substrates. While this configuration is convenient and does not require additional material for laser welding, it requires a suitable combination of dissimilar materials. Secondly it is not suitable for fabrication of transparent microfuidic devices since an opaque substrate is necessary to absorb the laser radiation to realize welding of the substrates. On the other hand, transparent microfluidic devices are desirable in many applications that require measurement of optical transmission for medical testing and diagnostics. In the previous work a thin film of carbon layer was used as an intermediate absorbing layer in laser welding of polymer substrates for microfluidic applications [130-132]. The layer of carbon black was deposited on a microfluidic substrate by spin-coating [130, 131] or by vacuum deposition [132] prior to fabrication of the microchannels on the polymer substrate, then a cover substrate was attached to the microfluidic substrate by the laser welding method [130-131]. Figure 2.25 shows a laser bonded channel structure, the channel width was 100 μm [130].

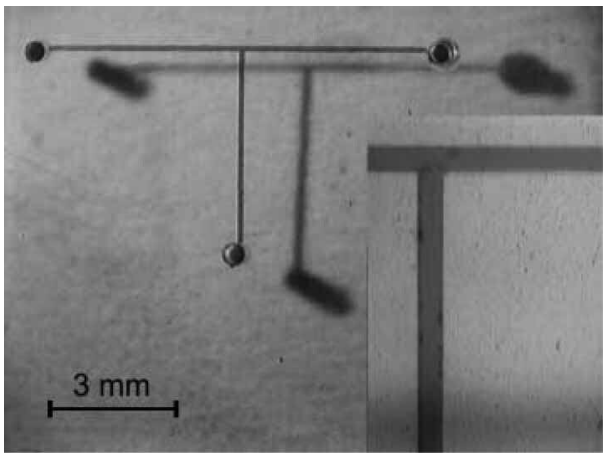

Figure 2.25: Successful COC microfluidic bonding with 100 μm width microchannels based on laser bonding method [130].

2.3.2 Laser Bonding of MEMS Devices

Laser bonding for packaging in microsystems applications has been studied for over a decade [55, 78, 133-149]. There are several advantages of laser bonding for MEMS encapsulation as compared to the other bonding methods [135, 138, 144, 145, 147]. Firstly, the laser bonding method is precise with controlled placement of the laser beam spot. Secondly, the temperature at the device position could be much lower than at the bonding site. Thirdly, the MEMS devices are not exposed to the total heat since the laser joining approach is a non-contact process which means the method can have less effect on the inner MEMS sensors. Lastly, this technique is suitable for chip to chip and chip to wafer MEMS packaging.

In comparison with the traditional bonding methods, the thermal distribution on the devices can be smaller than in the conventional techniques. As mentioned before, a wide range of wavelength is from infrared (CO_2 laser, Nd: YAG) to the ultraviolet (Excimer lasers etc) and the best wavelength can be selected to meet the bonding requirements. For localised laser bonding, there are usually two main methods which are direct bonding and intermediate layer bonding approach.

In the direct bonding process, a number of studies have been made in glass to silicon bonding using Nd: YAG lasers (1064 nm) [136-138, 147-149]. The bonding process is based on the laser transmission welding methods that needs one substrate with strong transmissivity and another substrate to have high absorptivity at the wavelength of the laser beam. In this method, a highly transparent glass, Pyrex, with 1 mm of thickness was used. The 1064 nm wavelength laser passes through the top glass substrate and is

absorbed by the silicon substrate. The mechanism is fusion bonding using the localised heating effect. To achieve strong bonds, a suitable pressure was applied on to substrates during the bonding process. A schematic diagram of the laser transmission bonding of glass to silicon is shown in Figure 2.26.

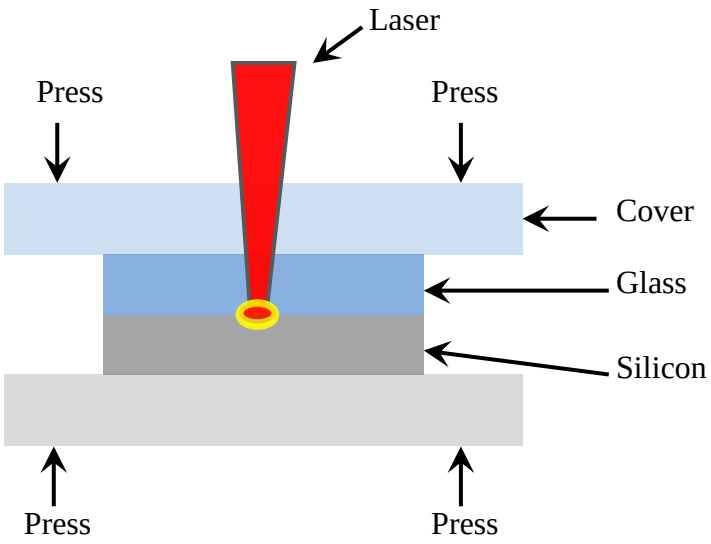

Figure 2.26: Schematic of the laser welding glass to silicon.

There is also a number of studies of laser eutectic bonding of silicon to glass [55, 140, 141, 144]. In this approach an eutectic solder was used as the absorber to be heated by laser beam rather than the silicon substrate. A nanosecond pulsed Nd: YAG laser with a wavelength of 355 nm was used to bond silicon to glass using an intermediate indium layer [140]. Once the laser power was applied, the temperature at the interface of indium/silicon was up to 2500 ℃ and rapidly dropped to 760 ℃ in 1 μs and 43 ℃ in 1 ms respectively. In order to carry out selected laser bonding, a mask was used as shown in Figure 2.27.

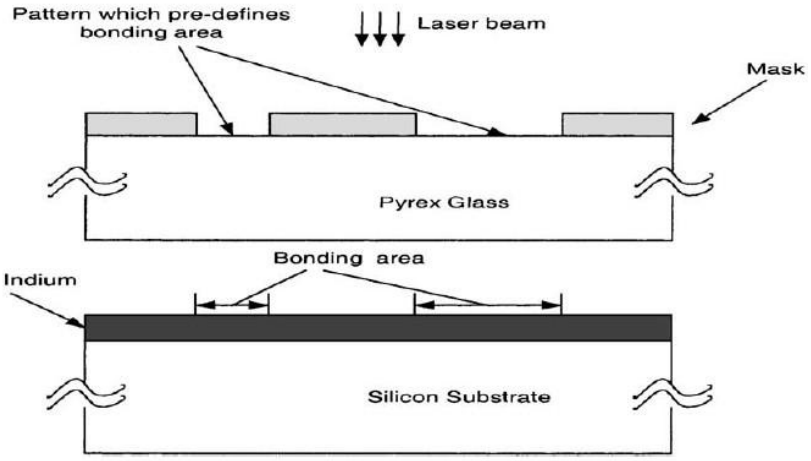

Figure 2.27: The experimental schematic of glass to silicon bonding using an intermediate indium layer [140].

After bonding strength test, the bond strength was found to be up to 2.6 MPa. After forcefully breaking the bonded samples, the interface between the glass substrate and silicon substrate can be clearly observed as shown in Figure 2.28.

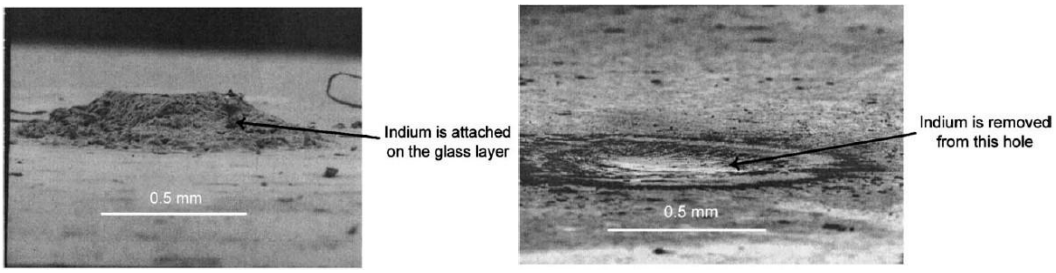

(a) (b)

Figure 2.28: (a) A cross-sectional view of the glass surface after broken test. (b) A cross-sectional view of the silicon surface after broken test [140].

In addition, a 355 nm ns-pulsed Nd: YAG laser was used to bond silicon and glass using a gold-tin eutectic alloy [55, 144]. In this method, high quality bonds were achieved without defects and the bonding strength was as high as 15 MPa. Another study of laser bonding of glass to silicon using aluminum or gold demonstrated bonding strength of 40 MPa [141]. In this work, the laser source is a Nd:YAG laser at 1064 nm. In order to obtain reliable bonding, the bonding parameters such as laser power and the speed in contour based bonding, have to be controlled precisely during the joining process.

Although the laser direct and eutectic silicon to glass bonding techniques have been studied for a few years, it is still under development for industrial applications. Several package bonding technologies based on CO_2 lasers have been demonstrated in actual manufacturing applications [133, 142, 143, 145, 146]. Off-the-shelf ceramic quad flat-packs (CQFP) are usually used in packaging of RF-MEMS and an intermediate solder preform (Au-Sn) used to bond the substrate and a Kovar^{TM} lid in the oven based process. However, this heating method is not desirable for RF-MEMS [146]. A localised laser based packaging method has been applied, instead of using a Kovar^{TM} lid, a metallised silicon lid was used. The silicon lid was bonded using a CO_2 laser to heat the edge of the lid as shown in Figure 2.29 to reflow an Au-Sn based sealing ring. The results of mechanical pull test showed tensile strength of 275 MPa. The results of hermeticity testing showed that this bonding technique is capable of hermetic packaging meeting the *MIL-STD-883E* standard.

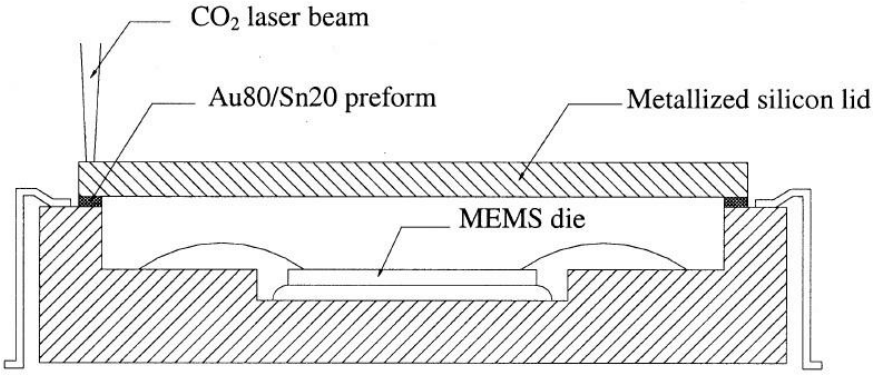

Figure 2.29: Schematic of CO2 laser sealing silicon lid to MEMS devices in off-the-shelf ceramic quad flat-packs (CQFP) [146].

Wafer-level bonding of silicon to silicon using lead-tin solder for vacuum packaging has also been demonstrated [142, 145]. A CW CO_2 laser was used as the heat source for localised bonding, the laser beam was incident on the silicon substrate in a vacuum environment at a pressure of 10^{-3} Torr. Although the bonding temperature was up to 183 ℃ during bonding process, the temperature at the center of the device was only 100 ℃ meaning less thermal impact on the inner parts. After pull tests of 12 bonded samples, it was found the bonding strength was in excess of 2-4 MPa. Also from the results of hermeticity testing, it was shown that the helium leak detection met the requirements of MIL-STD-883E and the gross leak tests achieved more than 1×10^{-4} atm cc/s. In order to achieve high bonding strength and prevent oxidation, several thin metal layers were deposited on the silicon surface as shown in Figure 2.30.

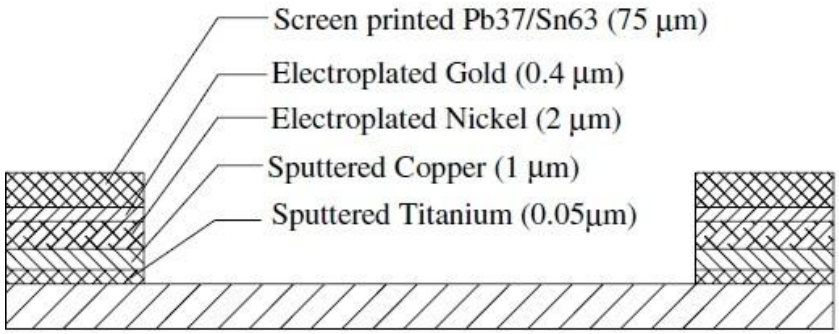

Figure 2.30: Thin metal layers were deposited on silicon using solder screen printing method [142].

Laser bonding using an intermediate glass frit layer has also been investigated for MEMS applications [78, 135, 150-152]. Laser based glass frit packaging of leadless chip carrier (LCC) packages in both air and vacuum have been successfully demonstrated [150, 151]. A fibre-delivered high-power CW diode laser from Laserline emitting at a wavelength of 940 nm with an optical output power of 200 W was used. A schematic sketch of the laser setup is shown in Figure 2.31. During these processes the

maximum laser bonding temperature was 375 ℃, but at the center of the package, the temperature was approximately 140 ℃ which is much lower than the bonding temperature. Similarly, an inner temperature of 220 ℃ was much lower than the bonding temperature of 440 ℃ in vacuum packaging. The shear strength was up to 880 N and hermetic bonding was also achieved.

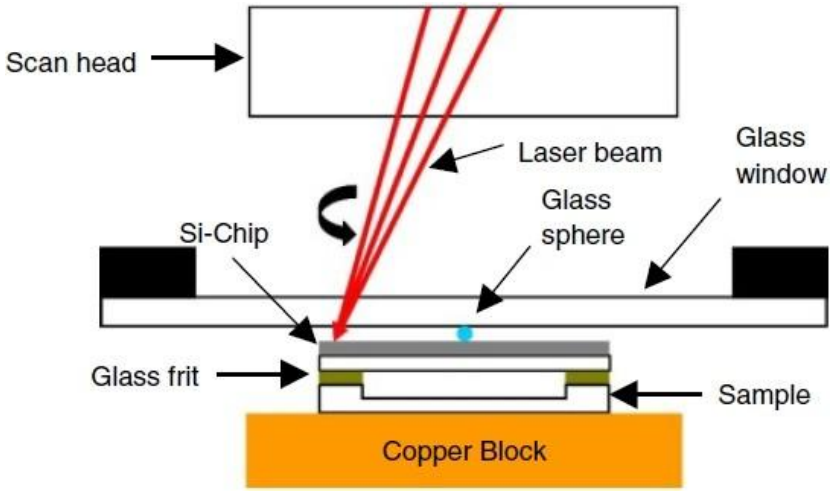

Figure 2.31: Schematic of laser bonding setup using glass frit layer [150].

Polymers have been widely used in laser bonding for MEMS packaging, in particular BCB which has been discussed before in the adhesive layer based bonding methods. For MEMS applications, BCB is a widely used polymer as the intermediate layer [153-158]. In laser bonding of microsystems with the BCB polymer, a DILAS-Rofin Sinar diode laser at wavelength of 810 nm was used [153]. The surface of the temperature of the load glass substrate was monitored using an IR pyrometer. The shear tests showed bonding strength of 20 kgf (nearly 200 N). The hermeticity test showed a leak rate of 1 x 10^{-10} $mbar\ l\ s^{-1}$.

2.4 Conclusions

In this chapter, several bonding methods for packaging of thermoplastic material based microfluidic devices have been described. Then the comparisons with the traditional materials such as silicon, glass, metals and ceramics in microfluidic systems are also discussed. The two main techniques for microfluidic bonding are indirect and direct bonding. Therefore, the main bonding techniques include adhesive bonding, thermal fusion bonding, solvent bonding, and localised bonding. Then some traditional approaches of MEMS packaging have been covered which are anodic bonding, eutectic bonding, glass frit bonding and adhesive polymer layer bonding. The methods of laser

bonding have been described including laser bonding methods and materials. Also the bonding methods based on laser technology for microfluidic systems and MEMS have been described and discussed.

Chapter 3 Laser Microwelding of PMMA Substrates for Assembly of Microfluidic Devices

In this chapter, the development of a diode laser based microwelding method for assembly and packaging of polymer based microfluidic devices is presented. In the bonding process, a diode laser was used to bond two PMMA substrates together at the interface using a thin film metal spot based intermediate layer design as a localised absorber. A broad laser beam with a top-hat profile was used to carry out all of the laser microwelding work in this study. The effects of laser power and processing time on the resultant heat affected zone and the melted zone were investigated. For large area welding, a 2x2 array of thin film metal spots were used to investigate the effect of separation between the spots on the resultant interfacial bond between the two polymer substrates. For comparison, a larger area titanium film with a comparable size to that of 2 x 2 array was also studied. The results of tensile measurements show that a strong bond between the substrates can be obtained. Finally, a microchannel was successfully produced using the laser microwelding method. A colour liquid based leak test showed leak-free operation of the microchannel.

3.1 PMMA Materials

Normal polymethacrylates are polymers of the esters of methacrylic acids and the most widely used material among them is poly (methyl methacrylate) (PMMA). The PMMA polymer is generated by free-radical polymerisation of methyl-methacrylate in mass or suspension polymerization according to the process shown in Figure 3.1 [159]. It is not specially a type of glass, but sometimes it is called acrylic glass.

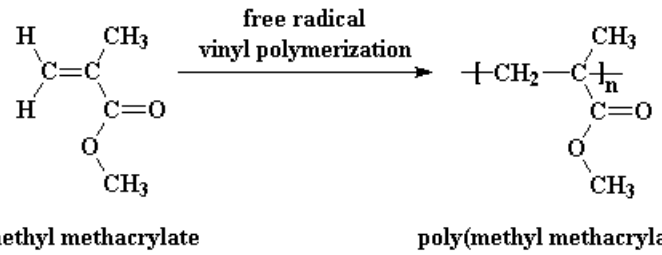

Figure 3.1: PMMA is made from the monomer methyl methacrylate by free radical vinyl polymerization [1].

Polymethyl-methacrylate (PMMA) was used as the polymer material for fabrication and

laser bonding of microfluidic devices. A wide range of PMMA materials with different glass transition temperatures are commercially available allowing material choice depending on application requirements and processing constraints. In this study, the PMMA material is from RS Components with a thickness of 2 mm for bonding devices and the 0.5 mm thick version for mask fabrication, respectively. According to the supplier [160], nearly 92% of light can be transmitted through the material and the PMMA material also has excellent long term weather resistance with no discoloration. Since taking into account moisture effects, the maximum operating temperature is at least 30-40°C below the $\boldsymbol{T_g}$ of the material. The typical properties of the PMMA material are shown in Table 3.1. The roughness of PMMA surface was measured on a white light interferometer (Zygo) and is shown in Figure 3.2.

Table 3.1: Types properties of PMMA [160].

Property	Value	Units
Density	1.18	g/cm^3
Tensile strength	60	MPa
Impact strength	18	kJ/m^2
Thermal conductivity	0.19-0.21	W/m ·K
Glass transmission temperature	132	°C
Max operating temp long term	80	°C

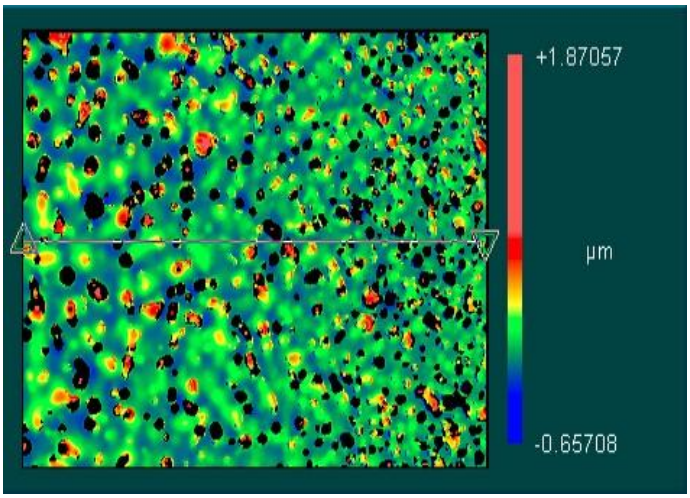

Figure 3.2: The roughness of PMMA surface in our study.

The PMMA polymer is an important substrate material which has been studied in the area of microfluidic applications. This polymer has significant advantages as the structural material for microfluidic devices, including low cost, easy fabrication and

good physical and chemical properties. Besides due to the low melting temperature of PMMA substrates, the device bonding can be made at low temperature.

3.2 CO_2 Laser Micromachining for Substrate Fabrication

Microfabrication is an increasing application of lasers based on the micromachining processes. The laser based cutting method has several advantages over the other approaches including flexibility, scope of automation, ease of control in depth of cut, cleanliness, non-contact processing, speed, negligible heat affected zone, and narrow kerf [161]. A schematic of the laser assisted cutting setup is shown in Figure 3.3 [162]. The material is placed on a stage, and the laser beam is applied to irradiate the material surface at different power and speed so as to generate controlled removal of material from the surface. The main parameters in the laser assisted cutting method are power or intensity, interaction time and covering environment [163].

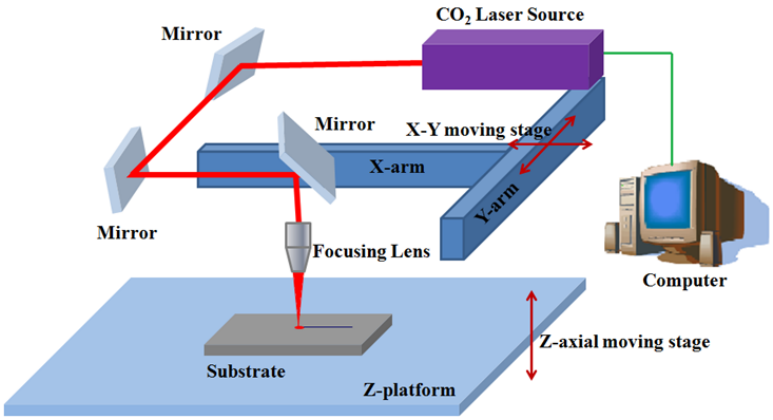

Figure 3.3: Schematic of the laser assisted cutting setup [162].

In this work, a CO_2 laser (Epilog Mini 18) at 10.6 μm of wavelength with a 18" x 12" engraving area is used. The maximum output of this laser is up to 40 W. The spot size of this laser can be varied from 0.003" to 0.005" (or 76.2 μm to 127μm). The substrate pattern is created using computer software in either AutoCAD or CorelDraw. The quality of the cutting zone is controlled by the laser parameters such as laser power density, position of the laser beam with respect to the surface and x-y stage speed. It has been shown that the relationship of laser power (P, W), material thickness (d, mm), cut width (s, mm) and cut speed (V, mm/s) can be given by:

$$P = 390 \cdot d^{0.21} \cdot s^{0.01} \cdot V^{0.16} \quad (3.1)$$

while ignoring variation of thermal properties of cutting material with temperature [163]. A photograph of the Epilog Mini18 CO_2 laser system is shown in Figure 3.4.

Figure 3.4: A photograph of Epilog Mini18 laser system.

3.3 PMMA Mask and Substrate Design

In order to study the effect of spot separation in the laser welding experiments, several circle spot patterns and square spot patterns were designed using CorelDRAW Graphics suite X5 (COREL). Then the 0.5 mm thick PMMA sheet is cut into plates of 55 mm x 50 mm on the CO_2 laser system. Figure 3.5 displays the different patterns used for the study. These masks have alignment marks for making precise alignment in the subsequent process for thin metal film deposition.

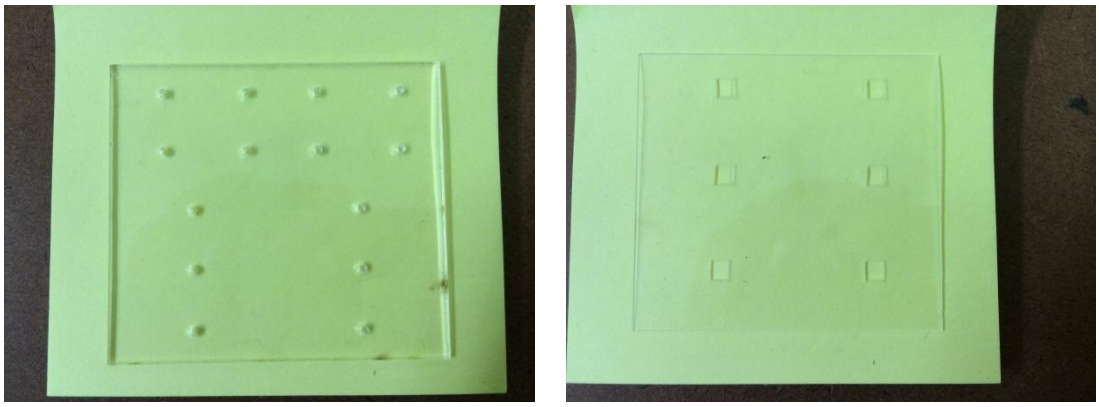

(a) (b)

Figure 3.5: Samples of PMMA mask, (a) circle pattern and (b) square pattern.

3.3.1 PMMA Substrate Fabrication

Figure 3.6 shows a schematic illustration of the deposition process for producing thin titanium film patterns on PMMA substrates using a shadow mask based approach.

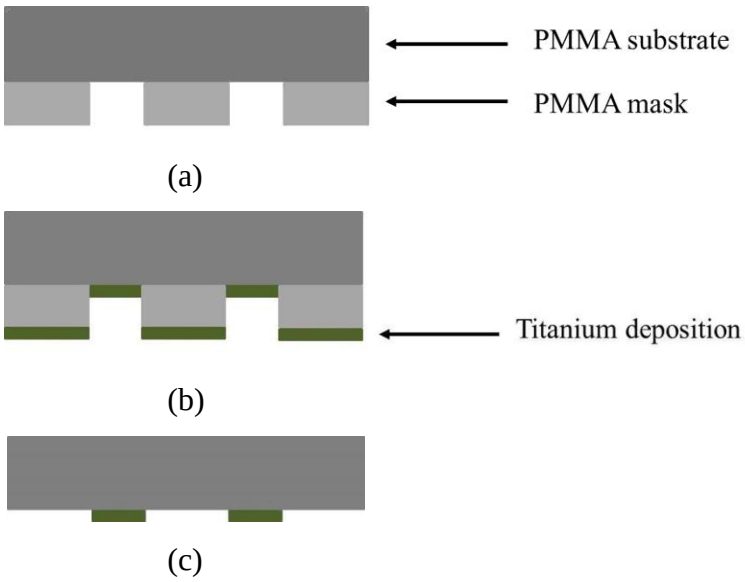

Figure 3.6: Illustration of the steps for titanium film deposition on a PMMA substrate using a shadow mask based vacuum deposition method. (a) A PMMA shadow mask on a substrate, (b) Titanium film deposition and (c) Titanium film spot pattern on substrate after removing the shadow mask.

The titanium deposition work was carried out using an electron beam based vacuum evaporation system and a PMMA based shadow mask with 1 mm diameter apertures. The mask was fabricated using a CO_2 laser based polymer machining system (Epilog Mini 18). The thickness of the PMMA plate for mask fabrication is 0.5 mm. Aperture arrays with separations of 0.6, 0.8, 1.0 and 1.2 mm were fabricated to determine the optimum value for continuous joining between the substrates using discrete titanium film patterns.

3.3.2 Preparation of PMMA Mask and PMMA Substrate

In order to mount the PMMA mask and PMMA substrate for E-Beam deposition of titanium film, 3-inch soda lime glass wafers were used as the carriers. All of the processes were carried out in the cleanroom.

Figure 3.7: The glass container was placed in an ultrasonic bath.

After CO_2 laser cutting, the PMMA masks and substrates as well as the glass wafer carriers were cleaned. The cleaning process was to ensure all of the materials were free of dust particles and contamination. Then the PMMA masks and substrates, and the glass wafers were placed on a wafer holder and washed using deionised water. After that, the wafer holder with the PMMA substrates and glass wafers was inserted into a glass container filled with a biodegradable decontamination liquid (Decon 90) mixed with deionized water. The concentration of Decon 90 was between 2% and 5% which was found to be sufficient for the work. Subsequently, the glass container was placed in an ultrasonic bath as shown in Figure 3.7.

Through this cleaning process, the micro-particles and contaminants are removed from the surface of the PMMA substrates and glass wafers. After 50 minutes in the ultrasonic bath, the substrates and glass wafers were rinsed using running deionized water and then inserted into another glass container with deionized water. The glass container was placed in the ultrasonic bath again for rinsing for 50 minutes. The aim of this cleaning process is to remove the residues of the Decon 90 from the surface of substrates and wafers. This process is also critical since the residues of contamination or grease from the Decon 90 solution would influence quality of the thin titanium film spots after the film deposition process.

After cleaning and preparation, the PMMA substrates and glass wafers were dried by pure nitrogen using an air-gun to remove the water from the surface of the substrates and wafers. Then the samples were placed into an oven for drying for approximately 60

minutes. Since the PMMA material and glass wafer have different heat distortion temperatures, the oven was operated at 70°C for the PMMA substrates and masks and 120°C for the glass wafer respectively. A photograph of the oven that was used is shown in Figure 3.8.

Figure 3.8: A photograph of oven for drying materials.

3.3.3 Deposition of A Titanium Layer on PMMA Substrate

As discussed in section 3.3.1, the PMMA mask and PMMA substrate are mounted on a glass wafer using a high temperature tape. Then the glass carriers with the PMMA substrates and the covering masks were plated into the E-Beam deposition chamber. In the deposition process, the titanium layer was deposited in the high vacuum chamber by electron beam evaporation as shown in Figure 3.9. Six glass wafers each carrying the PMMA masks and substrates were placed in the wafer holders of the electron beam evaporation chamber. The distance between the wafer holder and titanium source in a crucible was roughly 100 mm. A schematic of the electron beam evaporation principal is shown in Figure 3.10 [164].

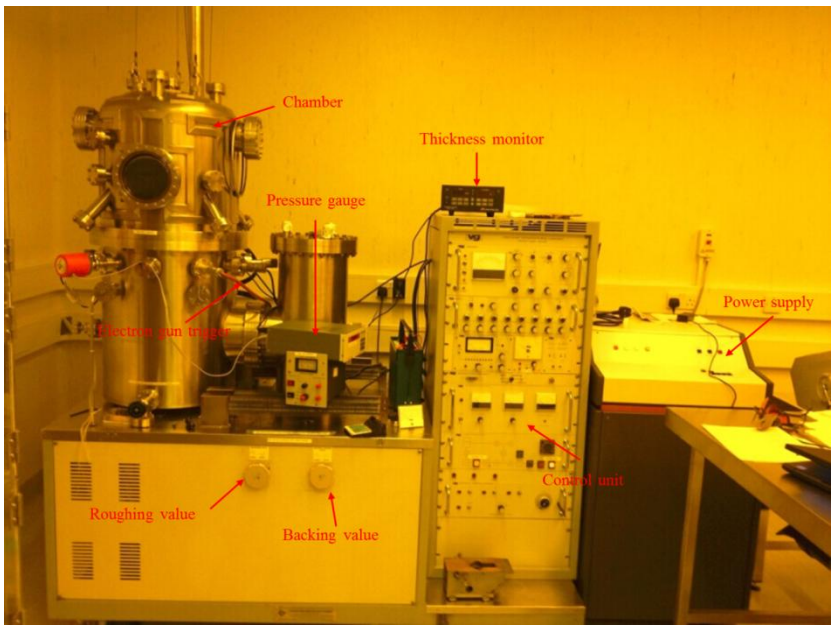

Figure 3.9: A photograph of electron beam evaporation.

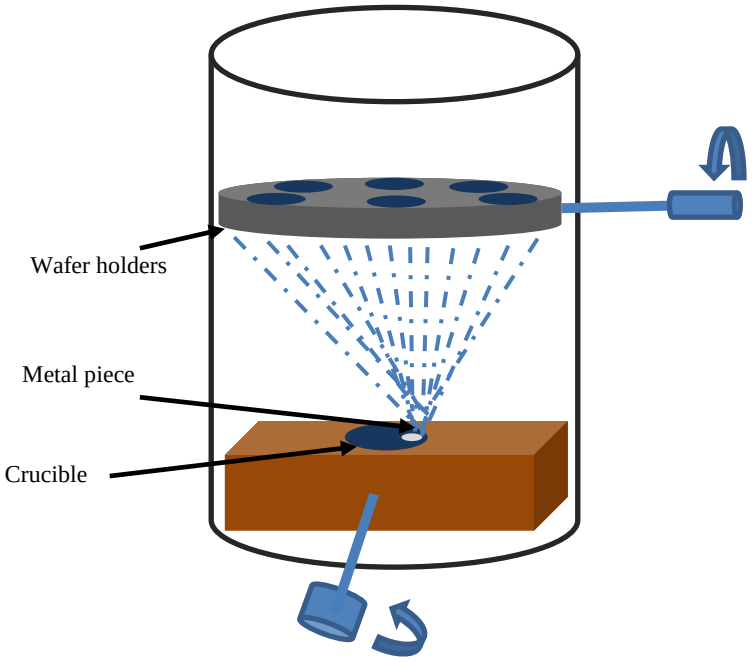

Figure 3.10: Schematic of electron beam evaporation chamber [164].

Before deposition, the pressure in the vacuum chamber must be low to prevent the titanium target from oxidizing when the titanium is heated to the melting point. Furthermore, in order to ensure that the metal vapour reaches the substrates with minimal collisions with the particles in the chamber, the pressure must be in the region of free molecular flow [164]. In our deposition process, the chamber pressure was around 2 x 10^{-5} *mbar* before the evaporation process was carried out. The pumping process is usually between 1.5 and 2 hours.

The electron beam was generated by a tungsten filament. The electrons are emitted from the tungsten filament and are guided by an arrangement of permanent magnets and electromagnets onto the titanium piece to be evaporated [164]. The electron direction can also be controlled by an emission control box. By turning the emission control the filament will begin to heat up and the electron production process is initiated, and the glow from the filament is visible inside the chamber. The deposition conditions are 60 mA of electron current and 5 minutes to produce approximately a 500 nm thick titanium layer and 60 mA with 10 minutes for a 1 μm thick titanium layer on the surface of the substrates, respectively.

Moreover it is also important to measure the thickness of the titanium layer after the E-Beam deposition. In our work, Zygo optical profiler was used to measure the thickness of the titanium films. The method is based on white light interferometry. When the two separate waves from the surface of the substrate and the titanium film combine, the resulting pattern is determined by the phase difference between the two waves. The waves in phase produce constructive interference, but when they are out of phase destructive interference occurs. The measurement of the thickness of the titanium film can be obtained using a computer and associated software. A picture of the Zygo optical profiler is shown in Figure 3.11.

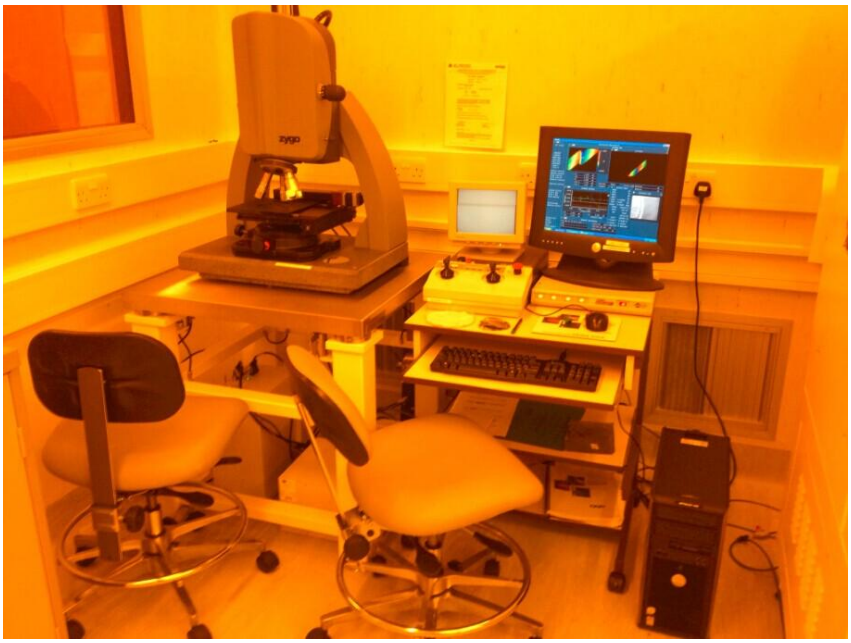

Figure 3.11: The photograph of Zygo optical profiler.

3.4 Laser Bonding Setup

3.4.1 Laser Bonding System

This diode laser operates in the near infrared wavelength region at 970 nm. The laser system housed in a 19'' plug-in compartment is connected with the laser coolant system, the electrical mains power supply and the laser control unit. The laser beam is transmitted to the work platform by a fibre optic cable. A schematic sketch of the diode laser system is shown in Figure 3.12.

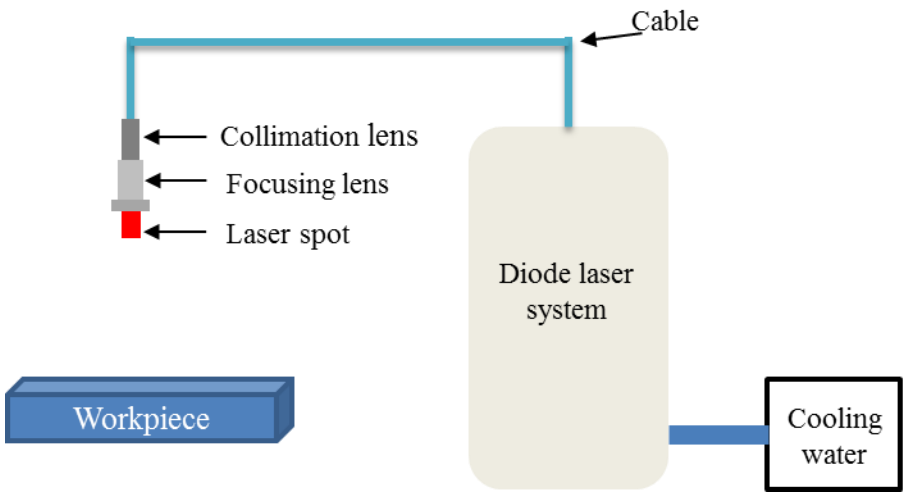

Figure 3.12: Schematic of the fibre coupled diode laser system.

3.4.2 Laser Bonding Setup

In the bonding process, PMMA substrate to PMMA substrate bonding with the metal intermediate film is described. A schematic of the laser bonding setup is shown in Figure 3.13. All of the samples are processed on a stainless steel bonding platform. A high-power diode laser system with a fiber-coupled output at 970 nm is used as the laser source. The laser output from the beam delivery fibre is transformed into a large square beam with top-hat intensity distribution. A broad beam allows easy alignment and processing of the substrates in the laser microwelding method. The top-hat beam is also desirable for microwelding with a small heat affected zone beyond the melted (weld) zone. The beam profile is produced using a custom-designed beam forming optical element [19]. The beam size is 6 x 6 mm^2.

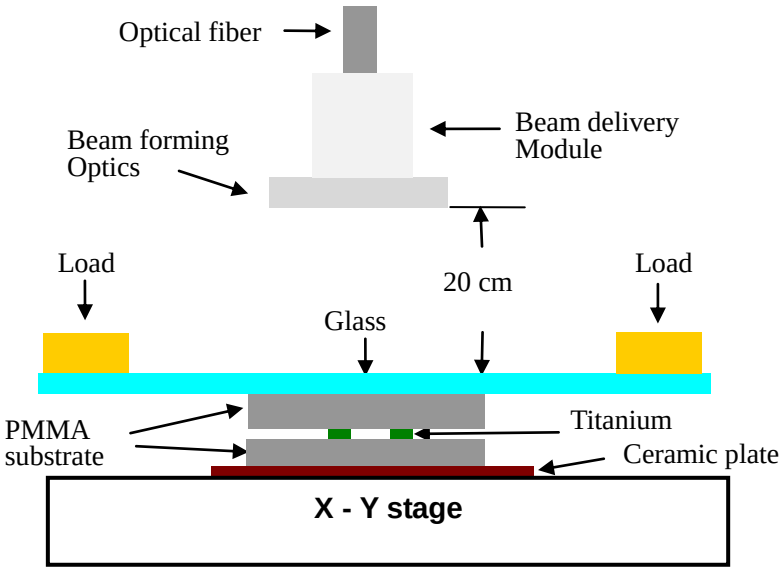

Figure 3.13: Schematic setup of the laser bonding setup.

Figure 3.14 shows a schematic of the experimental setup. The beam transmission module consists of collimation optics followed by a focusing lens with a focal length of 20 cm. The PMMA substrates were placed on an X-Y translation stage. A ceramic plate of thickness of 0.9 mm was placed under the PMMA substrates to improve thermal efficiency [20]. The substrate area with a titanium film is aligned to the laser beam. A glass plate was placed on the PMMA substrate assembly for supporting a metal ring based mechanical load. This is to ensure good contact between the two PMMA substrates during laser bonding.

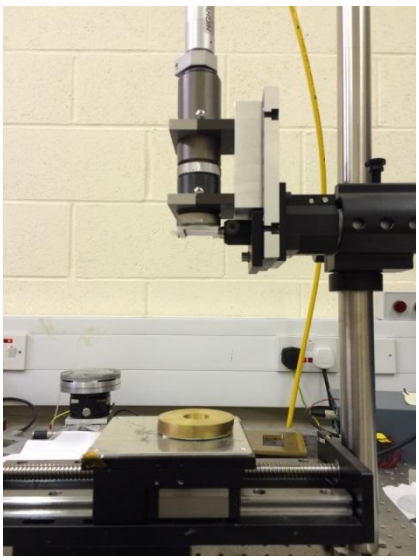

Figure 3.14: Photograph of the laser bonding setup.

3.5 Laser Microwelding of PMMA Substrates

3.5.1 PMMA Substrates Welding Method

In order to confirm the feasibility of laser bonding of PMMA substrate to PMMA substrate using the intermediate layer absorber, initial process tests were carried out. Figure 3.15 shows the images of laser welded PMMA substrates showing the area of titanium film, the heat affected zone and the melted zone. The thickness of the titanium film for Figure 3.15 (a) is 1 μm and it is 500 nm for the sample in Figure 3.15 (b). Both samples were produced at a laser power of 25 W and a processing time of 15 s. The heat affected zone (HAZ) and melted zone (MZ) are defined to be the zones beyond the perimeter of the circular titanium thin film as illustrated in Figure 3.15.

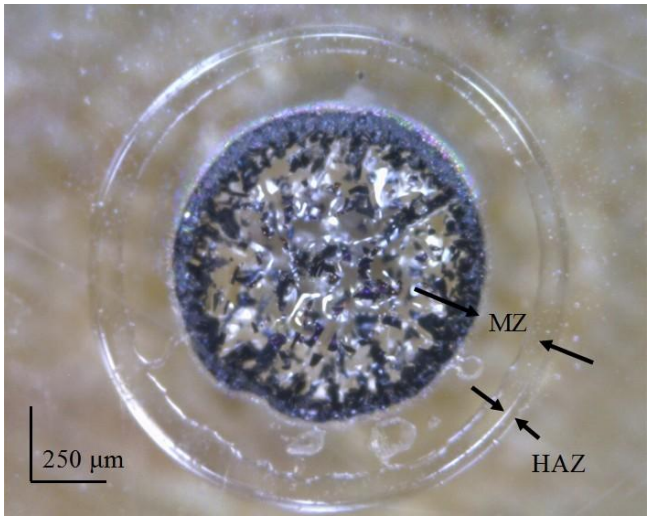

(a)

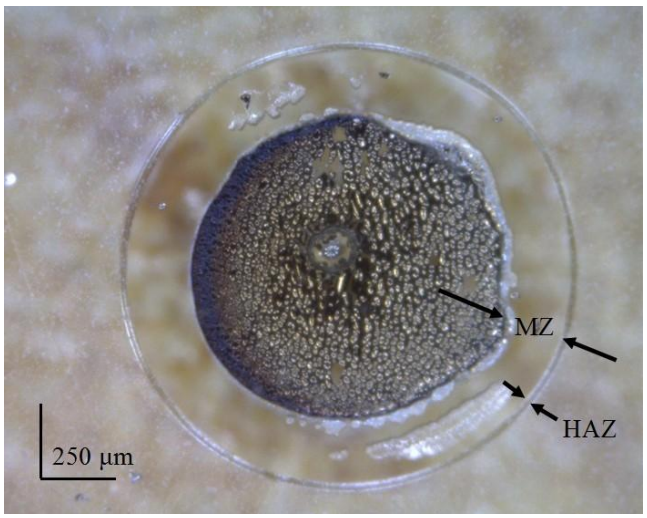

(b)

Figure 3.15: Optical images of laser welded PMMA substrates showing melt zone and heat affected zone for different titanium film thicknesses, (a) 1 μm and (b) 500 nm. The laser power and processing time were 25 W and 15 s respectively.

After testing, several PMMA samples were bonded using the diode laser system. The PMMA substrates were coated with titanium spots (1 mm diameter) of thickness of 500 nm and 1 μm respectively. Figure 3.16 shows the photographs of the bonded PMMA substrates using a 500 nm thick titanium layer and Figure 3.17 shows the photographs of the bonded PMMA substrate using a 1 μm thick titanium layer.

(a)

(b)

(c)

(d)

(e)

Figure 3.16: Bonded PMMA substrates using a 500 nm thick titanium layer, (a) 20 W of 15 s, (b) 20 W of 20 s, (c) 25 W of 15 s, (d) 25 W of 20 s, (e) 30 W of 10 s.

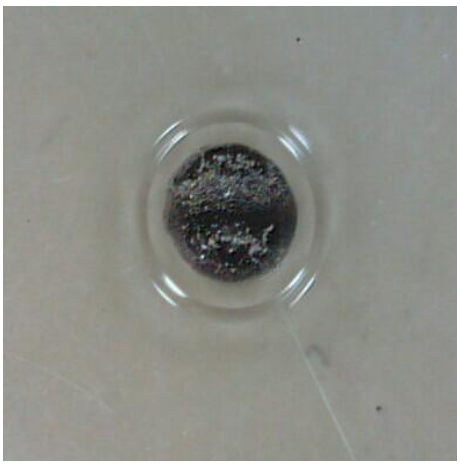

(a)

(b)

(c)

(d)

(e)

Figure 3.17: Bonded PMMA substrates using a 1 μm thick titanium layer, (a) 20 W of 15 s, (b) 20 W of 20 s, (c) 25 W of 15 s, (d) 25 W of 20 s, (e) 30 W of 10 s.

From Figure 3.16 and Figure 3.17, it is found bonds are created within all the bonding parameters. However, the melted zone and heat affected zone are different for different bonding parameters. Based on the same laser power, the melted zone and heat affected zone increase when the processing time increases by 5 seconds for both of the 500 nm and 1 μm thick titanium layers. Another phenomenon is that the titanium spot is nearly disintegrated when the process time is 20 seconds. In addition at the same processing time of 15 seconds, more laser power also generated wider melted zone and heat affected zone. In fact, it is easy for the titanium layer spread to create wider melted zone at higher laser power but the disadvantage is that a large heat affected zone is also generated.

Figure 3.18 shows the optical pictures of PMMA substrates bonded at 30 W of laser power and processing time 15 seconds. Although good bonding can be made, the intermediate titanium layer has significant deformation. This occurred because the polymer was over-melted to a liquid state after the excessive laser heating effect.

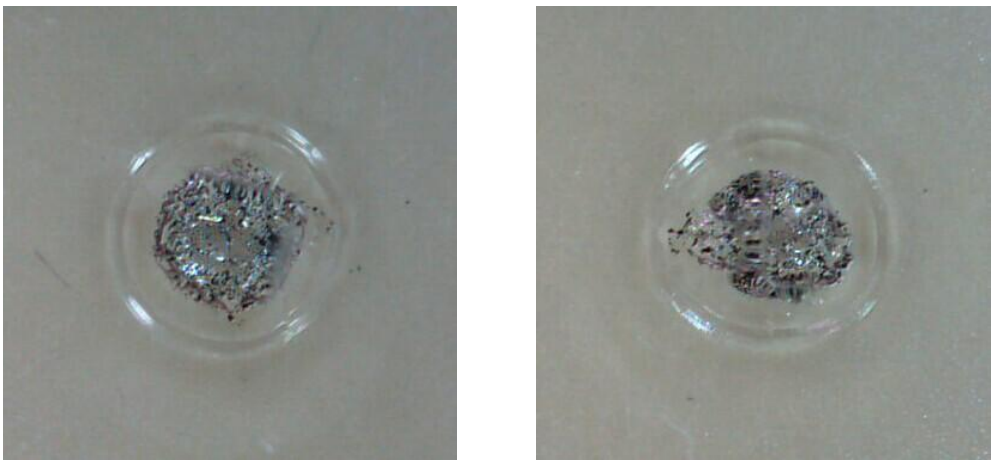

(a) (b)

Figure 3.18: Optical images of laser welded PMMA substrate (laser power is 30 W and processing time is 15 s), (a) 500 nm thick titanium layer and (b) 1μm thick titanium layer.

3.5.2 Analysis of Heat Affected Zone and Melted Zone

In order to determine the effect of laser welding conditions on the melted (weld) zone and the heat affected zone as shown in Figure 3.17, a number of samples were produced and analyzed using an optical microscope. Figure 3.19 and Figure 3.20 show the results of the measurements of the melted zone and heat affected zone. Each value represents an average of three independent measurements. As expected both of the melted zone and the heat affected zone increase as the laser power increases. The results are similar for the processing time since the laser induced temperature increases until the steady-state is reached. On the other hand the results indicate that the time to reach steady state of the laser induced thermal effect is longer than 25 s since the width of the heat affected zone is still increasing until then. The results for processing times beyond 25 s were not obtained since substrate deformation was observed consistently at all of the laser power levels. This is due to the absorption of more laser power resulting in melting of a larger volume of the substrate material and hence causing the subsequent substrate deformation [165].

Figure 3.19 displays the width of melted zone and heat affected zone for the 500 nm thick titanium layer. It is clearly observed that the melted zone is much larger than the heat affected zone, however the heat affected zone is increasing gradually with the process time and laser power. Although the area of the melted zone still increases after the bonding time of 20 s, it is already in the over-heating region not only increasing the melted zone and heat affected zone but also causing deformation of the samples.

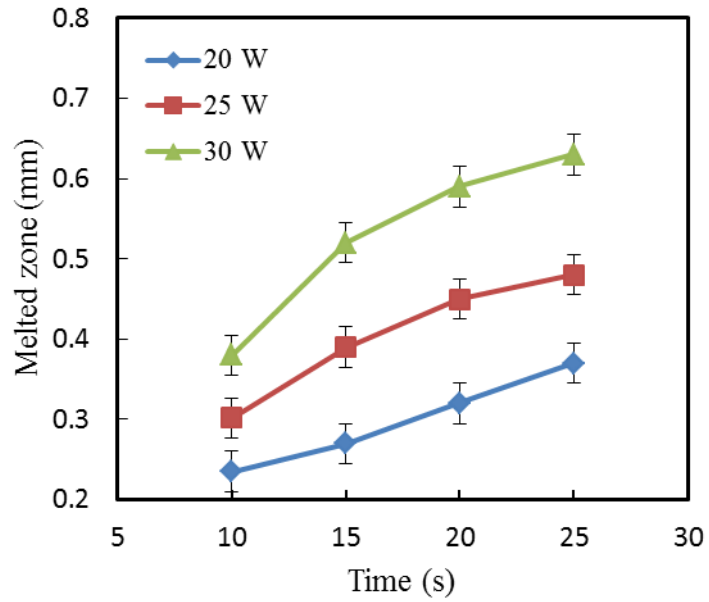

(a)

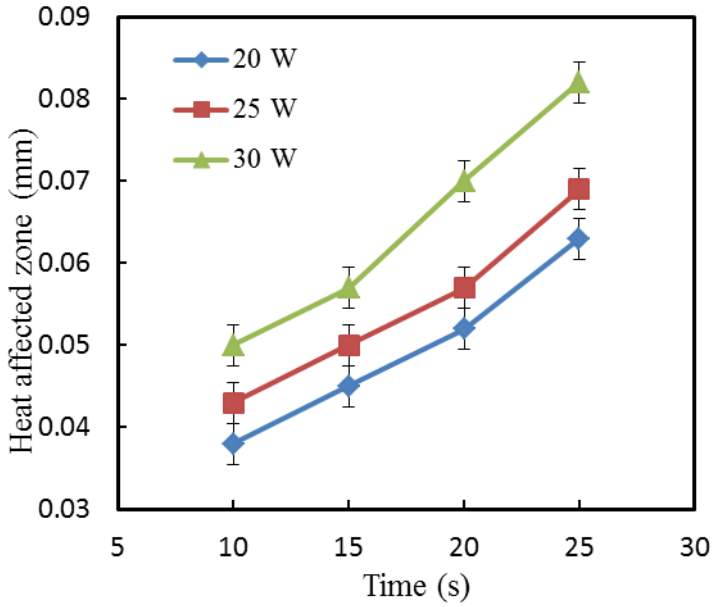

(b)

Figure 3.19: Results of measurements of (a) melted zone and (b) heat affected zone for different laser processing conditions. The thickness of the titanium film is 500 nm.

Comparing the results in Figure 3.20 (a) and Figure 3.20 (b), the width of the heat affected zone is about a factor of 10 smaller than that of the melted zone. This is a highly desirable effect for encapsulation of microfluidic devices since the thermal effect on the neighboring region of the functional structures such as microchannels is minimized. Based on the results of optical inspection after bonding for uniform welding contour and minimal substrate deformation, It is found that the optimum conditions for laser microwelding are 25 W for laser power and 15 s for processing time or 30 W for

laser power and 10 s for processing time.

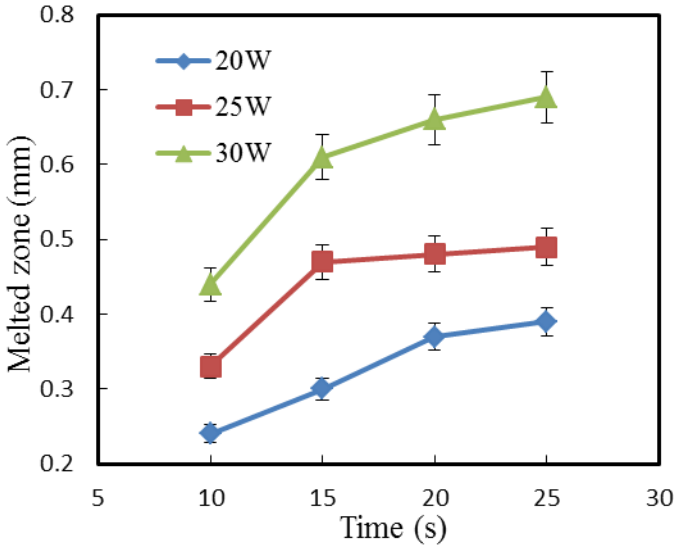

(a)

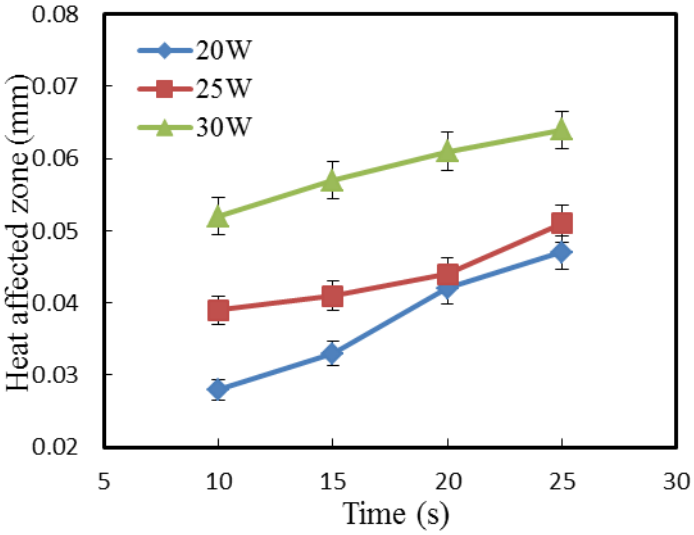

(b)

Figure 3.20: Results of measurements of (a) melted zone and (b) heat affected zone for different laser processing conditions. The thickness of the titanium film is 1 μm.

Comparing Figure 3.19 with Figure 3.20, it is found that the melt zone and heat affect zone of all samples increase with increasing laser power and processing time. In analysing the melted zone, it is observed that the melt zone is 0.1 mm larger for the 1 μm thick titanium film than that of the 500 nm thick titanium film at 30 W of laser power. As for the 20 W of laser power, the effect is the same. Regarding the heat affected zone, the measurements show that the width increases rapidly for the 500 nm thick titanium layer as shown in Fig. 3.19 (b). Although the heat affected zone also increases in the samples with the 1 μm thick titanium layer, the increasing amplitude is

smaller than samples with 500 nm thickness titanium layer. This is because the thicker intermediate absorbing layer produces more thermal diffusion to generate a larger melt zone rather than the heat affect zone.

3.5.3 Studies of Separation Between Two Adjacent Film Spots

For microfluidic applications it is necessary to produce a closed loop welding line for sealing and encapsulation. As analysed in section 3.5.2, the width of the melt zones ranges from 0.3 mm to 0.6 mm. So in order to study the design parameters of the titanium patterns and in this case it is the separation between two neighbouring titanium spots, laser welding was carried out for substrates with spot separations of 0.6, 0.8, 1.0 and 1.2 mm.

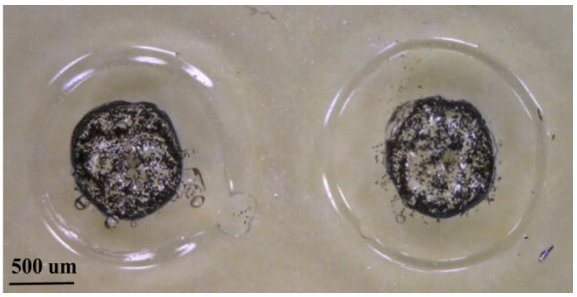

(a)

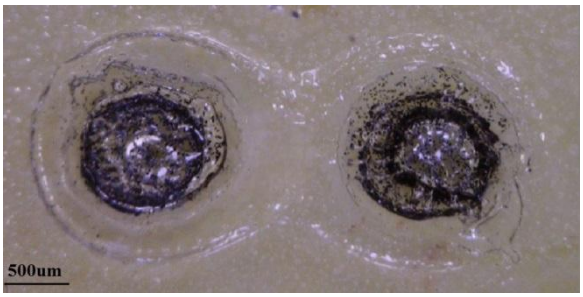

(b)

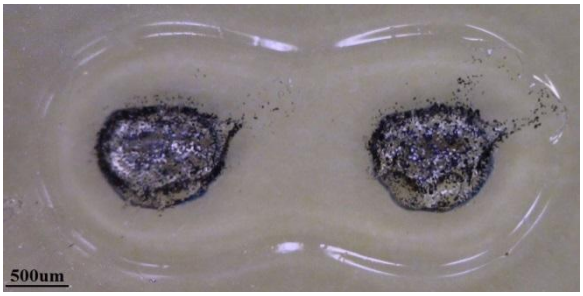

(c)

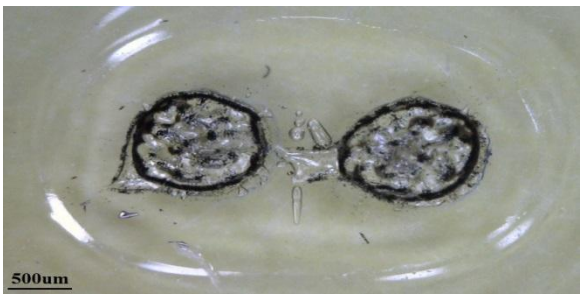

(d)

Figure 3.21: Effect of separation between two titanium film spots for continuous welding between substrates for the 500 nm thick titanium film. (a) 1.2 mm, (b) 1.0 mm, (c) 0.8 mm and (d) 0.6 mm.

Figure 3.21 shows the effect of separation between two titanium film spots for continuous welding between PMMA substrates for the 500 nm thick titanium film. The separate distance between two titanium film spots was in the range 1.2 mm to 0.6 mm. As discussed in section 3.5.1, it was found that the best process parameters of PMMA substrates for bonding are 25 W and 15 s for laser power and processing time respectively. Since there is more thermal diffusion to the middle of the two titanium spots when the separation is less, the titanium spots become more irregular as shown in Figure 3.21 (d).

In Figure 3.22, the thickness of the titanium film is 1.0 μm. It is found that this film thickness produces well defined melted zones. Films thicker than 1 μm are also suitable but require a longer deposition time. The laser power and welding time are 25 W and 15 s respectively. It can be seen that for the largest separation of 1.2 mm there is no contact between the two melted zones. But as the separation decreases the two melted zones are joined to produce a continuous line. At the separation of 0.6 mm, the two melted zones merge into one with a seamless transition. The results show that it is possible to produce a well defined continuous welding line using discrete spot based film absorbers. Although a circular spot design was used in this work, other spot geometries can also be used.

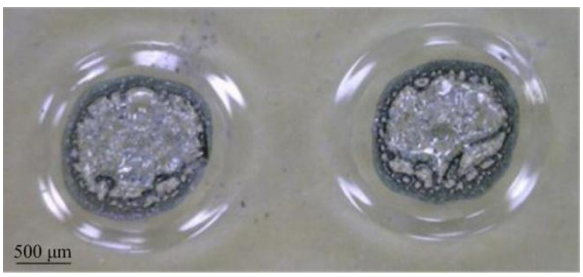

(a)

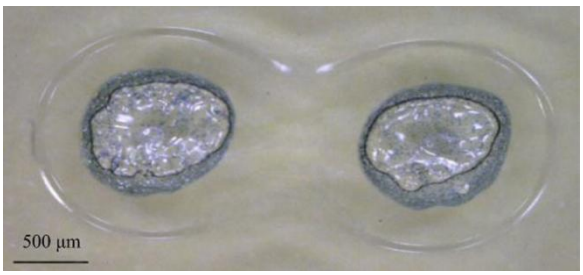

(b)

(c)

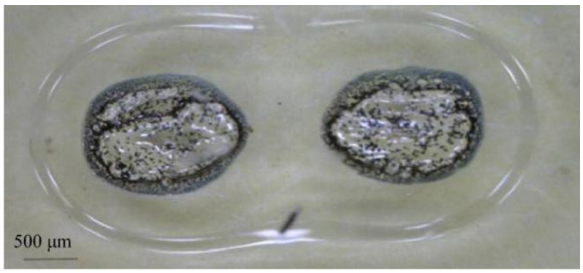

(d)

Figure 3.22: Effect of separation between two titanium film spots for continuous welding between substrates for the 1 µm thick titanium film. (a) 1.2 mm, (b) 1.0 mm, (c) 0.8 mm and (d) 0.6 mm.

Comparing Figure 3.21 with Figure 3.22, most of the samples were well defined melted zones to bond two PMMA substrates but there are differences between the samples for the 500 nm and 1 µm thick titanium layer. In Figure 3.21, the titanium spots becomes irregular after laser heating because the thinner titanium film is less rigid or robust. Moreover as it can be seen in Figure 3.21, the boundaries of the melted zone are not as well defined as in Figure 3.22 since the thicker titanium film has better mechanical integrity resulting in less disintegration of the film. Therefore for better quality, a titanium film of thickness of about 1 µm is preferred. In addition the effect of larger melt zone and smaller heat affect zone is another important factor for PMMA bonding. From Figure 3.22 and section 3.5.2, it is found that the sample with 1 mm of separation between two adjacent titanium film spots has the best melt zone and bonding effect although its heat affect zone is not the smallest. Finally, the optimal design is 1 mm for separation between two titanium film spots and 1 µm for the film thickness.

3.5.4 Studies of Large Area Joining

Large area joining has also been studied, this work was carried out using samples with 2x2 arrays of titanium film spots. Large area joining between the substrate surfaces can produce a high bond strength that may be required in applications where a high pressure fluid flow is necessary. The spot separation was 1.0 mm and the titanium film thickness was 1.0 μm. The laser power was 25 W and the welding time was 15 s. For comparison of a similar area of welding, a single large square titanium film (3x3 mm^2) was used to join two PMMA substrates under identical conditions as for the 2x2 array of circular titanium film spots. Figure 3.23 shows the images of the assembled PMMA substrates. Although the total joined area is similar in both designs, there was significant distortion of the top surface of the PMMA substrate that is not shown in Figure 3.23 (b). This was due to the excessive thermal energy from absorption of the laser radiation by the large titanium film. Therefore the results show the advantage of using an array of titanium film spots for large area substrate joining.

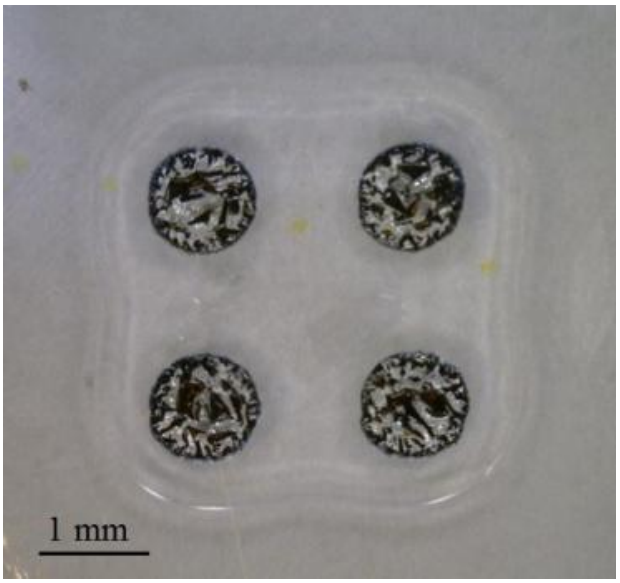

(a)

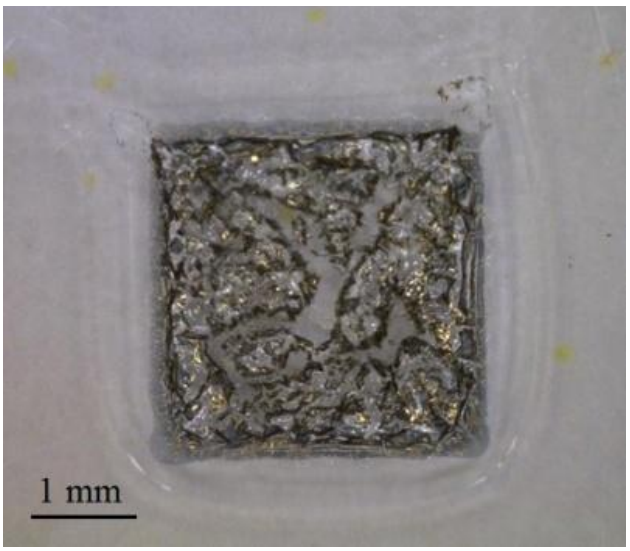

(b)

Figure 3.23: Optical images of laser welded PMMA substrates using (a) a 2x2 array of 1 mm diameter titanium film spots and (b) a square titanium film of 3 x 3 mm2.

3.5.5 Cross-sectional Studies of Weld Interface

In order to study the laser welded interface in detail, the cross-sections of the assembled substrates are obtained and examined under an optical microscope. Figure 3.24 shows the images of the cross sections of samples produced at the laser power of 20 W, 25 W and 30 W respectively. The titanium film thickness is 1 μm and the processing time was 15 s. At low laser power, the temperature rise at the interface is just above the melting temperature (135°C) of the PMMA substrate material. In this case welding occurs but does not cause breakup of the titanium film. As the laser power is increased to 25 W, the temperature at the center of the film spot region is significantly higher than the melting temperature of the PMMA material resulting in melting of a larger volume of the PMMA substrate material as shown in Figure 3.24 (b). As the laser power is increased further to the value of 30 W, the melted interface region extends further into each substrate as can be seen in Figure 3.24 (c). It has been observed that the excessive melt region shown in Figure 3.24 (c) causes deformation of the substrate surface of the sample. Therefore it is necessary to control the laser processing conditions in order to obtain a reliable bond between the substrates and at the same time not causing substrate deformation. After comparison, the optimum bonding parameters are 25 W with processing time of 15 s which is shown in Figure 3.24 (b).

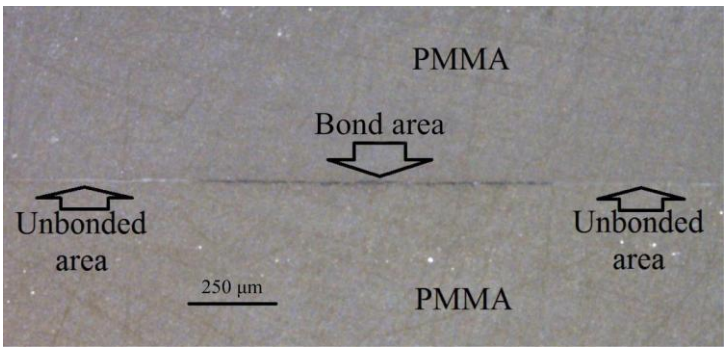

(a)

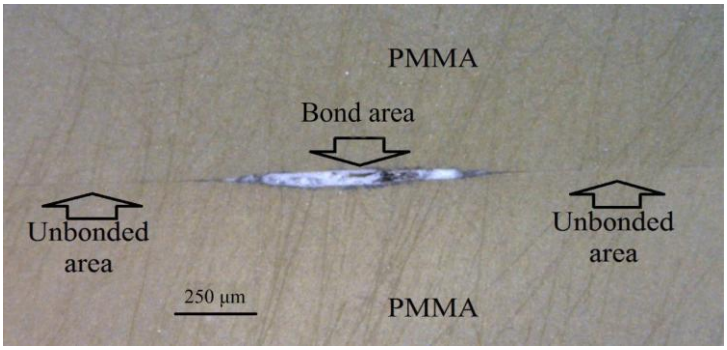

(b)

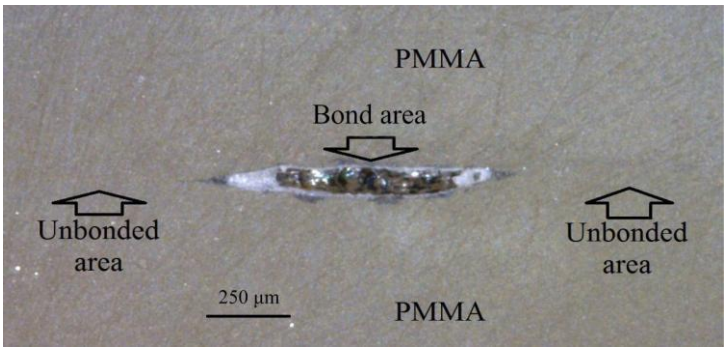

(c)

Figure 3.24: Optical images of cross-sectional view of the laser weld interface between two PMMA substrates produced at the laser powers of (a) 20 W, (b) 25 W and (c) 30 W respectively. The thickness of the titanium film is 1 µm and the processing time is 15 s.

3.5.6 Bonding Strength Measurement

In this study, tensile testing was applied to measure the mechanical stability of the bonded PMMA substrates. A cylindrical or a plate shaped specimen is deformed by applying a uniaxial force. One end of the sample is fixed in a static grip while the other end of the specimen is pulled at a constant velocity until a mechanical break occurs. The tensile measurements were carried out to determine the interfacial bond strength of the laser weld PMMA substrates. Figure 3.25 shows the schematic configuration of a laser welded PMMA substrate assembly for tensile strength testing. An acrylic circular rod was attached to each PMMA substrate using an epoxy glue (Everbuild Stick 2 Rapid) [166]. The two polymer rods were aligned along a straight line to ensure minimal shear

stress during tensile testing. The rods were secured to the grippers of the test rig and a tensile load was applied to the sample. In our study, the measurements were made using a commercial tensile strength tester (Instron, model 2715-015) which is shown in Figure 3.26. The tensile strength for each sample was obtained from the measured load extension characteristic at a pulling speed of 1 mm/min.

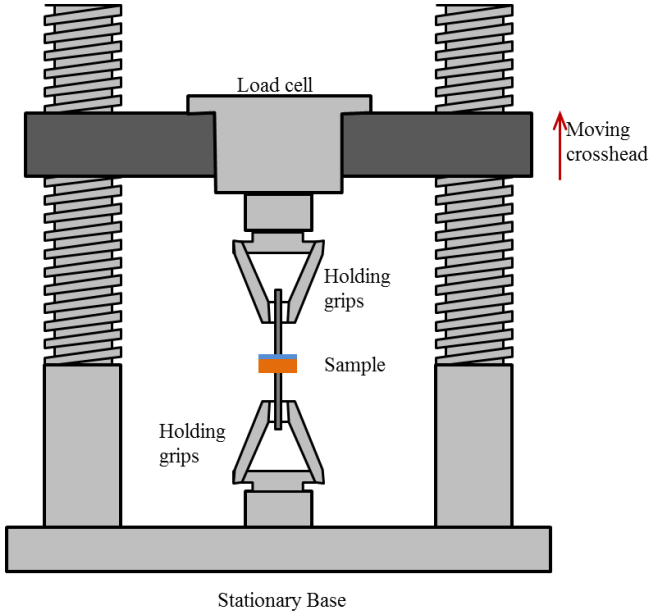

Figure 3.25: Schematic of sample mounting [166].

Figure 3.26: The photography of Instron tensile tester.

The results of tensile strength measurements are given in Table 3.3. A 2x2 array of titanium spot pattern and a single square titanium film were used in the comparative study. The separation and diameter of the film spots in the 2x2 array design are both 1

mm. The area of the square titanium film is 3 x 3 mm^2. The processing time and load of 15 s and 4 N respectively were the same for all samples. The total weld area for each sample was measured from the corresponding optical image of the resultant PMMA substrate assembly and used to determine the values of tensile strength shown in Table 3.2. As can be seen in Table 3.2, sample 2 has the best tensile strength among the samples without suffering from substrate deformation. Compared with the previous polymer bonding methods, the new method produces higher tensile strength [19, 26, 29, 41, 42]. For the titanium film of thickness of 1 μm, the tensile strength for the 2x2 array design is better than that for the large area square film. At the laser power of 30 W, surface deformation was observed for both sample 3 and sample 6. As discussed in Section 3.5.1 in this case the higher laser power produced a large volume of melted PMMA material from the two substrates causing excessive softening during the welding process and therefore the subsequent surface deformation after cooling.

Table 3.2: Tensile strength at different laser welding conditions.

Sample No.	Titanium film pattern	Titanium thickness (μm)	Laser power (W)	Tensile strength (MPa)	Substrate deformation
1	2×2 array	0.5	25	2.88	No
2	2×2 array	1.0	25	5.08	No
3	2×2 array	1.0	30	6.14	Yes
4	Square film	0.5	25	3.18	Yes
5	Square film	1.0	25	4.31	No
6	Square film	1.0	30	4.93	Yes

The results also show that the tensile strength is higher for the thicker titanium film. Therefore the film thickness of 1 μm is better for laser welding of PMMA substrates and this is in agreement with the results shown in Figure 3.22 in order to achieve a well controlled weld zone. Figure 3.27 (a) shows the picture of one of the two PMMA substrates of sample 3 after tensile testing. Figure 3.27 (b) shows a similar picture for one of the substrates of sample 6. It was found that a similar amount of titanium film residue was left on each substrate of the samples as shown in Figure 3.27. This failure modes show that the cracks occurred on both surfaces of PMMA substrates which indicating highly strong bonds generated at the interface of PMMA substrates.

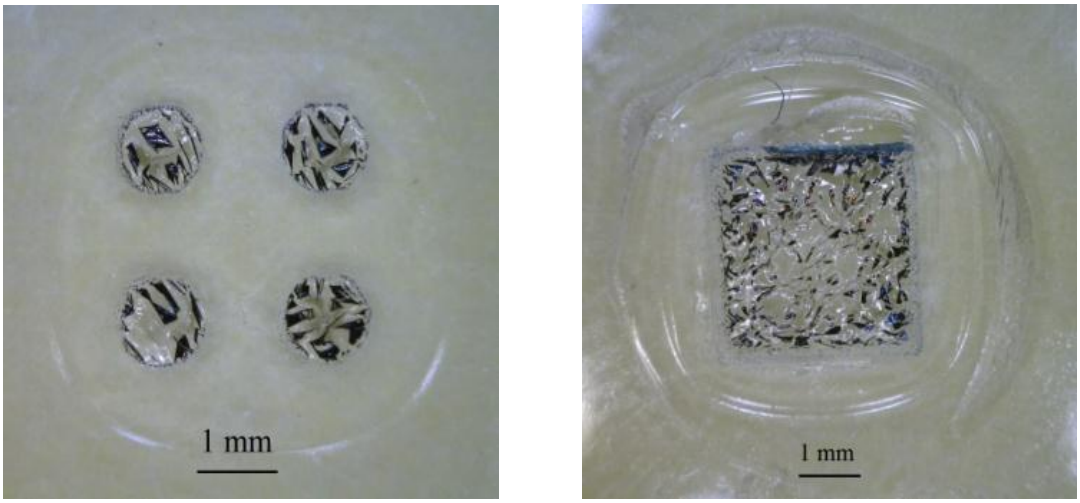

(a) (b)

Figure 3.27: Sample mounting configuration and optical pictures of the PMMA substrates after destructive tensile testing. (a) optical picture of one PMMA substrate for sample 3, and (b) optical picture of one PMMA substrate for sample 6.

3.6 Laser Fabrication and Encapsulation of Microfluidic Channels

As bonding of blank PMMA substrates bonds has already been investigated, structured substrates are used to carry out experiments to study the demonstration of its ability to seal microchannels and ports. Based on the results described in the previous sections several microfluidic structures are designed and manufactured for testing the laser microwelding method.

3.6.1 Laser Fabrication of Microchannels in PMMA Substrates

For laser machining PMMA material, a CO_2 laser system (Epilog Mini 18) was used which has been detailed in section 3.2 and section 3.3. Normally residues and bump formation and their growth within polymer melts are highly complex problems. The ablation of polymers can be presented by the process depth (d) as function of laser power (P) and moving speed (v) of the laser beam [167]:

$$d \propto \frac{P}{v} \qquad (3.2)$$

The laser power and speed are the main factors in continuous wave laser ablation.

A larger number of process parameters for PMMA micromachining were carried out and the results are shown in Table 3.3.

Table 3.3 Results of channel depth in CO2 laser ablation.

Speed (mm/s)	Power (W)	Approx Depth (μm)
17.6	6	80
17.6	8	100
17.6	10	180
17.6	12	220
17.6	14	300
23.5	8	60
23.5	10	120
23.5	12	180
23.5	14	200
29.3	6	35
29.3	8	50
29.3	10	80
29.3	12	130
29.3	14	185
29.3	16	225
29.3	18	260
29.3	20	285

Since the CO_2 laser beam has a Gaussian intensity distribution, the geometry of the channels can be regarded as a Gaussian function [167]. Figure 3.28 shows an example of the cross-section of a microchannel. Although the residues were generated on the surface after laser machining, there is no occurrence of any bump formation.

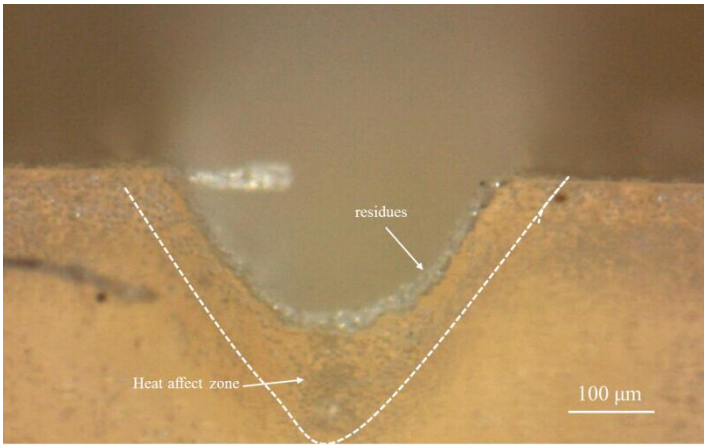

Figure 3.28: Cross section of laser ablated microfluidic channel (P= 8 W, v=17.6 mm/s).

3.6.2 Design of Microfluidic Devices

The microfluidic device is a channel structure with reservoirs which is used to test the laser welding method for microfluidic applications. The length, width and depth of the channel are 28 mm and 150 µm and 200 µm respectively. The thickness of the two PMMA substrates is 2 mm. In this study, the quality of the inner channel walls was not considered as an important factor. The diameter of the titanium spot is 1 mm and the separation between the adjacent spots is also 1 mm based on the investigation described in section 3.5.3. The design of the microfluidic channel is shown in Figure 3.29. To create the channel two ellipse reservoirs with a diameter of 7 mm were laser micromachined into a PMMA substrate. Two microfluidic devices are bonded with 25 W for 15 s. And other two microfluidic devices are bonded with 30 W for 15 s. For all the sealed samples, it is needed at least 15 s for cooling. Pressure is applied to provide a bonding pressure of 0.4 kg for all samples.

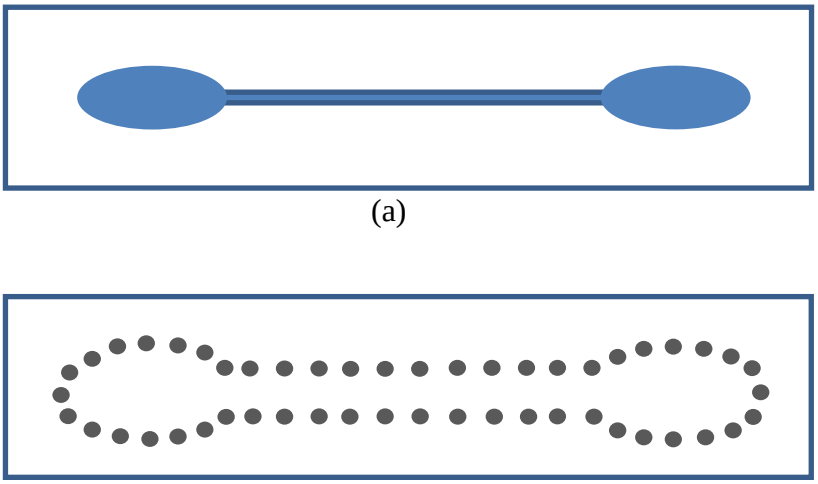

(a)

(b)

Figure 3.29: (a) Design of microfluidic channels, (b) design of titanium layer.

3.6.3 Results

The titanium spots were deposited on the top PMMA substrate as the lid (Fig. 3.30). Holes were also machined on the top substrate to provide inlets to the microfluidic channel. A bonding force was applied and the same setup was used as shown in Fig 3.14. The bonding force was generated using a mechanical load of 0.4 g. Ten samples were bonded. Most of these samples are successful except two which were broken since they were not aligned correctly.

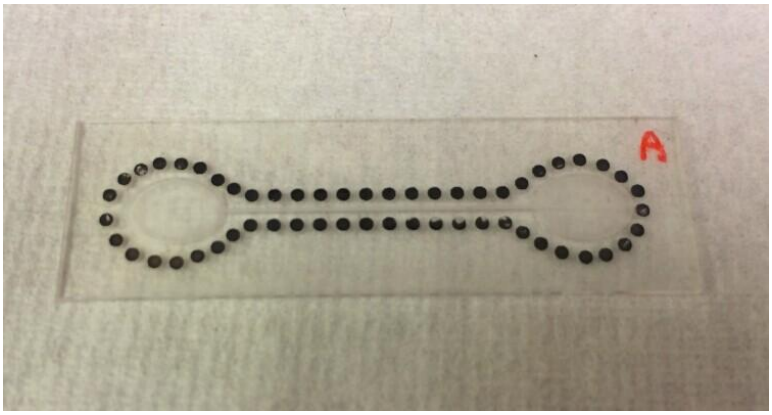

Figure 3.30: Titanium spots were deposited on PMMA substrate.

In order to test the bond quality of the devices, a coloured liquid was injected into the inlet reservoir to flow through the channel by capillary effect. Although the samples were carefully placed and processed, two of the samples with bonding parameters of 30 W and 10 s are not leak free structures. The coloured liquid leaked between the two PMMA substrates as shown in Figure 3.31. Overall most of the samples showed leak free performance as shown in Figure 3.32.

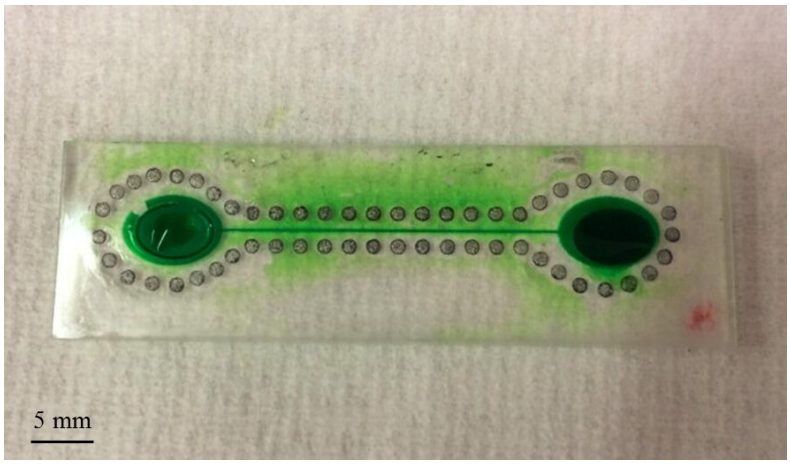

Figure 3.31: Leaking microfluidic device.

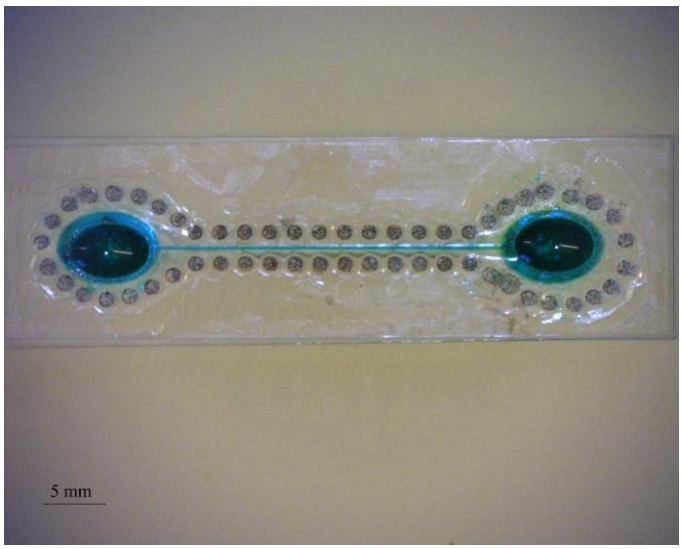

Figure 3.32: Successful microfluidic device injected with ink.

Moreover after several hours, the samples still showed no leakage and all of the devices were flushed by water through the left reservoir to right one using a syringe to remove the coloured ink. Then these samples were tested again after a few hours. There was no leakage in the samples which had passed the initial test. To further assess the quality of the successfully sealed samples, the cross section of the devices was obtained as shown in Figure 3.33. It can be seen that bonding is created around the fluidic channel.

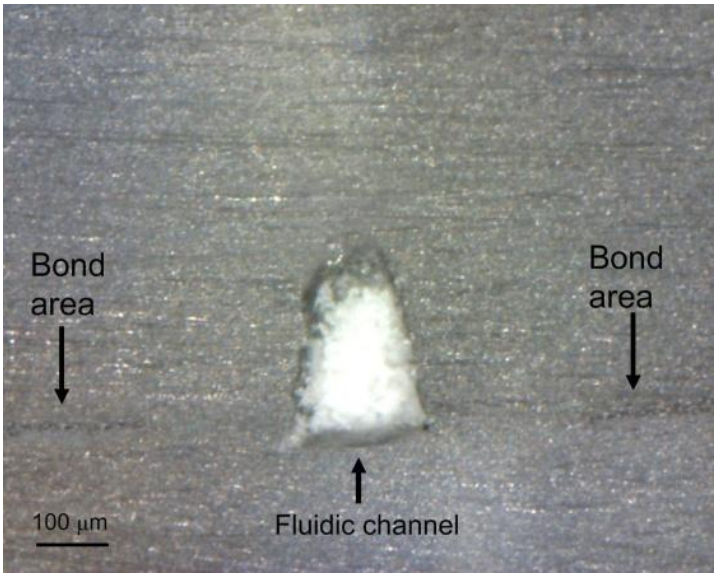

Figure 3.33: An optical image of a cross-sectional view of the microchannel showing no channel distortion after bonding.

3.7 Conclusions

A novel laser microwelding method has been studied for bonding of PMMA substrates using an intermediate metal film spots design for fabrication of microfluidic devices for

lab-on-chip applications. In this approach the bonding contour is defined by the pattern of the titanium film spots and thus allowing easy alignment with a broad laser beam resulting in a greater process tolerance than the previous approaches. The thin film spots can also be produced using an inkjet based low cost printing method. The dependence of the weld zone and heat affected zone on laser power and processing time has been investigated. It has been found that a laser power of 25 W corresponding to a beam intensity of about 70 W/cm^2 is sufficient to produce a good bond with a processing time of 15 s. A continuous weld between the adjacent circular titanium film spots can be achieved by controlling the separation between the film spots. The results on studies of different film patterns show that for large area substrate joining the spot array design is better than a large thin film patch in order to minimize the effect of substrate distortion. Both cross-sectioning and tensile strength measurements have been carried out to study the reliability of the laser weld PMMA substrates. The tensile strength of the laser produced weld is about 6 MPa which is comparable to that of the previous work in laser welding of bulk polyvinyl chloride (PVC) materials [168]. The laser microwelding method has been used successfully in encapsulation of a microchannel device as shown by leak-free operation. The results of the work show a potential application of the laser microwelding method for packaging of future microfluidic devices.

Chapter 4 Laser Assisted Bonding Using an Intermediate LCP Film For Microsystem Packaging

This chapter presents a study of an LCP film as an adhesive layer for packaging of MEMS devices using a diode laser system. There are several advantages using the LCP material for packaging of microsystems such as RF devices. The development of a laser processing method using an LCP film with a short bonding time is presented. A temperature monitoring method and quality testing of the bonded devices are also described. In order to enhance the performance and the integration of systems, the MEMS packages have to be made to be small and light. As discussed in Chapter 2 the LCP polymer is a highly stable material with good moisture properties for near-hermetic package performance. Besides as an attractive thin plastic material, LCP can be used successfully for packaging applications with low temperature requirements.

A laser-assisted bonding technique using an LCP film for cavity based packaging applications is investigated. Laser based LCP bonding of both planar silicon and glass substrates and also a molded LCP package will be described. For glass-glass bonding, a thin film titanium absorber in a spot pattern was used to facilitate absorption of laser beam in the bonding region for melting the LCP sealing ring to achieve substrate bonding. An embedded temperature sensor was used to monitor the temperature change at the bonding interface in bonding of a silicon cap to a molded LCP package. Shear and leak tests were performed to assess bonding strength and hermeticity of the laser bonded samples.

4.1 Properties of LCP polymer

The study of LCP materials in electronics has been only for a few decades, although the first research of the LCP material by scientists was in 1923 when Vorlander synthesised LCP by applying benzene rings linked through ester groups [169]. The term “liquid crystal” refers to a state of relation that reveals both partly solid and partly liquid properties. While the liquid crystal flows like normal liquids, the molecules retain an original direction. Normally, LCP materials are in solid phase at room temperature. If the liquid crystal materials are heated to change from the solid state to the liquid-crystal state, they are called as thermotropic materials. Furthermore, if the liquid crystal materials are observed when they are in solution then the materials are called lyotropic

[170]. The reason that LCP has been widely applied in electronic integration is because of its unique properties. Figure 4.1 shows illustrations of the structures of liquid crystal polymers in solid phase and in fluid phase [170].

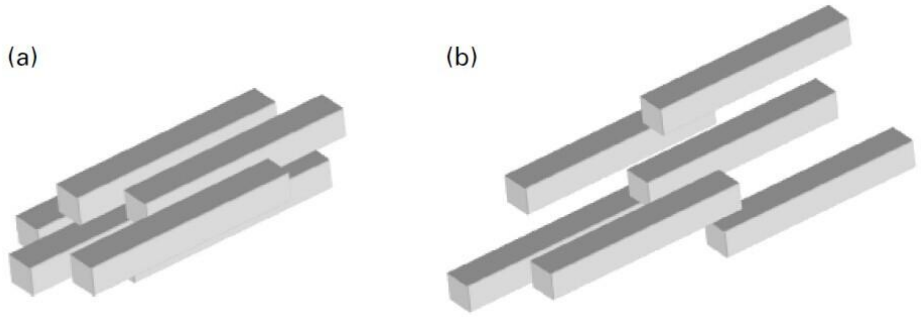

Figure 4.1: (a) A liquid crystal solid phase and (b) A liquid crystal fluid [170].

The molecular structure of LCP that is a totally aromatic polyester is shown in Figure 4.2 [170]. The two groups are linked together by an ester bond (-O-CO-) that provides long range rotational adaptability. This movement is referred to as crankshaft rotation in the chemistry field. The benzene rings, also refers to aromatic rings, are shown as hexagons in the chemical diagrams of the two groups. The left group is p-hydroxybenzoic acid (HBA) and the right group is 6-hydroxy-2-napthoic acid (HNA). Because of the significant feature of the aromatic rings, LCP materials exhibit a greater stability. The aromatic rings also have the abilities to stack on the top of each other to generate a strong attachment. This property makes the LCP to possess low diffusivity and permeability for high density polymer packing [170].

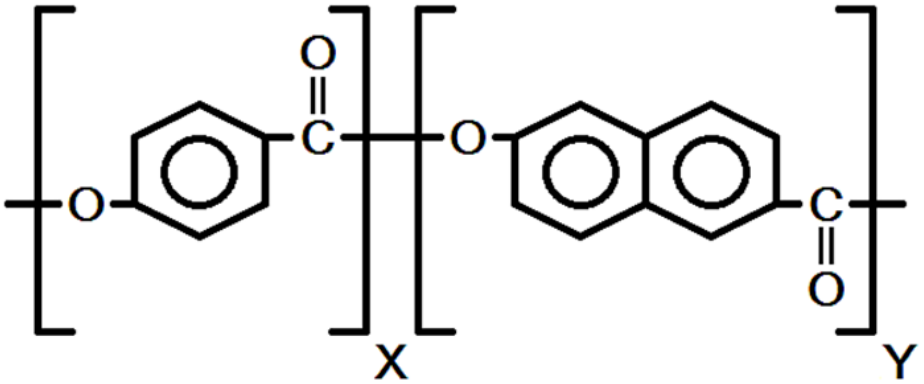

Figure 4.2: Molecular structure of the LCP [170].

LCP has been used in chemical applications and produced with diverse characteristics. The Coefficient of Thermal Expansion (CTE), which is the change in the physical dimension as temperature, ranges from 8 to 17 ppm/K (X and Y). LCP materials have

the property of less than 0.004% of water absorption [106, 115]. The melting temperature is between 280 ℃ to nearly 350 ℃ depending on the material composition. LCP has a specific property of heat distortion temperature that is the temperature at which the LCP starts to deform within a certain pressure. The heat distortion temperature of the LCP is 260 ℃ which is about 20 ℃ lower than minimum melting temperature.

There are several types of LCP materials available from different manufacturers, such as Kevlar, Vectran, Zenite and Rogers. In this study, the ULTRALAM 3908 bondply from Rogers Corporation is used as a bonding film. The standard thicknesses are 25 μm and 50 μm. Furthermore, it exhibits a number of features and benefits:

- Excellent electrical properties
- Low modulus
- Extremely low moisture absorption
- Flame resistant

The typical properties of the ULTRALAM 3908 bondply are given in Table 4.1 [171].

Table 4.1: The typical values of ULTRALAM 3908 bondply [171].

Property	Value	Unit
Tensile Strength	216	MPa
Coefficient of Thermal Expansion	X:17, Y:17, Z:150	ppm/ ℃
Melting Temperature	280	℃
Dielectric Constant (10 GHz, 23 ℃)	2.9	
Water Absorption (23 ℃, 24 hrs)	0.04	%

4.2 Micromachining of LCP

In order to produce a microcavity after bonding two planar surfaces, a laser processing approach was studied to machine LCP rings from the thin film material. Unlike traditional mechanical drilling, laser processing of LCP does not need deburring and the laser technology provides more precision. The mechanical drilling approach is not suit able for LCP cutting in this study because it is not easy to produce circular rings.

The same CO_2 laser (Epilog Mini 18, 10.6 μm in wavelength) as described in Chapter 3

was used which has been detailed in section 3.3. There are many advantages of CO_2 laser for LCP cutting:

- The CO_2 laser system is a safe equipment, the laser beam is ready to use when it is switched on and can be switched off immediately by an interlock mechanism when the protection cover is opened by accident. It also does not need a warm-up and a cooling down procedure for operation.
- Unlike the other laser systems such as the excimer laser, the CO_2 laser system is more reliable. As for issues such as unstable power supply, critical gas tube mixtures maintenance and burn marks on laser optics, the CO_2 laser system does not suffer from these problems.
- The CO_2 laser is the fastest system for cutting holes, sample edges and random patterns such as circular rings out of an LCP film in this work.

Figure 4.3 shows two samples of LCP layers which were machined using the Epilog CO_2 laser system.

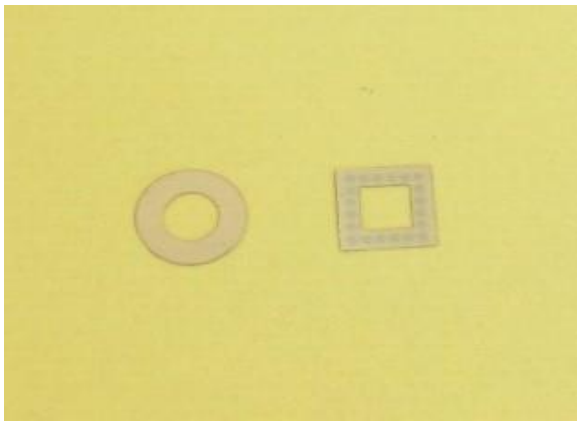

Figure 4.3: LCP rings produced by the Epilog CO2 laser system.

However there are also some disadvantages in the CO_2 laser cutting method:

- The worst issue is the burn residues of carbon ash still adhered at the edges of the cutting area which can smear the samples. The typical solution to clean the burn residue is to use oxygen plasma.
- Although the CO_2 laser system could cut good cavities, holes and edges, it does not have the precision of some other lasers.
- The CO_2 laser system can only produce feature sizes of larger than a hundred

microns since the laser spot size is larger than other lasers.

4.2.1 Mask Fabrication and LCP Film Preparation

For bonding glass and glass substrates, PMMA masks for depositions on LCP rings circular titanium spot patterns are designed using CorelDRAW Graphics suite X5 (COREL). The diameter of the apertures on the mask is 0.6 mm and the separation between two adjacent apertures is 0.7 mm. The 0.5 mm thick PMMA sheet is cut into 55 mm x 50 mm plates for mask fabrication. The PMMA masks were fabricated using the CO2 laser machining method as described in section 3.2. Figure 4.4 shows an explosive view of the arrangement for depositing titanium thin film spots on the LCP rings. The LCP rings were attached to the glass carrier and the masks were aligned each to the corresponding LCP ring using the alignment marks.

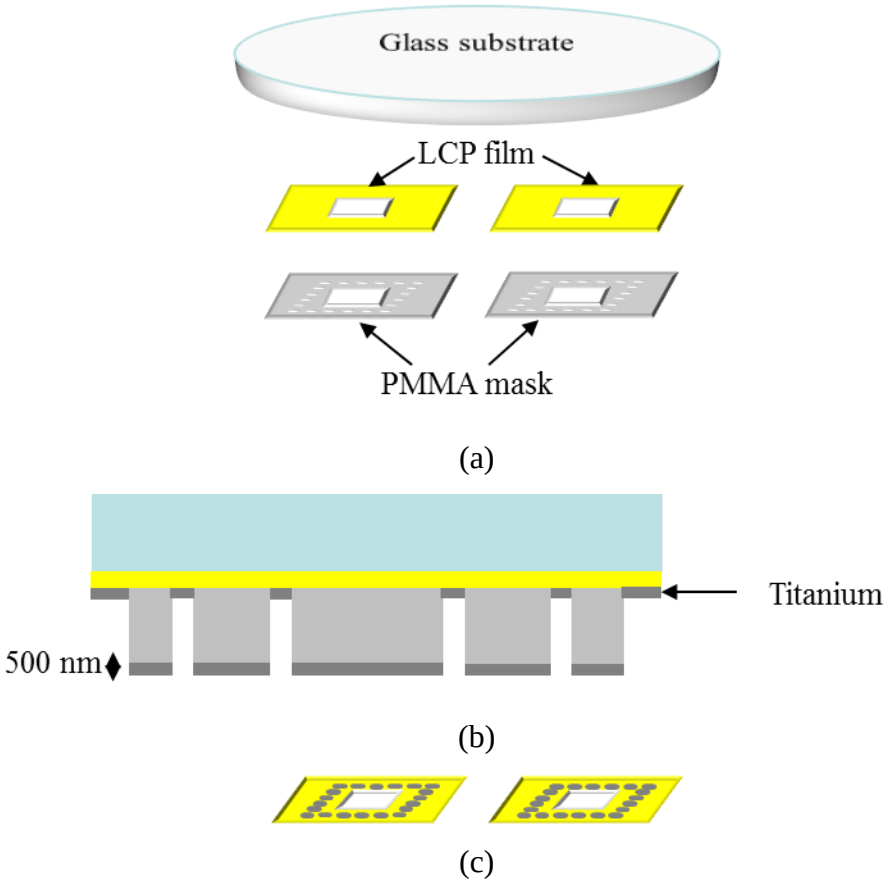

Figure 4.4: The main steps for titanium deposition on an LCP film using a shadow mask based vacuum deposition method. (a) Explosive view of the assembly for titanium deposition, (b) After titanium film deposition, and (c) Titanium film spots on LCP rings after removing the masks and the glass substrate.

Before mounting for titanium film deposition, glass substrates, PMMA masks and the LCP rings were cleaned following the steps described in section 3.3.2. The LCP rings

were fabricated using the method described in section 4.2. The deposition process for thin film spots on the LCP rings were carried out using the method which was detailed in section 3.3.3.

4.2.2 LCP Package Preparation

The LCP packages used in this study are the cavity style package designs as shown in Figure 4.5. It was designed for packaging of sensors and electronic chips for industrial applications. This package material is a 35% glass reinforced LCP polymer (Vectra S135, Ticona) with a deflection temperature of 335°C. The outer dimensions of the substrate are 8.9 mm x 8.9 mm x 2 mm and the inner dimensions are 7 mm x 7 mm by 1.5 mm. The peripheral ridge was to produce a smooth surface for LCP bonding. A silicon lid with dimensions of 10 mm x 10 mm x 0.6 mm and the ULTRALAM 3908 LCP film with the same size as the silicon lid were used for laser bonding with the LCP package.

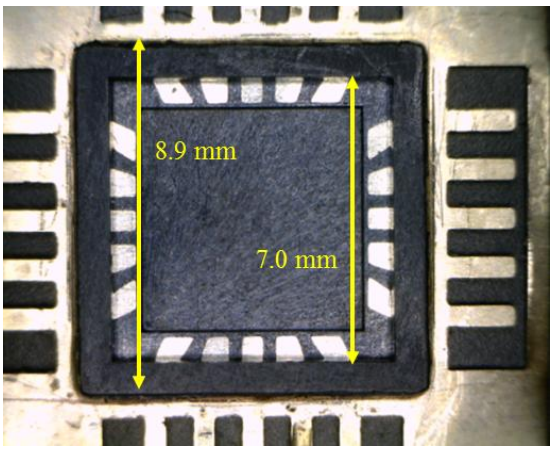

Figure 4.5: Photograph of an LCP package after polishing.

4.3 Design Configurations

The substrate and package configurations for laser based LCP bonding are shown in Figure 4.6. Glass to glass bonding in Figure 4.6 (a) is based on a square LCP ring with a thin film titanium spot pattern. The titanium film pattern absorbs laser radiation to produce the required temperature above the melting point of the LCP film in order to produce a bond between the substrate surfaces after cooling. The titanium film spots were produced by vacuum deposition. The diameter and the thickness of the spots were 0.6 mm and 500 nm respectively. The separation between the adjacent spots was 0.7 mm. The inner dimensions of the LCP ring were 4 mm x 4 mm and the width was 1.5

mm. For silicon-glass and silicon-silicon bonding as shown in Figure 4.6 (b) and (c), the silicon substrate absorbs the laser radiation for bonding. The inner diameter and width of the LCP ring were 4 mm and 1 mm. Figure 4.6 (d) shows the configuration of bonding a silicon cap to the molded LCP cavity package which is shown in Figure 4.5. In all cases the dimensions of the silicon and glass substrates were 10 mm x 10 mm. The thickness of the silicon substrate was 0.6 mm and it was 0.5 mm for the glass substrate.

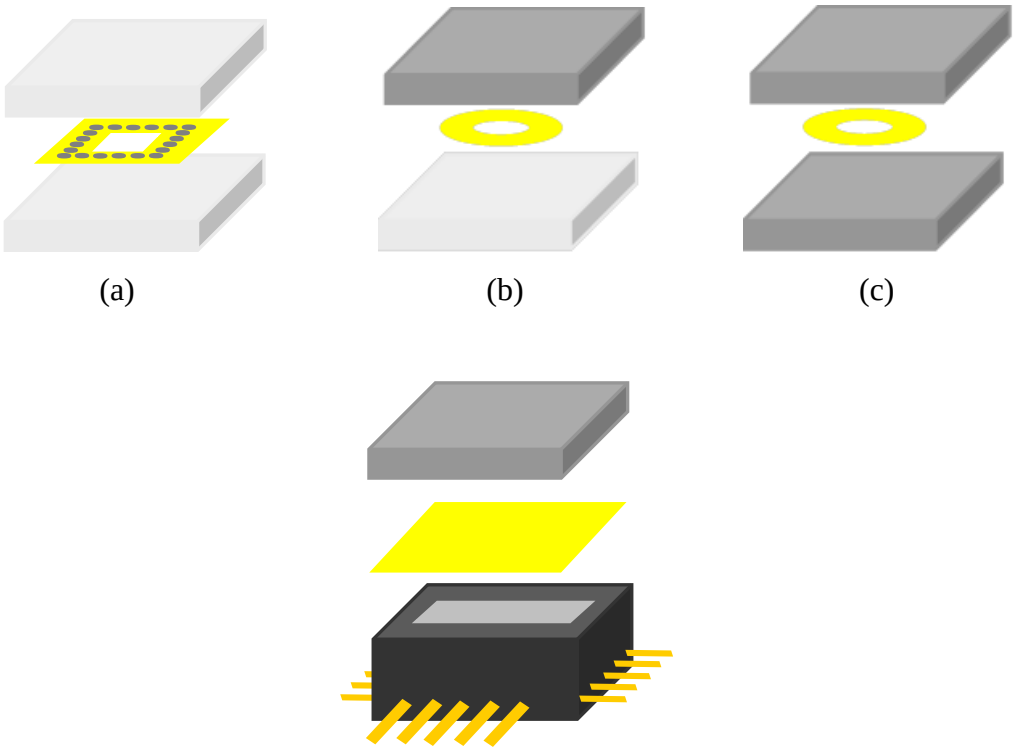

Figure 4.6: (a) Schematic view of glass to glass bonding with titanium-coated LCP film, (b) Schematic view of silicon to glass bonding with LCP ring film, (c) silicon to silicon bonding with LCP ring film and (d) Schematic view of silicon to LCP package bonding with LCP film.

4.4 Laser Assisted LCP Bonding

In this work, the same high-power diode laser system with a fiber-coupled output at 970 nm as described in Chapter 3 was used. A schematic of the experimental setup is shown in Figure 4.7. The beam transmission module consists of collimation optics followed by a focusing lens with a focal length of 20 cm. The samples were placed on an X-Y translation stage. A ceramic plate with thickness of 0.5 mm was placed under the samples to reduce thermal diffusion [23]. The glass, silicon substrates and the LCP package are aligned with the LCP film as necessary for each of the bonding configurations shown in Figure 4.6. A glass plate was placed on the sample assembly for supporting a metal ring based mechanical load. This is to ensure good contact between

the LCP ring and the surfaces of the bonding partners.

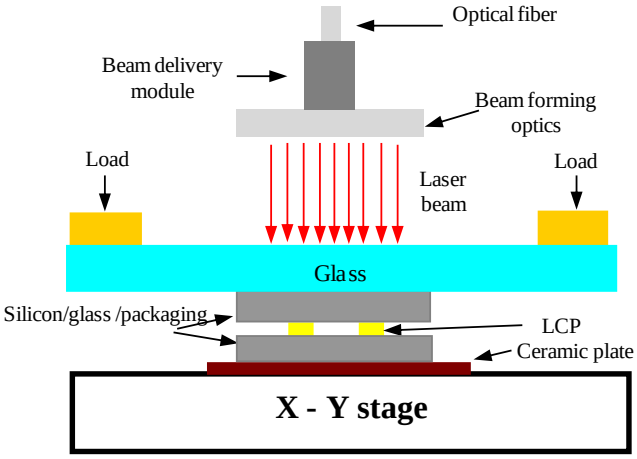

Figure 4.7: Schematic of laser bonding setup using an LCP film.

4.4.1 Glass to Glass Bonding

Basically the glass to glass bonding process with the LCP intermediate layer is a transmission bonding process. Both the lid glass and substrate glass have almost total transmission at the laser wavelength of 970 nm, and the laser beam is absorbed by the metal layer that has been deposited on intermediate LCP film. A cross-sectional view of the bonding setup is shown in Figure 4.8.

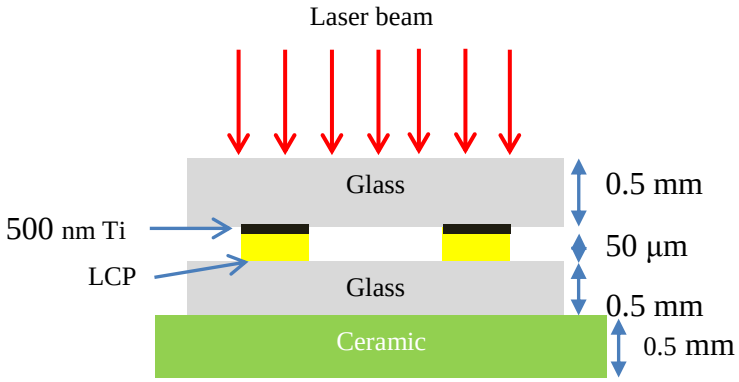

Figure 4.8: A schematic diagram of the setup for glass to glass bonding.

After laser radiation is absorbed by the titanium layer and a laser heating effect is created to melt the LCP layer for bonding purpose. A 0.5 mm thick ceramic plate was placed below the samples to reduce heat dissipation from the bonding interface.

Several initial bonding tests were carried out to determine the effects of the bonding parameters. The laser induced temperature in the LCP ring needs to be above the

melting temperature of the LCP material and in this case it is 285 ℃. A larger number of samples were tried and information obtained using different processing parameters.

As discussed above, several experiment sets were conducted to investigate the laser bonding process. In most of the traditional studies of LCP bonding, the processes were usually carried out for a few hours at different pressure and temperature conditions. But in our method, fast laser bonding can be achieved in 75 s. Two metal blocks (0.2 kg each) were placed on the top of samples resulting in successful joining with a bonding pressure of 4 N. A series of process parameters were tested, for example, 48 W for 50 s to 70 s; 45 W for 60 s to 78 s; and 43 W for 70 s to 90 s. In the case of 45 W and 78 s, LCP was over melted but in the case of 43 W and 70 s no bonding can be obtained since the temperature is below the melting point of the LCP material. After testing the optimal bonding parameters were 45 W of laser power and 75 s in bonding time. Good results were also achieved using the parameters listed in Table 4.2.

Table 4.2: Laser bonding parameters for glass to glass bonding.

Sample Number	Laser Power (W)	Bonding Time (s)
1	43	85
2	43	95
3	45	65
4	45	70
5	45	75
6	45	78
7	48	50
8	48	55
9	48	60
10	48	65

The bond quality was inspected by visual inspection. Figure 4.9 (a) shows an optical picture of a good sample with less deformation of the LCP ring, while Figure 4.9 (b) shows a sample with excessive deformation of the LCP ring. More details of reliability studies will be described in sections 4.6-4.8.

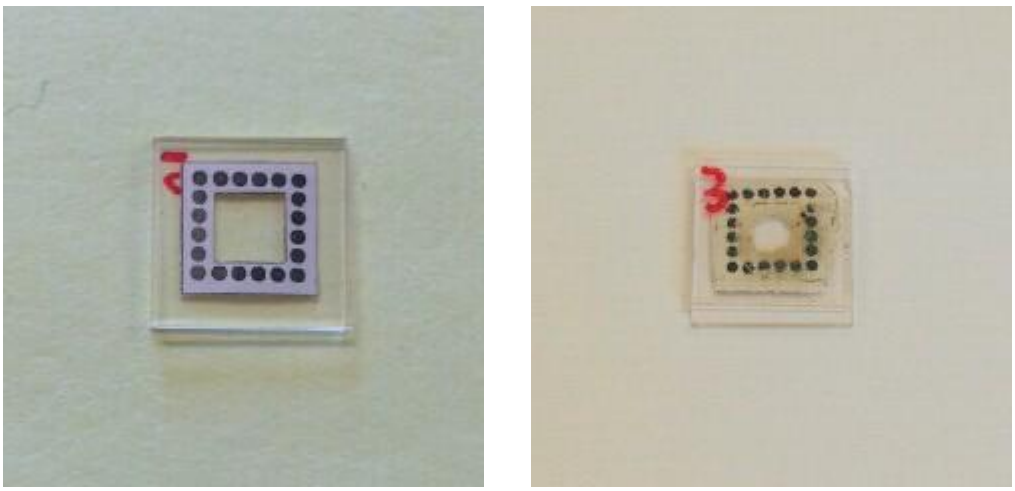

(a) (b)

Figure 4.9: Optical images of glass to glass bonding using an LCP ring. (a) Successful bonding with less LCP deformation of 48W and 60 s, and (b) excessive LCP deformation of 45 W and 78 s.

4.4.2 Silicon to Glass/Silicon Bonding

Similar to glass to glass bonding, the silicon to glass/silicon bonding process with an LCP intermediate layer was studied. However in this case the laser beam is absorbed by the top silicon substrate. Unlike silicon to glass bonding, silicon to silicon bonding with the LCP layer requires higher laser power since the thermal conductivity of silicon is two orders of magnitude higher than that of glass as shown in Table 4.3. Therefore, heat dissipation is faster resulting in low thermal efficiency of the laser heating effect [156]. A schematic of the bonding process is shown in Figure 4.10.

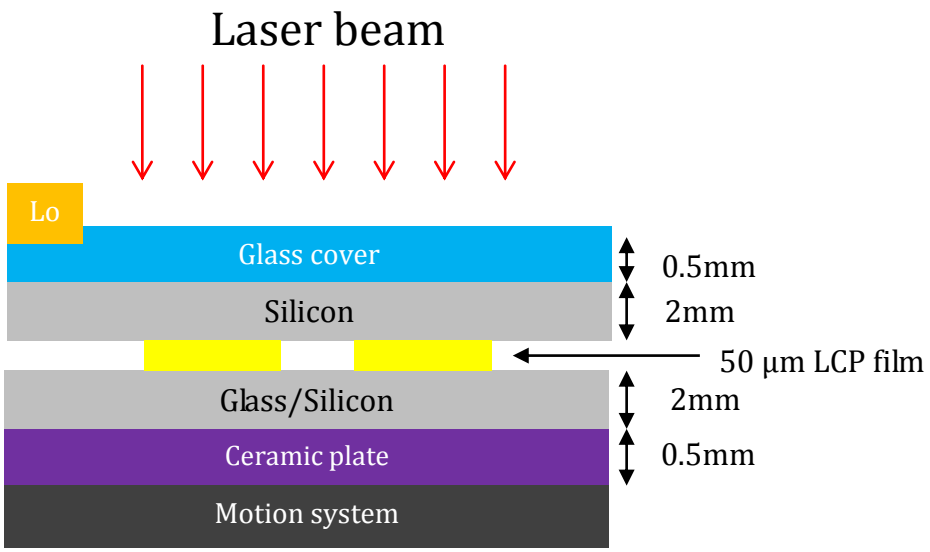

Figure 4.10: A schematic of laser bonding of silicon to glass/silicon.

Table 4.3: Thermal conductivities of substrate materials [156].

Materials	Thermal Conductivity (W/(m Ƙ))
Silicon	130
Glass	0.8-1.4
Ceramic	35
Stainless steel	237

The 0.5 mm thick ceramic plate was placed below the substrate assembly to improve the thermal efficiency of the bonding setup. The silicon and glass substrates with dimensions 10 mm x 10 mm were used. The thickness was 0.5 mm for the glass substrate or 0.6 mm for the silicon substrate. The thickness of the LCP ring is 50 μm and the inner and out diameters are 3.6 mm and 5.6 mm respectively. The load for applying the bonding force was 0.4 kg.

Several initial bonding tests were performed using different bonding parameters. A number of samples were produced under different processing parameters. A bonding force of 4 N was used for all of the samples based on the results of glass to glass bonding. For silicon to glass bonding, the processing conditions were 21 W for 55 s to 65 s, 23 W for 30 s to 45 s and 25 W for 20 s to 35 s. The time for the LCP film to reach its melting point is shorter for higher laser power. It was found that the optimal bonding parameters were 23 W for laser power and 40 s for bonding time. Good bonding results were also obtained using the parameters listed in Table 4.4.

Table 4.4: Laser bonding parameters for silicon to glass bonding.

Sample Number	Laser Power (W)	Bonding Time (s)
1	21	55
2	21	60
3	21	65
4	23	30
5	23	35
6	23	40
7	23	45
8	25	20
9	25	25
10	25	30

The quality was assessed by visual observation and good bond was indicated qualitatively by adequate but not excessive deformation of the LCP film. Figure 4.11 shows a bonded sample with less deformation of the rings and a sample with excessive deformation of the LCP rings.

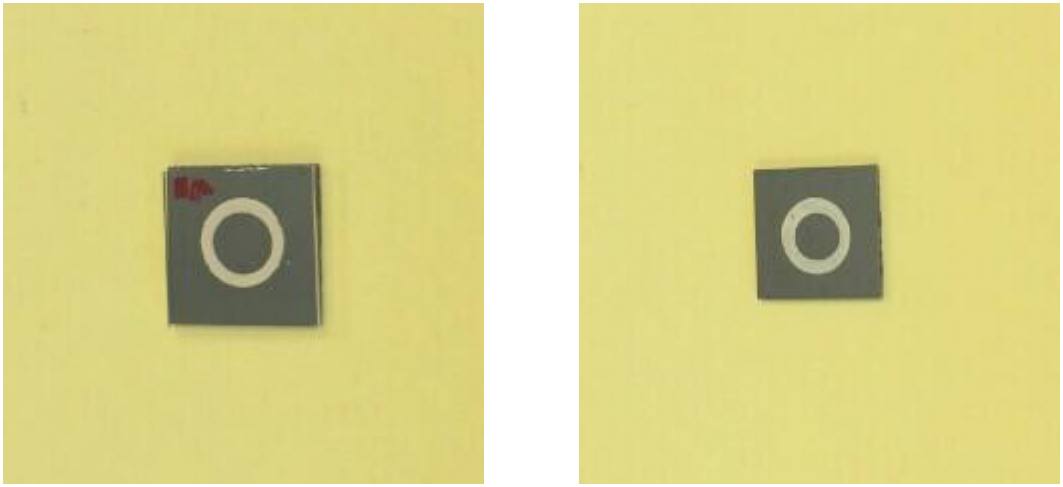

(a) (b)

Figure 4.11: Laser processing silicon to glass intermediate LCP layer result in (a) low deformation of 25 W and 25 s, and (b) high deformation of 23 W and 45 s.

For silicon to silicon bonding, a series of processing parameters were tested, for example, 32 W for 55 s to 65 s, 35 W for 30 s to 45 s and 38 W for 20 s to 35 s. Since both substrates are opaque, destructive inspection was made by breaking the bonded silicon substrates and observing the level of deformation of the LCP film. It was found the optimal bonding parameters are 35 W of laser power and 40 s of bonding time. Good bonding was also obtained based on the other parameters shown in Table 4.5.

Table 4.5: Laser bonding parameters for silicon to silicon bonding.

Sample Number	Laser Power (W)	Bonding Time (s)
1	32	55
2	32	60
3	32	65
4	35	35
5	35	40
6	35	40
7	35	45
8	38	20
9	38	25
10	38	30

4.4.3 Silicon to LCP Package Bonding

In this experiment, a silicon substrate was used as the lid for cavity style LCP package shown in Figure 4.5.

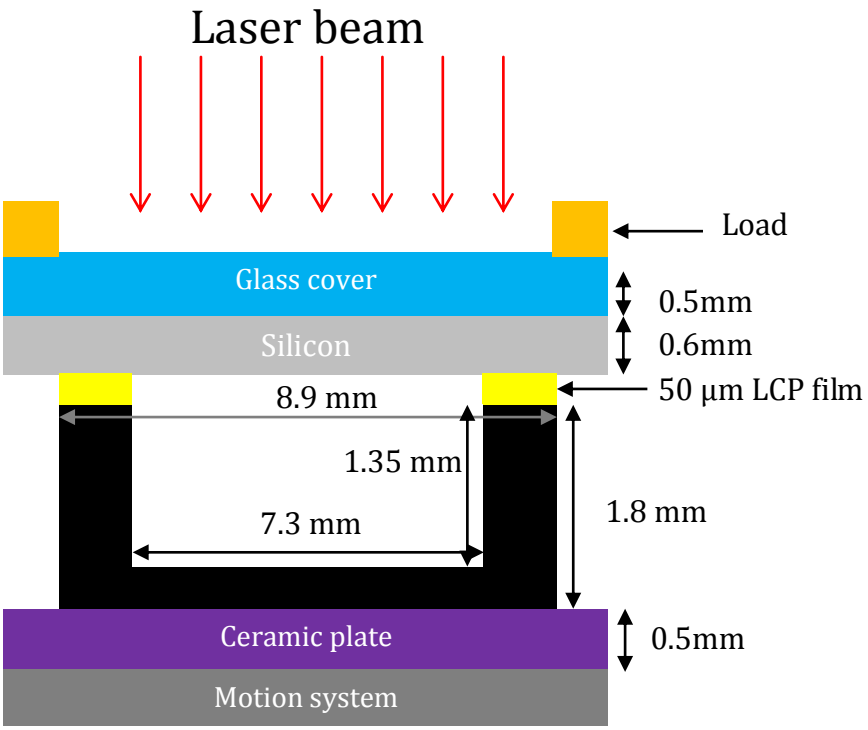

Figure 4.12: A schematic diagram of bonding of silicon lid to LCP package.

The outer dimensions of the LCP packages are 8.9 mm x 8.9 mm and the cavity dimensions are 7.3 mm x 7.3 mm by 1.35 mm deep as shown in Figure 4.12 which is a

cross-sectional view of the bonding setup. The bonding Pressure was applied to the bonding assembly using the metal-ring based load of 0.4 kg. The silicon substrate absorbs the incident laser beam to produce thermal energy to melt the LCP film to bond it to the LCP package.

A number of tests were carried out and the bonding conditions are listed in Table 4.6.

Table 4.6: Laser bonding parameters for silicon to LCP-package bonding.

Sample Number	Laser Power (W)	Bonding Time (s)
1	15	240
2	16	180
3	16	190
4	18	110
5	18	115
6	18	120
7	18	125
8	20	90
9	20	95
10	20	100

Since the quantities of LCP packages were limited, a package was used again after polishing to produce a fresh surface in the sequent bonding trial. On the other hand, if serious deformation or damage occurred after the previous bonding experiment, the LCP package was not used again.

4.5 Temperature Monitoring

Temperature monitoring provides important information about the temporal profile of the localized laser heating effect [152]. The actual bonding process will only start after the laser induced temperature has reached the melting temperature of the bonding medium, in this case, an LCP film with a melting temperature of 280°C. Figure 4.13 shows the results of temperature monitoring for the three substrate configurations shown in Figure 4.6 (a)-(c). The temperature was measured by placing the thermocouple under the bottom substrate and aligned to the center of the LCP bonding ring.

The monitored temperature was expected to be lower than the interface temperature for bonding due to the temperature gradient across the bottom substrate. Although a more accurate method for temperature monitoring using an embedded thin film sensor array has been reported [152], the method used in this work is much simpler to implement and the monitored temperature for bonding is not much lower than the expected temperature at the interface of the substrates. The behaviour of temperature increase in silicon-glass and silicon-silicon bonding are similar although a high laser power is necessary in silicon-silicon bonding. Heat dissipation when the bottom substrate is silicon is much faster than when it is glass since the thermal conductivity of silicon is about 10 times higher than silicon [152]. For glass-glass bonding the temperature rise is slower than in the other two substrate configurations. The top substrate is glass and the laser beam is absorbed selectively by the pattern of the titanium thin film spots. The rate of heat transfer is lower resulting in a longer rise time in the temperature profile. Since the absorption of the laser beam is less efficient thus requiring a higher laser power to reach the bonding temperature.

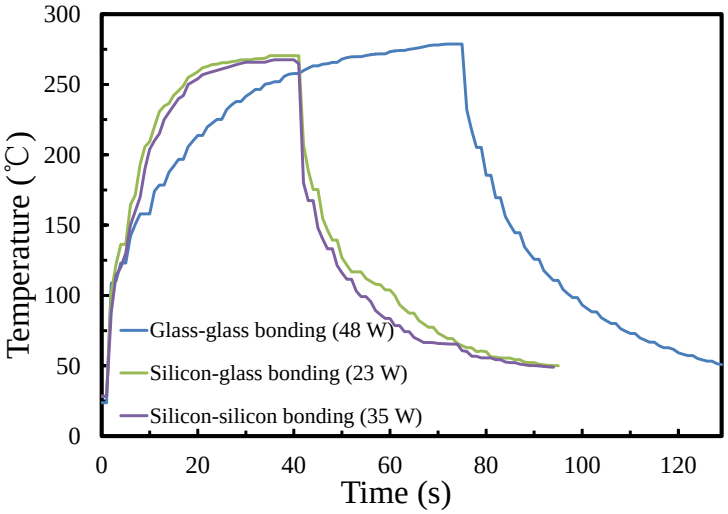

Figure 4.13: The measured temperature profile in laser bonding.

Figure 4.14 (a) shows the schematic illustration of the thermocouples embedded in the LCP packaging by drilling small holes on the package. The thermocouples were embedded in each hole using a small amount of glue. The results of temperature monitoring for bonding of silicon cap to the LCP package are shown in Figure 4.14 (b). The laser power was 20 W. The maximum temperature when the laser beam was switched off was ~270°C. This temperature is lower than the melting temperature

(280°C) of the LCP film, however the successful bonding indicates that the temperature at the bonding interface must have reached 280°C. This is because the main body of the temperature sensor is below the bonding interface and the laser induced temperature decreases below the surface of the LCP package. This is demonstrated in the output from the second sensor embedded at the center of the package base where the maximum measured temperature was only about 150°C. The more significance of the temperature monitoring work is that it illustrates one of the key advantages of the laser based bonding method, i.e. it is ideally suited to packaging of temperature sensitive devices. In this case, a temperature difference of ~ 130°C is obtained without using any active cooling as it was the case in [156] where a water-cooled copper block was used. The reason is that the thermal conductivity of LCP material is much lower than that of the ceramic package in [156] thus providing a poor heat pathway from the bonding region to the package base.

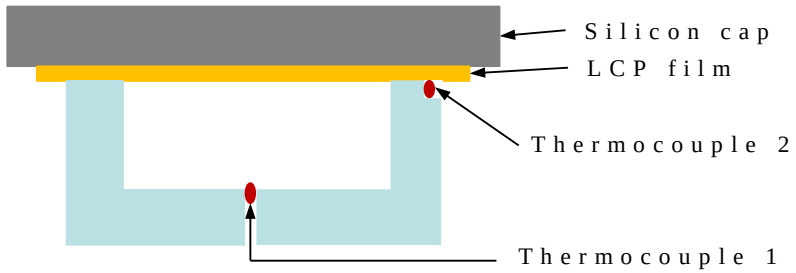

(a)

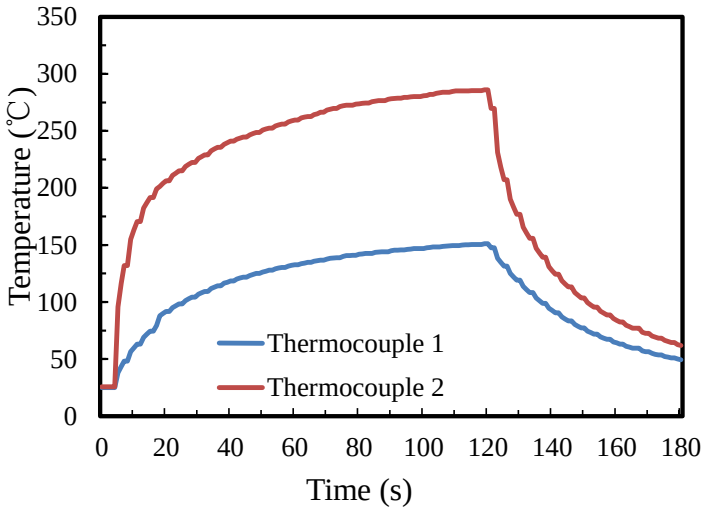

(b)

Figure 4.14: (a) A diagram showing positions of embedded thermocouples, (b) The measured temperature profiles from the thermocouples.

4.6 Cross-sectional Studies

The cross sections were prepared by dicing the selected sample followed by mechanical polishing to produce a high quality specimen for examination under an optical microscope or a scanning electron microscope (SEM).

The examples of SEM micrographs for glass to glass bonding are shown in Figure 4.15. From the pictures, it can be observed that defect free bonds can be obtained. The thicknesses of the LCP layers are 50 μm in Figure 4.15 (a) and 20 μm in Figure 4.15 (b) respectively. The results show that there is negligible change in LCP film thickness before and after bonding for the laser power and bonding time of 48 W and 75 s. However the LCP film thickness was reduced significantly for the laser power of 50 W and bonding time of 75 s. The latter is a result of significant melting of the LCP film during the bonding process when a higher laser power was used.

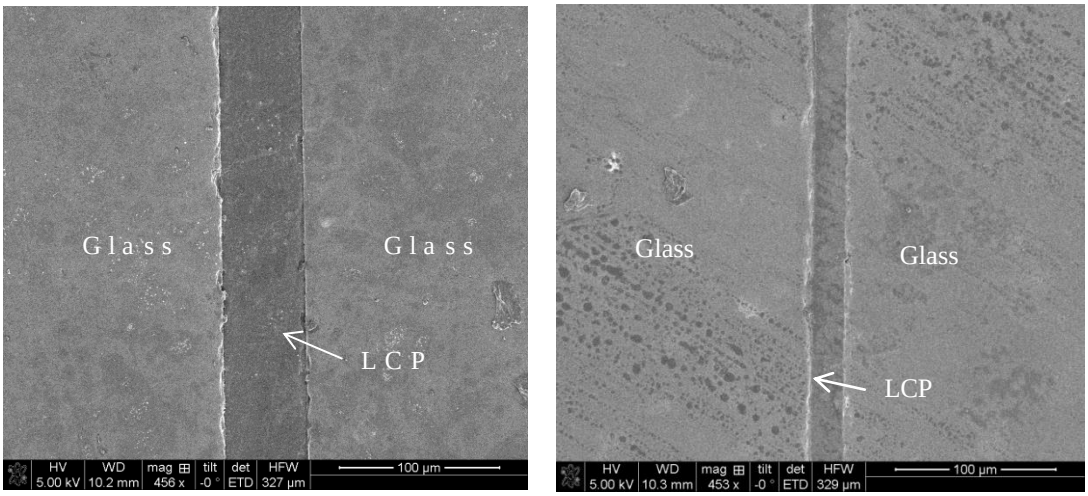

(a) (b)

Figure 4.15: SEM micrographs of samples for glass to glass bonding. (a) successful glass to glass bonding and (b) high deformation of glass to glass bonding. The thicknesses of the LCP layers are 50 μm in Figure 4.15 (a) and 20 μm in Figure 4.15 (b) respectively.

Figure 4.16 shows the cross-sectional views of silicon to glass bonding and silicon to silicon bonding samples. Although the bonding interfaces in Figure 4.16 (a) and (b) are not as clear as that in Figure 4.15, the reduction in LCP film thickness is not significant. The bonding conditions were 23 W and 40 s in Figure 4.16 (a) and were 35 W and 40 s in Figure 4.16 (b).

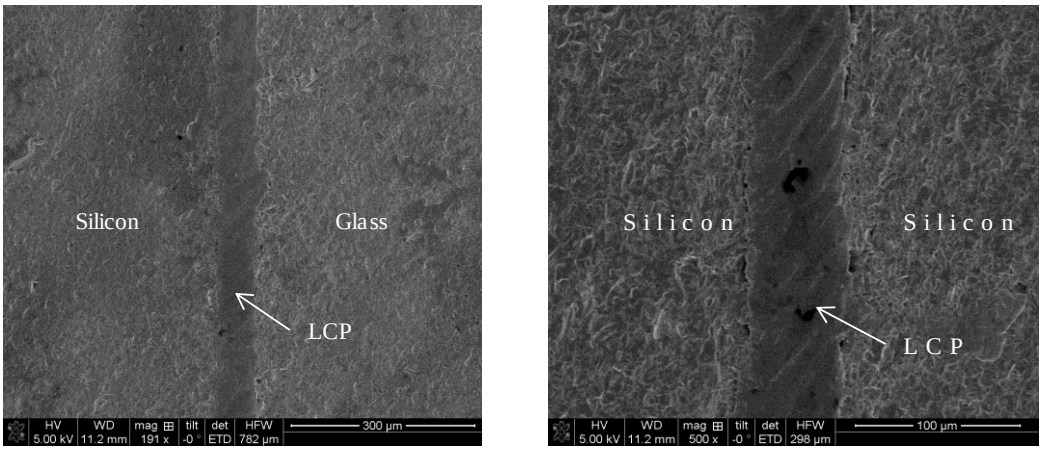

(a) (b)

Figure 4.16: SEM images of bonding interface using an LCP film, (a) Silicon and glass, and (b) Silicon and silicon. The thicknesses of the LCP layers are 40 μm in Figure 4.16 (a) and 40 μm in Figure 4.16 (b) respectively.

The SEM picture in Figure 4.17 shows that good interfacial bonding of silicon to LCP package is obtained using an LCP film. The cracks between the package and epoxy on the right of Figure 4.17 is caused during the specimen polishing process. The LCP film thickness is approximately 30 μm corresponding to the laser power of 20 W and bonding time of 120 s.

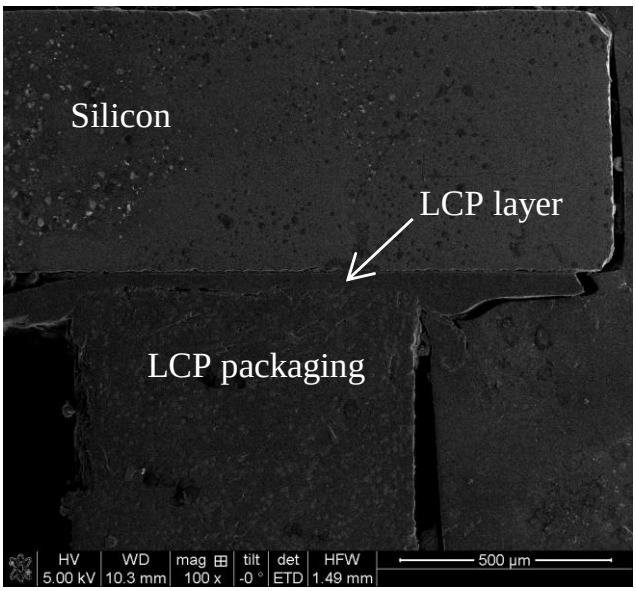

Figure 4.17: SEM images of bonding interface of silicon to LCP package with LCP layer. The thicknesses of the LCP layers is 30 μm.

4.7 Shear Force Test

Shear and tensile testing were applied to the bonded samples to measure the mechanical strength of the laser bonded samples. Since the LCP film in this thesis are being used to

bonding LCP packages, the shear test was chosen as the testing method because it provides the most useful information for LCP film that bonding LCP packages. In shear test, one of the substrates of a bonded sample is fixed in order to prevent sample movement while testing. A shear tool was applied at the edge of the other substrate to break the bond as illustrated in Figure 4.18.

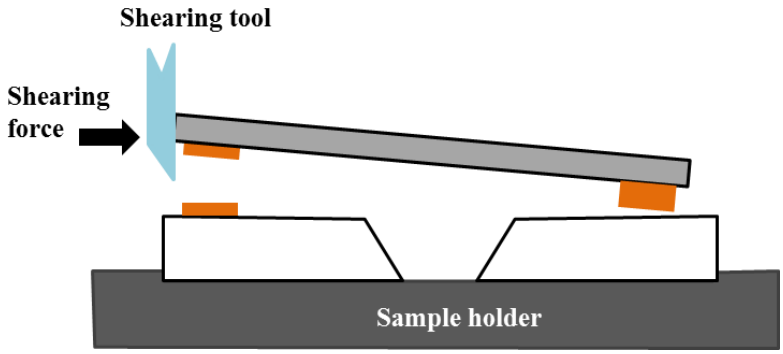

Figure 4.18: Illustration of shear test when the sample is split open [153].

For glass to glass bonding, nine bonded samples produced with three different bonding times (85 s, 75s, and 60 s) for laser powers of 43 W, 45 W and 48 W, were tested based on the procedures in MIL-STD-883G. The measurements were carried out on a commercial strength test experiment (Instron, model 2715-015). In this test the bottom substrate was fixed and the force was applied on the top glass substrate to make the sample split open. The results of the shear test are shown in Figure 4.19.

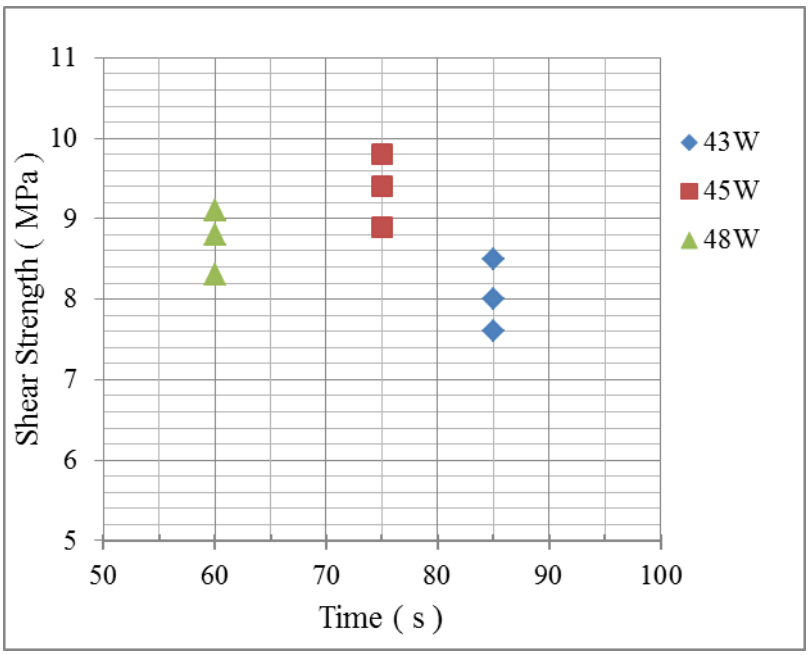

Figure 4.19: Results of shear test of glass to glass bonding samples.

According to the shear testing results in Figure 4.19, the highest and lowest bonding strengths were from the samples bonded at the laser power of 45 W for 75 s and 43 W for 85 s, respectively. After shear force tests, it was found that most elements of the LCP layer remained on the bottom glass substrate. This is because the titanium layer was deposited on the surface of the LCP film which was bonded to the top glass substrate. The titanium film spots have poor adhesion with a glass surface. Therefore, the bond strength of the LCP film to the bottom substrate is much higher than at the interface with the top glass substrate.

For silicon to glass bonding, the test samples were at laser power of 21 W, 23 W, and 25 W and bonding time of 60 s, 75 s, and 85 s, respectively. According to Figure 4.20, it can be found that the average bond strength is 7.7 MPa. After the shear test, most of the LCP residues were found on the top silicon substrate. This is probably due to the factor that the LCP material has better adhesion to silicon than glass. It could be also due to the effect of temperature gradient across the LCP layer in the bonding process.

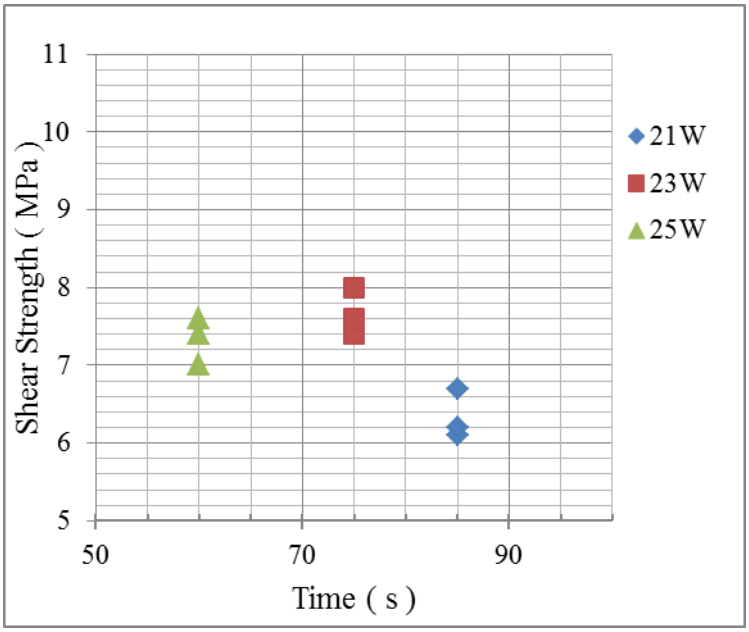

Figure 4.20: Shear test results for silicon to glass bonding.

For silicon to silicon bonding, the test samples were made at the laser power of 32 W, 35 W, and 38 W and bonding time of 60 s, 75 s, and 85 s, respectively. The laser power is much higher than silicon to glass bonding with LCP layer since the thermal conductivity of glass is two orders of amplitude lower than that of silicon. According to the Figure 4.21, it can be found that the average bond strength is 8.5 MPa. After the

shear test, the LCP ring residues were found adhered on both top and bottom silicon substrates. The results also indicate that the LCP material has better adhesion to silicon than glass when companied with the results in Figure 4.19. This is in agreement with the observation that most of the LCP ring remained on the silicon surface after the destructive test of the laser bonded silicon to glass samples.

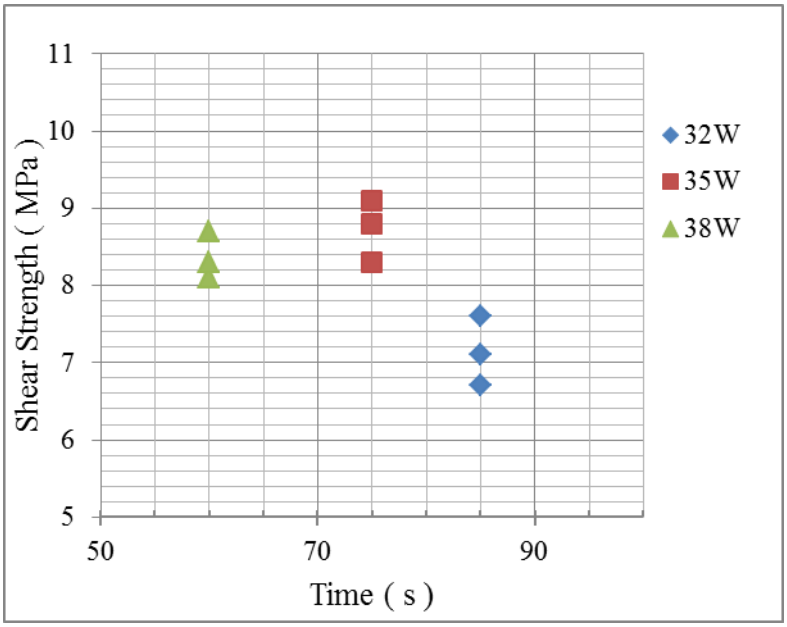

Figure 4.21: Shear test results for silicon to silicon bonding.

For silicon to LCP package bonding, the test samples were produced at the laser power of 16 W, 18 W, and 20 W and bonding time of 60 s, 75 s, and 85 s, respectively. According to Figure 4.22, it can be found that the average bond strength is 11.6 MPa. After shear test, the LCP film residues remained on both the silicon substrate and the LCP package. Several black residues from the LCP package were also seen on the LCP layer. This phenomenon indicates that the intermediate LCP layer and LCP package forms a strong good bond after laser bonding.

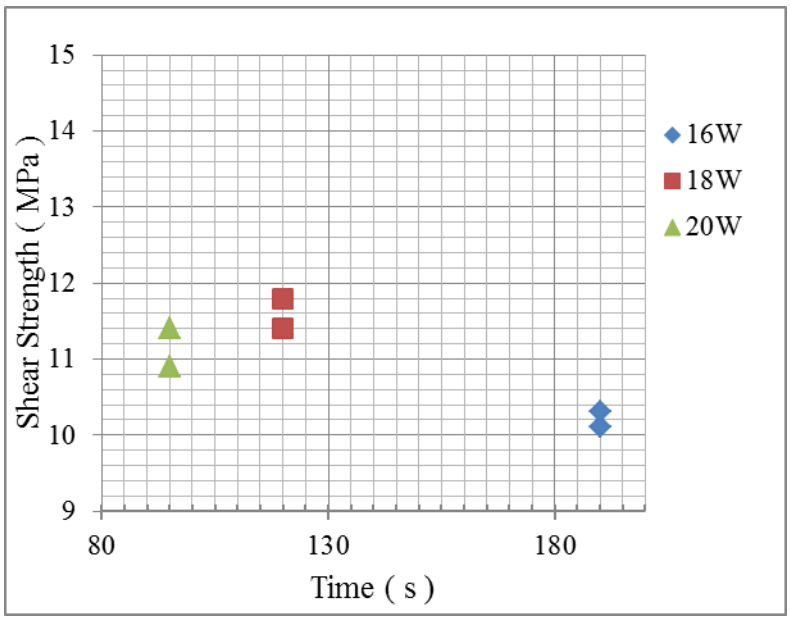

Figure 4.22: Results of shear force testing of silicon to LCP-package bonding.

4.8 Leak Testing

Two main leak test methods were used which are the gross leak test and the helium based fine leak test. In leak test, the gross leak test is carried out first and the helium based fine leak test is made for the samples which have passed the gross leak test. Another simple method for leak test is the coloured liquid based approach by immersing a bonded cavity in the liquid and observing any ingress of the liquid into the cavity. Although helium fine leak test is the most usual hermeticity test used, it is needed to be combined with a gross leak test to achieve the range of leak rate. There are also some other leak test methods in the military standards which are gross and fine leak test techniques, gross leak tests use liquids for detection and fine leak tests use a tracer gas [173]. After discussing hermeticity test, the methods to achieve the bonding strength has also been described.

4.8.1 Color Liquid Leak Testing

A coloured liquid test was performed to find any significant leak at the bonding interfaces. This method has been used before by immersing the MEMS devices into a coloured liquid for a few hours for near-hermetic testing [174], [175]. The coloured liquid can be clearly observed in the cavity if there is a significant leak through the bonded interface. In the thesis work, all of the samples were tested and all of them passed the coloured liquid test. Figure 4.23 shows the optical images of two samples for glass to glass bonding and one for silicon to glass bonding, after immersing the samples in coloured water for 24 hours. As can be seen there is no coloured liquid in the cavity

in both cases indicating good water resistance.

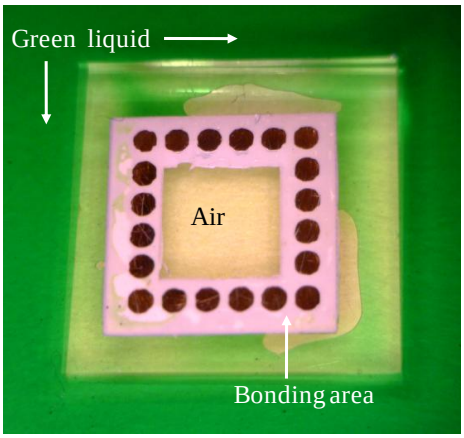

(a)

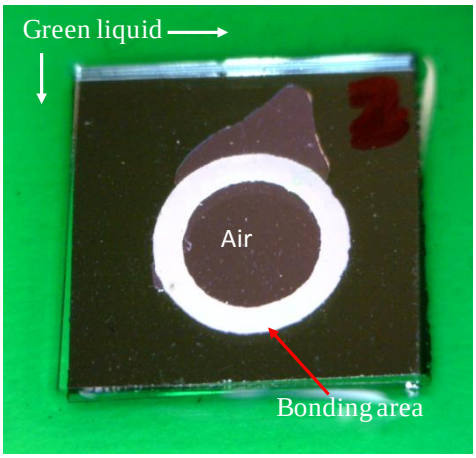

(b)

Figure 4.23: Optical pictures of bonded samples after immersion in a green color liquid for 24 hours showing no leak, (a) glass to glass bonding and (b) glass to silicon bonding.

4.8.2 Gross Leak Testing

The gross leak test was carried out based on the *MIL-STD-883E* standard for testing hermeticity of microelectronic packages. In our work, twenty samples produced under different bonding conditions were tested. Two fluorinert liquids were used, FC-84 and FC-40 respectively, with corresponding boiling temperatures of 80°C and 155°C. The samples were emerged into the FC-84 for 24 hours at room temperature, and then transferred to a beaker containing the FC-40 liquid which was placed on the hotplate at 110°C. Bubbles would emerge from the cavity if there are any defects in the bonding track causing a significant leak. Among the 21 samples we tested, 20 of them passed the gross leak test. The one which failed the gross leak test was a sample of silicon bonded to the LCP package. Subsequent destructive inspection revealed that the leak was caused by package distortion due to the overheating effect resulting from misalignment

of the laser beam.

4.8.3 Helium Based Fine Leak Testing

In the helium fine leak test method for microelectronic packages, a helium bomb chamber and a helium leak detector are used. Before the helium fine leak test, the device has to be pressurised in a helium atmosphere for 2 to 10 hours in the bomb chamber. This process is called bombing and the gas will come into the cavity if the packaged device has a leak. The amount of gas coming into the device depends on the size of the leak, the bombing pressure and the bombing time. After the helium bombing step, the device is taken from the bombing chamber and placed onto a helium leak detector chamber for a certain time [172]. The leak rate depends on the volume of helium in the device, the size of the leak and the volume of the cavity.

The reject decision for a device could be achieved in one of two ways: by using a look up table or by calculation using an equation to calculate. The test parameters and reject limits from *MIL-STD-883H T.M.1014. 13* are shown in Table 4.7 [172].

Table 4.7: Helium fine leak test parameters and reject limits from *MIL-STD-883H T.M.1014.13* [172].

Volume of package in cm^3	Bombing conditions			Reject limit atm. $cm^3.s^{-1}$ He.
	Pressure (psi) +/- 2	Min. exposure time (Hours)	Max. dwell time (hours)	
<0.05	75	2	1	5×10^{-8}
≥0.05 - <0.05	75	4	1	5×10^{-8}
≥0.5 - <1.0	45	2	1	1×10^{-7}
≥1.0 - <10	45	5	1	5×10^{-8}
≥10 - <20	45	10	1	5×10^{-8}

The through hole leak test method developed for MEMS devices is based on the technique shown in Figure 4.24. This method is based on helium fine leak test and usually for small cavities. In this method, no helium bombing is required. The test is performed using a through hole on the base of a package. The package is mounted on the helium defector using an O-ring with vacuum grease to make a sealed contact. Then helium is sprayed around the bonding ring. Leaks will be shown by the detected helium rate above the background level and this test method has sensitivity around 10^{-9} atm · cm^3 · s^{-1}. A schematic sketch of the through hole test setup is shown in Figure 4.24.

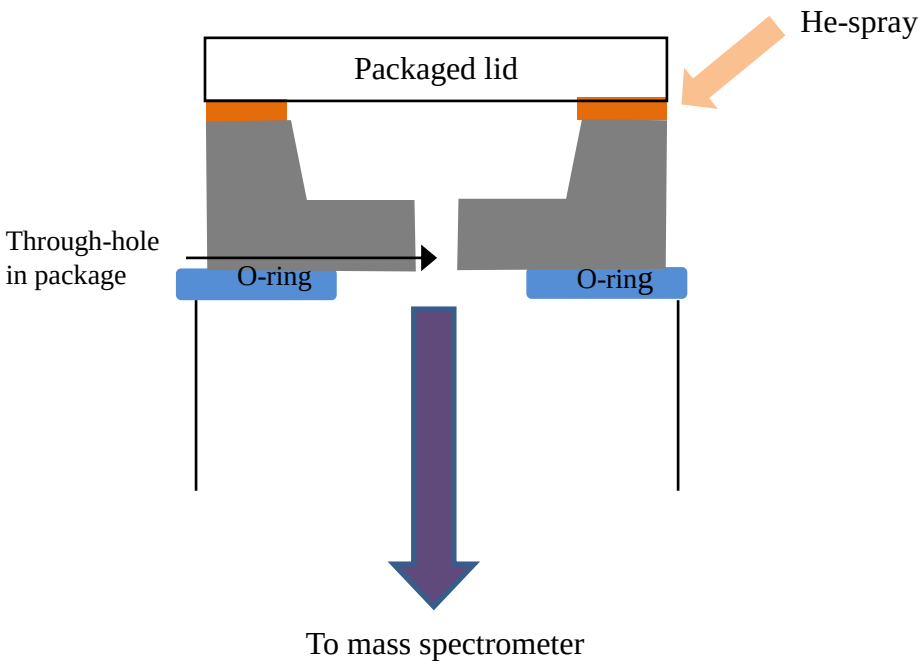

Figure 4.24: A schematic of the through-hole helium fine leak test setup.

A portable ULTRATEST UL 200 helium leak detector was used which is shown in Figure 4.25 (a). A custom designed holder shown in Figure 4.25 (b) was made and used to mount the samples for testing on the helium detector.

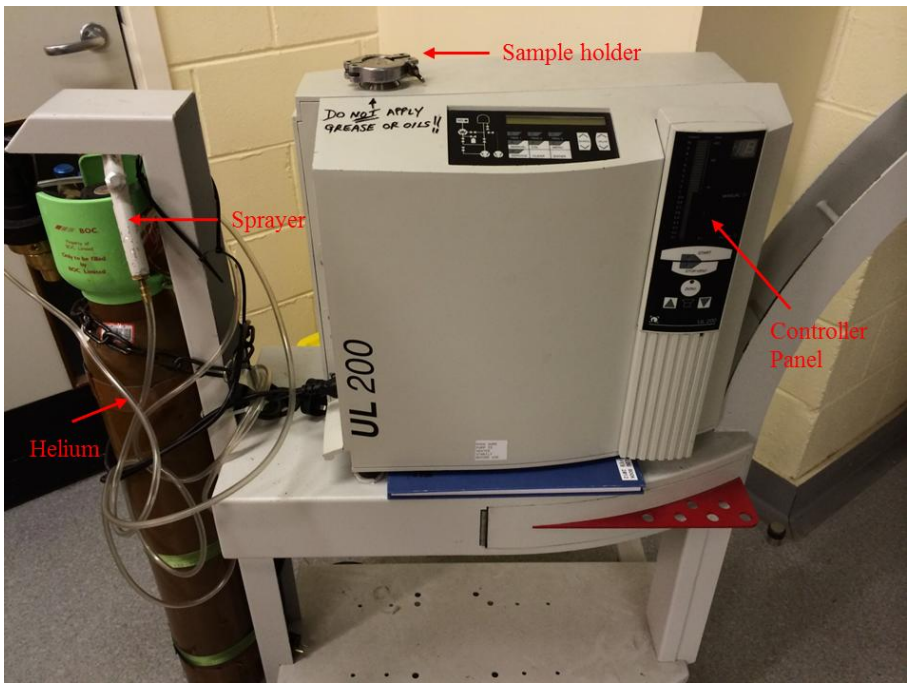

(a)

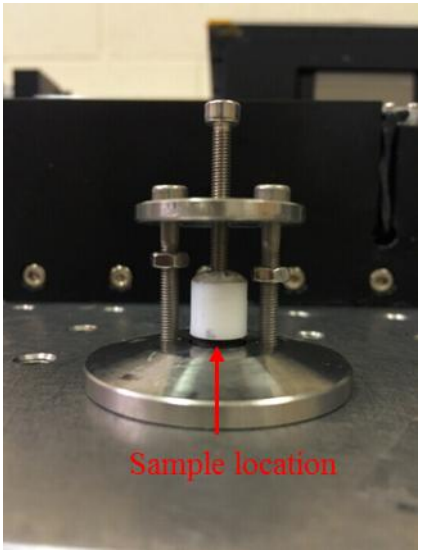

(b)

Figure 4.25: (a) A photograph of UL 200 helium leak detector and (b) a picture of sample holder.

The detection limit of the helium leak tester is about 5.5 x 10^{-11} *mbar l* s^{-1}. All of the samples used for the helium test already passed the gross leak test. For the through-hole leak test, the results of the average leak rates are shown in Table 4.8-4.11. The values of the leak rates indicate that most of the samples showed near-hermetic performance. For glass to glass bonding with laser power of 43 W and bonding time of 85, the leak rates of 8.6 x 10^{-6} *mbar l* s^{-1} was achieved and demonstrated that the samples failed the leak test because the heat of titanium is insufficient to melt the LCP to form strong bonds.

Table 4.8: Leak rate of laser bonded glass to glass cavities.

Laser Power (W)	Bonding Time (s)	Leak Rate (*mbar l* s^{-1})
43	85	8.6 x 10^{-6}
45	75	1.8 x 10^{-10}
48	60	2.1 x 10^{-10}

Table 4.9: Leak rate of laser bonded silicon to glass cavities.

Laser Power (W)	Bonding Time (s)	Leak Rate (*mbar l* s^{-1})
21	85	6.4 x 10^{-9}
23	75	2.0 x 10^{-10}
25	60	2.5 x 10^{-10}

Table 4.10: Leak rate of laser bonded silicon to silicon cavities.

Laser Power (W)	Bonding Time (s)	Leak Rate ($mbar\ l\ s^{-1}$)
32	85	2.3×10^{-10}
35	75	1.3×10^{-10}
38	60	1.9×10^{-10}

Table 4.11: Leak rate of laser bonded silicon to LCP packages.

Laser Power (W)	Bonding Time (s)	Leak Rate ($mbar\ l\ s^{-1}$)
16	190	2.6×10^{-10}
18	120	1.7×10^{-10}
20	95	1.2×10^{-10}

4.9 Conclusions

Laser bonding of the combinations of glass and silicon substrates using an LCP film has been studied. A novel laser bonding method has been studied for creating glass – glass based microcavities using an intermediate LCP film with thin film metal spots. It has been shown that the laser bonding process can be between 40 s and 120 s. Temperature monitoring methods have been used to characterize the laser induced temperature in the bonding process. In laser bonding of a silicon lid to a molded LCP package. The bonding strength of these samples was found to be high from 7.7 MPa to 11.6 MPa, which are quite high in the field of MEMS packaging. Moreover hermeticity tests were conducted and demonstrated that most of the samples passed both the gross leak and fine leak tests. A coloured liquid based leak test method was also used for the samples of glass to glass bonding. No traces of coloured water were found inside the cavity after immersion in the water for 24 hours. Cross-sectional studies were conducted to inspect the integrity of the bonding interface. The SEM micrographs show no delamination or trapped air bubbles at the interface between the substrates.

Chapter 5 Modelling and Simulation

5.1 Introduction

In Chapter 3 and 4 the experimental studies of a laser assisted polymer based bonding method were described. In this chapter, the main approach of this study is to estimate the temperature of the melting area using the laser generated heat to melt substrates. In order to achieve the optimized bonding parameters such as laser power and bonding time, it is essential to study the numerical simulation of the bonding process. For laser bonding, temperature is an important factor during the substrates fabrication processing since at the optimal temperature, the best hermeticity of devices is achieved but also the heated samples can be protected. In the process of microfluidic fabrication, the titanium layer absorbs the laser beam generate heat to melt the surrounding areas of the two PMMA substrates. But for MEMS packaging, the LCP film is melted and the cap and the substrate are bonded together after the LCP material is solidified again. The optimal bonding parameter of laser processing needs the knowledge of the estimate temperature *T*. In order to study this key factor, a two-dimensional time dependent model of heat transfer is described. The two-dimensional model results and a three-dimensional time of heat transfer model in COMSOL to determine the temperature distribution is presented.

5.2 Transfer

5.2.1 Fundamental Theory of Heat Transfer

The aim of this section is to introduce the basic concepts, equations and the parameters which affect the heat conduction required for thermal modelling of the laser bonding process. Thermal conduction is one of the most important parts in the heat transfer process. By conduction, heat transfer happens because of the molecular motion within a medium from high temperature to low temperature. From Fourier's law, the heat flux within a target is relative to the temperature gradient in the direction of the heat transfer and this law can be described as [176],

$$q_x = -k_x \frac{\partial T}{\partial X} \tag{5.1}$$

where q_x is heat flux at the x direction, k_x is thermal conductivity at the x direction and T

is temperature distribution.

In the three-dimensional Cartesian space, a normal heat conduction equation can be written as:

$$\rho C_p \frac{\partial T}{\partial x} = \frac{\partial}{\partial x}\left(k_x \frac{\partial T}{\partial x}\right) + \frac{\partial}{\partial y}\left(k_y \frac{\partial T}{\partial y}\right) + \frac{\partial}{\partial z}\left(k_z \frac{\partial T}{\partial z}\right) + Q \tag{5.2}$$

where ρ is the density of the material, C_p is the specific heat capacity, Q is the generated heat, k_x, k_y and k_z are the thermal conductivities in the x, y, z-directions, respectively.

In this work, the laser beam was absorbed by a medium (metal film or silicon) to generate heat and achieve the required temperature for bonding. The heat generation starts in terms of the laser power absorbed through the material. The top surface of the bonding setup is exposed to the air and the heat transfer is by convection. From Newton's law of cooling, the convective heat flux is described by [177],

$$q_{conv} = Ah\left(T_S - T_\infty\right) \tag{5.3}$$

where A is the area of the surface, h is convection heat transfer coefficient, T_s is the surface temperature and T_∞ is the fluid temperature. Convection can be classified as a forced or free convection depending on the flow property. For example, if the flow is caused by an external influence, a forced convection occurs. If the flow is caused by a buoyancy force due to the temperature difference in the fluid, a free convection happens. The coefficient of convective heat transfer depends on the geometry and fluid motion.

Radiation is another heat transfer mechanism generating electromagnetic waves. The difference between heat conduction and radiation is that heat conduction requires a medium but thermal radiation can pass through vacuum. The mid-range of the electromagnetic spectrum is from 0.1 μm to 100 μm including the infrared range (0.7 μm-100 μm) to generate thermal radiation [178]. A black body is defined as an object that absorbs all radiation that falls on the surface. Electromagnetic radiation is based on Planck's function which describes the spectral distribution of a black body and can be written as [178],

$$E_{\lambda b}(\lambda, T) = \frac{2\pi h c_0^2}{\lambda^5 \left[\exp\left(\frac{h c_0}{\lambda k T} \right) - 1 \right]} \tag{5.4}$$

where h (6.625 x 10^{-34} $J\,s$) and k (1.3805 x 10^{-23} J/K) are the Planck and Boltzmann constants respectively. c_o (2.998 x 10^8 m/s) is the speed of light in vacuum, T is the absolute temperature of the body, and $E_{\lambda b}(\lambda,T)$ is the spectral emissive power ($W/m^2 \cdot \mu m$).

The total power emitted by thermal radiation from a black body depends on the temperature (T) and surface area (A). Real surfaces usually emit less than the black body power, typically between 10% and 90%. The Kelvin temperature scale is used in the Stefan-Boltzmann formula because thermal radiation depends on the temperature above absolute zero. The Stefan Boltzmann law can be described as [179],

$$q_{rad} = \sigma \varepsilon \left(T_S^4 - T_\infty^4 \right) \tag{5.5}$$

where σ (5.67 x 10^{-8} $W/m^2\,K^4$) is Stefan Boltzmann constant, ε is the emissivity and T_∞ is the absolute temperature of the surroundings. In a black body, 100% of the surface energy is emitted (ε = 1.0). For a real surface, the emitted energy is a fraction of the ideal surface (ε < 1.0). The ratio of these two energy levels is the emissivity that defines the property of radiative surface and varies between zero and one.

The mathematical model in laser heating effect is based on a spatially and temporally diverse laser energy source. Since the laser beam radiates the devices from cap to the intermediate metal layer, a fraction of the incident light is reflected by the cap material and the residual laser energy going through the metal layer to heat. As most of the laser light heats the intermediate layer, with the probability of scattering, a part of the laser energy is absorbed which can be described by Beer's law [120]

$$I(z) = I_0 e^{-\alpha z} \tag{5.6}$$

where $I(z)$ is the optical intensity of a function of material depth; I_0 is the optical intensity at z=0; α is the absorption coefficient; and z is the material thickness.

5.2.2 Laser Beam Profile and Governing Equations

In this study, a top-hat shape laser beam is used as the heat source. This top-hat shape applies a uniform intensity well-defined spot to the material and enables sharp and accurate transitions in the material under process. Use of a top-hat laser beam can be prevented cracking of the thin film in substrates. In fact, a top-hat beam profile in the working plane with a steep slope is from a Gaussian-shaped beam. In most materials, the aim is to determine the effect of laser radiation on some material properties and the kind of geometry can represent an unnecessary complication. Therefore, the material is heated statically for a certain time and the intensity is always assumed to be constant over this time. These simplifications are usually necessary in order to make the issues mathematically easy or in order to reduce the computation time for numerical models. Many processes representatively involve a work-piece against a stationary beam (Figure 5.1 (a)). And the intensity of the beam may vary laterally or not (Figure 5.1(b)) [180]. In this model, the laser beam distribution is represented on Figure5.2.

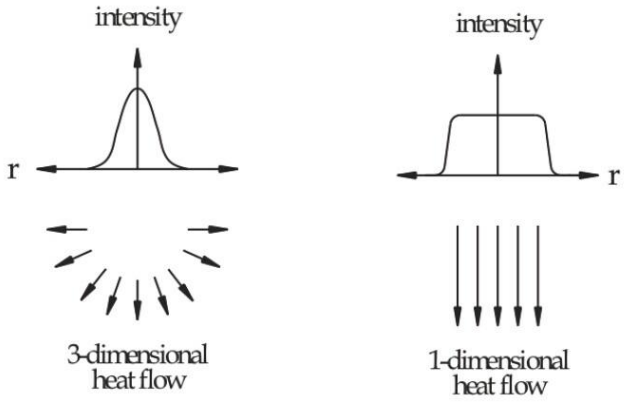

Figure 5.1: A stationary laser beam has a non-uniform intensity profile (a) Gaussian profile and (b) a top-hap profile [180].

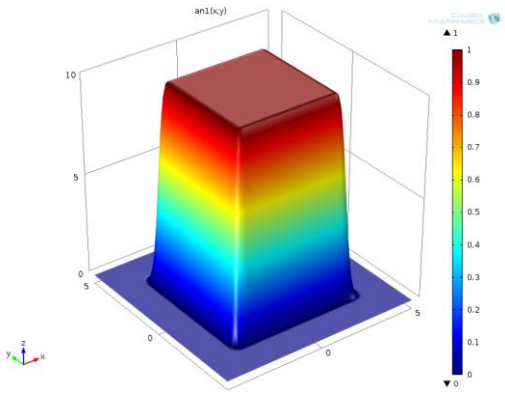

Figure 5.2: Top-hat profile of laser intensity distribution in this model.

As has been discussed above, the heat transfer law and the Beer's law is in section 5.2.1. If the intensity of laser beam is I_0 in W/m^2, then an intensity I_{in} is transmitted into the surface, where

$$I_{in} = I_o(1 - R) \tag{5.7}$$

R is the reflectivity.

Then the optical intensity decays exponentially inside the material is below:

$$I_Z = I_{in} \exp(-\alpha z) \tag{5.8}$$

where α is the optical absorption coefficient. Therefore, the general source in W/cm^3 is

$$Q = \alpha I_Z = \alpha I_0(1 - R)\exp(-\alpha z) \tag{5.9}$$

5.3 Properties of Materials

The main materials described in this chapter are PMMA, substrates and titanium thin films. Their thermo-physical properties at room temperature are listed in Table 5.1 [181,182].

Table 5.1: Physical properties of the material at room temperature [6, 7].

	Thermal conductivity (W/m K)	Density (g/cm^3)	Specific heat (J/kg K)	Melting temperature (℃)
PMMA	0.19	1.18	1466	160
Titanium	21.9	4.50	530	1668

When the temperature is close to the melting temperature of crystalline materials and the glass transition temperature of amorphous materials, the specific heat of the plastic is increased. PMMA produced by radical polymerization is atactic and totally amorphous [181]. Amorphous polymers have a lower thermal conductivity than semi-crystalline polymers and the thermal conductivity rises gradually up to glass transition temperature followed by a slow decrease [183, 184]. The temperature-dependent behaviours of the thermal conductivity of PMMA polymers are

shown in Figure 5.3 [185]. Since the PMMA material used in the thesis work is an amorphous material, the thermal conductivity does not change significantly over the temperature range between 150 ℃ and 200 ℃.

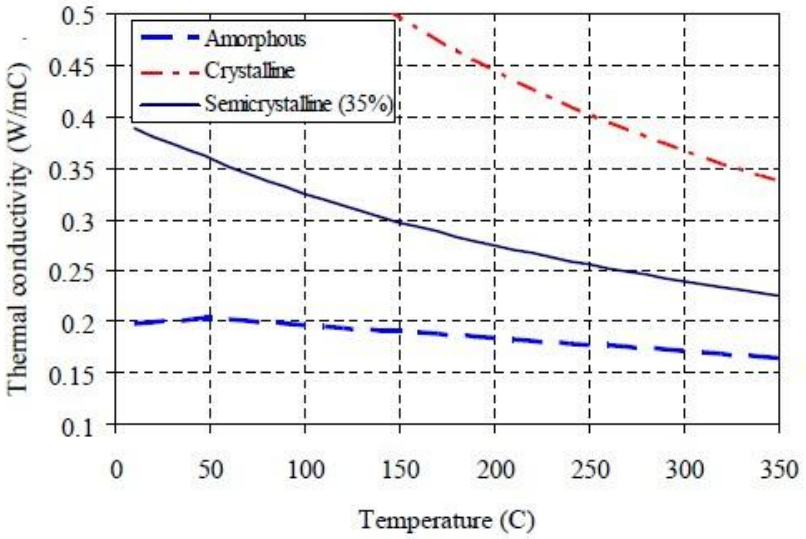

Figure 5.3: Thermal conductivity vs. temperature for amorphous [185].

Because the PMMA substrate has excellent transmission as shown in Figure 5.4 [186] at the laser wavelength, the titanium film is necessary to absorb the laser energy. This model is based on the stationary laser power to heat thin titanium film and analyze the accompanying temperature change in the material.

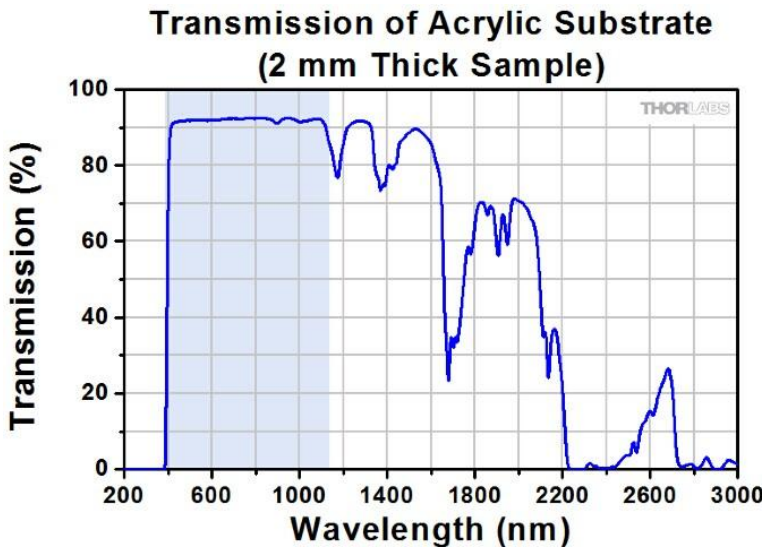

Figure 5.4: Transmission of acrylic substrate [186].

In the section of laser heating MEMS modelling, silicon as an important material is

highlighted and discussed including its optical properties and thermal conductivity which is temperature-dependent. The high reflectivity at wavelength of 970 nm on monocrystalline silicon is 31% and the reflectivity of silicon is shown in Figure 5.5 [187].

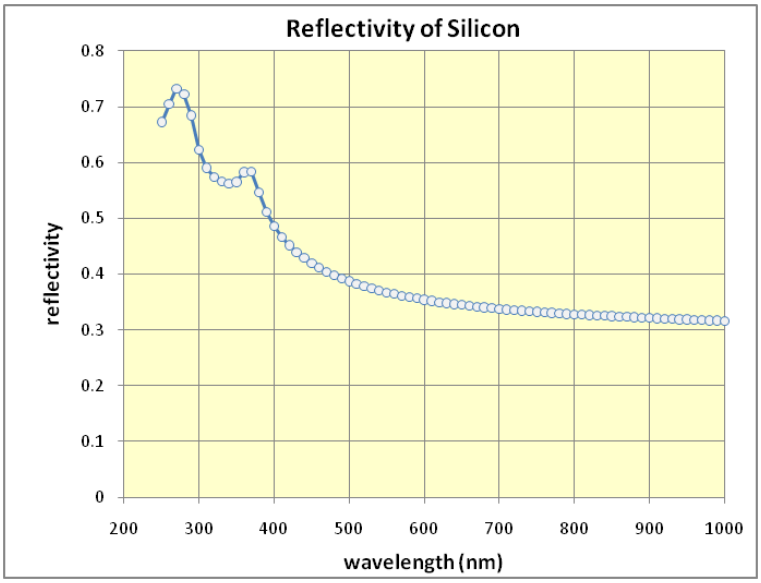

Figure 5.5: The reflectivity of silicon of different wavelength [187].

The absorption coefficient of silicon is extremely important for applications in semiconductor processing and MEMS packaging. It defines the penetration depth at which light of a certain wavelength penetrates into the semiconductor. If a material has a low absorption coefficient, light is barely absorbed. But if the material is thin enough, it would be transparent to the wavelength. So the absorption coefficient depends on the material and also on the wavelength of light. Because of light that has low energy below the band gap does not have enough energy to active an electron into the conduction band from the valence band, the semiconductor materials have a sharp edge in the absorption coefficient. The absorption coefficient for silicon is shown in Fig. 5.6.

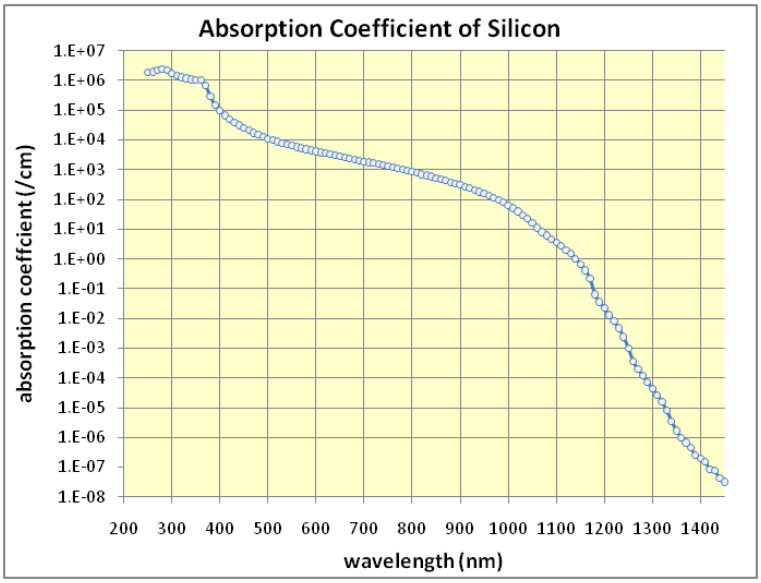

Figure 5.6: Absorption coefficient of silicon [187].

The absorption depth, $\delta \approx 1$ μm, depends on optical properties of silicon, refractive index n_1 and extinction coefficient n_2. The refractive index and the relationship between the assumption coefficient and assumption length are given by,

$$n = n_1 + in_2 \tag{5.10}$$

and the absorption coefficient α can be expressed by:

$$\alpha = \frac{2\omega n_2}{c} = \frac{4\pi n_2}{\lambda} = \frac{1}{\delta} \tag{5.11}$$

where ω is the angular frequency, c is the speed of light and λ is the wavelength. n_1 and n_2 are the real and imaginary parts of the refractive index. n_2 is also referred to as distraction coefficient . The penetration depth in silicon is shown in Figure 5.7.

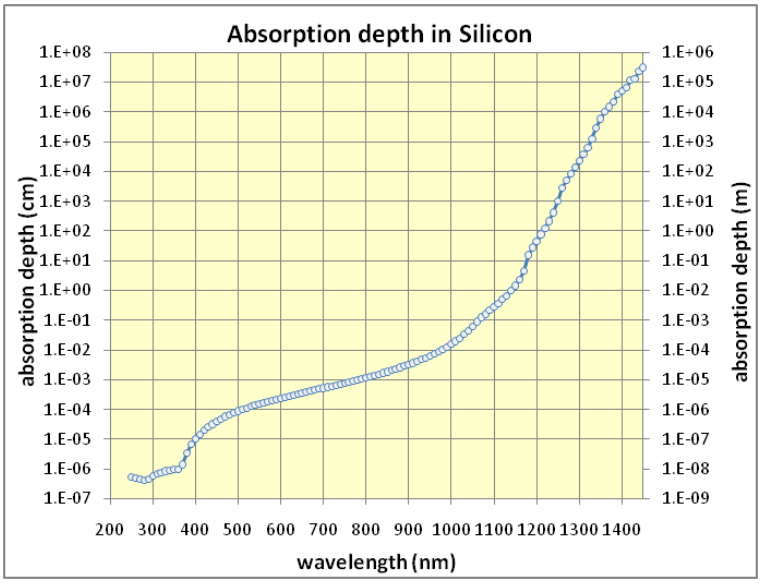

Figure 5.7: The absorption depth of silicon [187].

5.4 Software Tool For Modeling and Simulation

A commercial software, COMSOL Multiphysics, is used to carry out the simulation work. There are nearly 26 different modules to provide software solutions for multiphysics problems available as software packages. These modules can be easily applied to solve many engineering and physics problems. In addition to conventional physics-based user-interfaces, COMSOL also provides for entering coupled systems of partial differential equation (PDE). The COMSOL software has a powerful integrated desktop interface with a built-in model builder that one can use to enter all of the design dimensions and achieve an overview of the model. With the flexible graphical user interface (GUI) of COMSOL, one can work on several physical interfaces and carry out stationary and time dependent, linear and non-linear studies, eigen frequency and modal and frequency response based studies. COMSOL can also be used in conjunction with Matlab to perform data analysis and visualization, numerical computation, algorithm development, and application development. In the COMSOL Multiphysics tool, it solves the equations with the finite element method. In the physics interface builder, the materials and their physical properties and defining parameters are listed [188].

In this work the heat transfer module is used, and in this module all of the heat transfer effects including conduction, convection and radiation are included. The module for heat Transfer in solids was used in the work. Figure 5.8 shows sub-modules available in the heat transfer module. All of the modules can be applied in 1D, 1D axisymmetric, 2D, 2D axisymmetric and 3D for both stationary and time dependent studies. The

three-dimensional time dependent model for heat transfer in solids is used in this thesis. This deals with heat transfer by conduction based on the associated equation in the module.

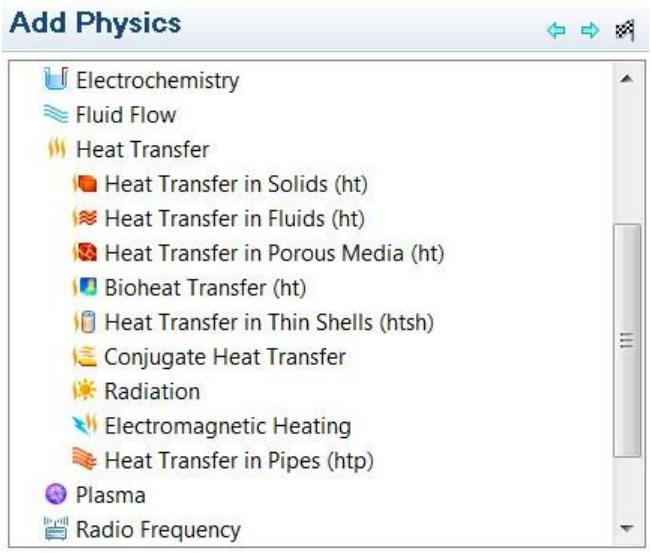

Figure 5.8: The interface of Heat Transfer Module.

5.5 Modelling of Laser Transmission Microfluidic of PMMA Substrates

5.5.1 Model Implementation

Figure 5.9 shows a schematic cross-sectional view of the substrate assembly in microfluidic of two PMMA plates described in section 3.4.2. The diameter of titanium spots is 1 mm. Two corresponding layouts are implemented in the user interface of the COMSOL tool as shown in Figure 5.10. All of the layers in Figure 5.9 and their dimensions are included in the model for simulation.

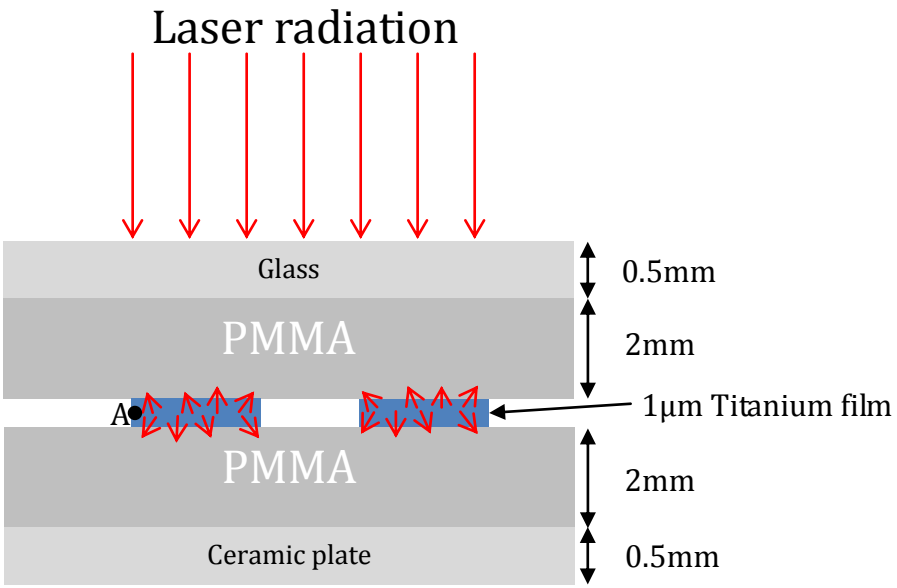

Figure 5.9: Schematic of laser bonding PMMA substrates.

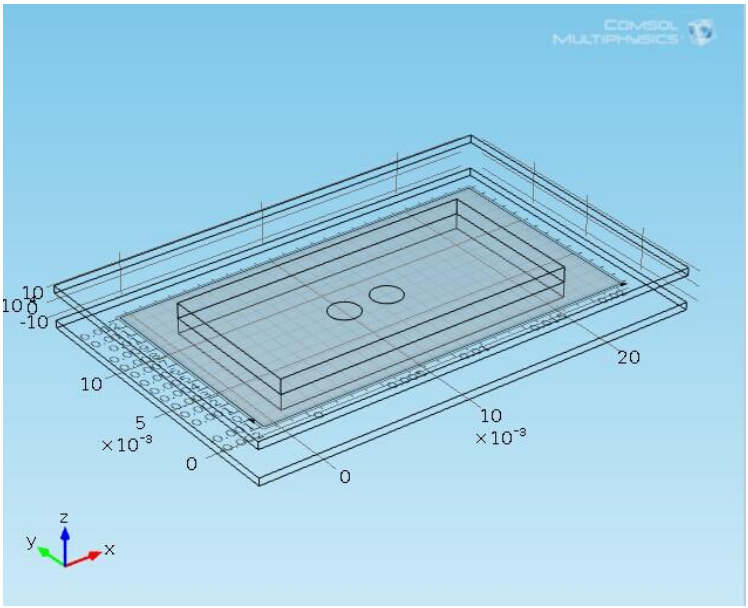

Figure 5.10: The 3D thermal model geometry of PMMA bonding configuration.

In the first step of this study, it is assumed that most of the laser power is transmitted through the top glass cover and the PMMA substrate to reach the intermediate titanium film and is absorbed totally by the titanium film. The sample used in the experiments is modelled in Figure 5.10. The dimensions of the glass cover and ceramic plate are 30 x 20 x 0.5 mm^3. And the dimensions of both PMMA substrates are 20 x 10 x 2 mm^3. The titanium film absorbs by laser energy to heat both PMMA substrates while the ceramic plate acts as an insulator.

In this model, the heat loss at the top surface of the glass cover and the edge surfaces of the assembly substrate is by convection to the environment because they are exposed to the surrounding air medium. An average heat transfer coefficient of h = 2 W/m^2 K is used for free convection correlations and the initial external temperature is 293.15 K. The rest of the surfaces are assumed to be adiabatic. As discussed before, the ceramic plate placed under the PMMA substrates can effectively reduce heat dissipation into the bottom metal platform. Figure 5.11 shows the mesh configuration in the simulation work, two intermediate titanium film parts are finely meshed to ensure the simulation accuracy and efficiency. The thickness of the titanium film layer is very small and it is between two PMMA substrates, consequently the mesh number of the titanium layer is significant. The material properties which are used in this modeling and simulation work are summarized in Table 5.2.

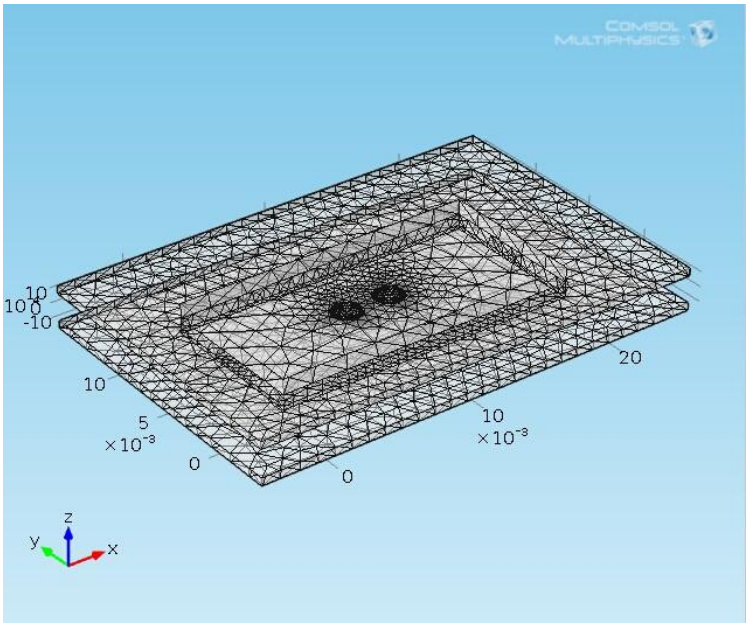

Figure 5.11: The mesh configuration of PMMA bonding.

Table 5.2: Thermo-physical properties of the materials [13].

	K(W/m ‐K)	Cp(J/kg ‐K)	ρ(kg/m^3)
PMMA	0.19	1420	1180
Titanium	21.9	522	4506
Glass	1.1	480	2200
Al_2O_3	30	730	3965
Steel	228	475	7850

5.5.2 Results and Discussion

The numerical simulations are intended to understand the influence of the bonding setup and conditions on the laser microwelding process. Figure 5.12 shows the results of evolution of the temperature distributions surrounding the laser heated titanium films. The maximum temperature of the titanium film is 500 K (200 ℃). The temperature of each titanium film and the heat affected zone both increase as time from the onset of the laser radiation.

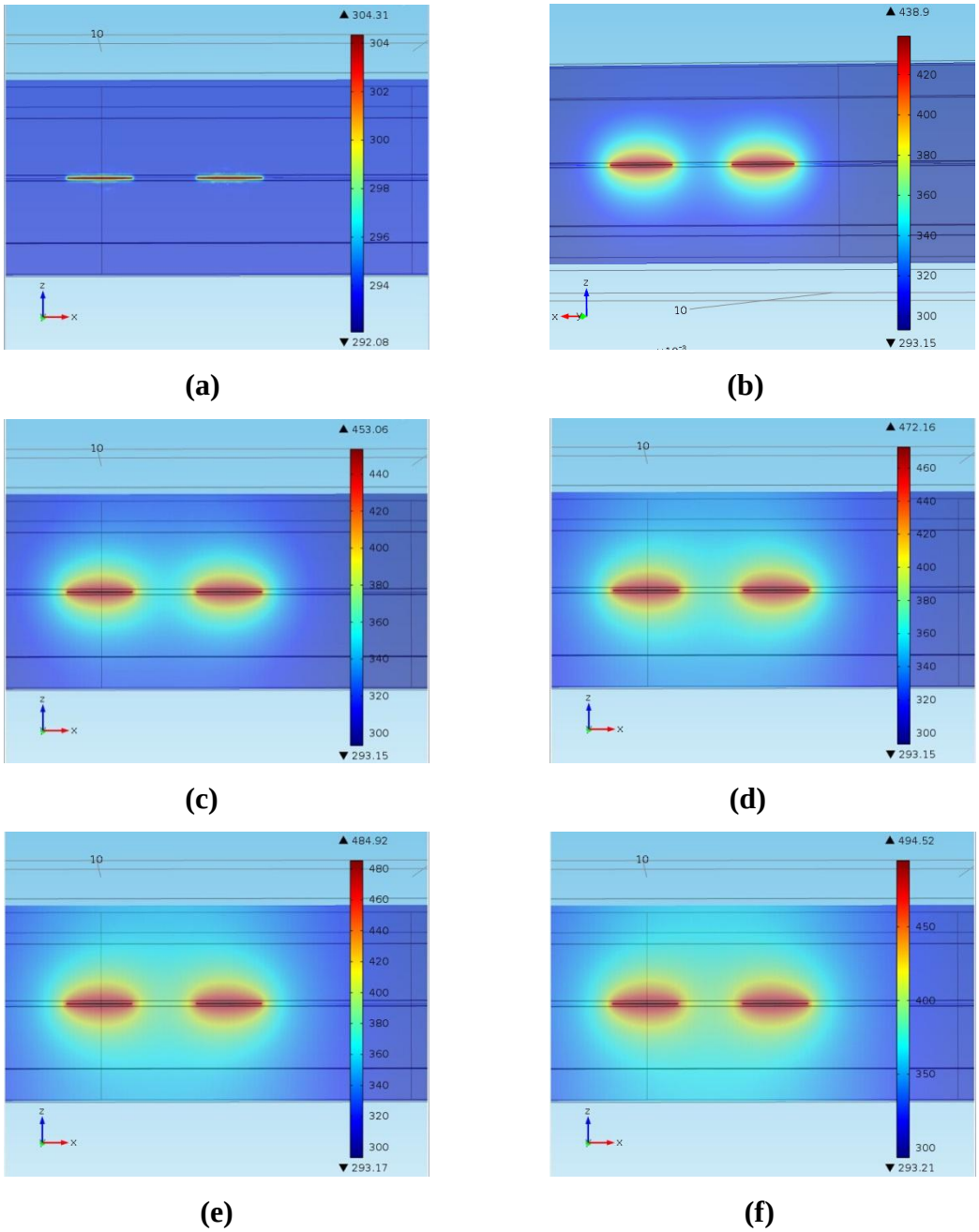

Figure 5.12: Temperature contours of time-dependent thermal modelling (input power is 25 W), (a) 1 s, (b) 3 s, (c) 5 s, (d) 10 s, (e) 15 s, and (f) 20 s.

Figure 5.13 shows the temperature at point 'A' (Figure 5.9) as a function of time. The temperature increases rapidly to about 430 K in 2 s and then gradually rises to 480 K in 18 s. From the results it is found that although the temperature at the edge of titanium layer is increased to 480 K, the temperature at the center of titanium film is nearly 500 K which is 20 K higher than temperature at the edge. It is because after the laser beam heating process, the titanium film absorbs the laser energy and the generated heat diffuses into the surrounding PMMA material. But the heat is mostly concentrated at the center of two metal films.

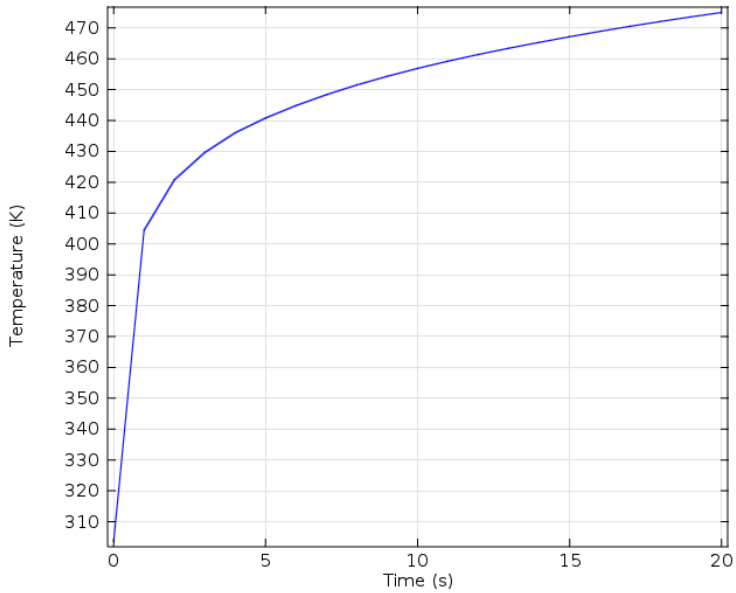

Figure 5.13: Temperature distribution of the edge (point 'A') of titanium film.

Figure 5.14 shows the temperature distribution across the centers of the two titanium film spots at several time intervals. The temperature in the center of the titanium film increases from 293 K to 430 K (137 ℃), 460 K (167 ℃) and 475 K (182 ℃) after 4 s, 12 s and 20s respectively. From Figure 5.14, it can be observed that the two peaks with the highest temperature correspond to the two circular titanium layers. Following the laser radiation, the two circular titanium layers generate heat which melts the surrounding area of the PMMA substrates to form a strong bond after the laser radiation is removed.

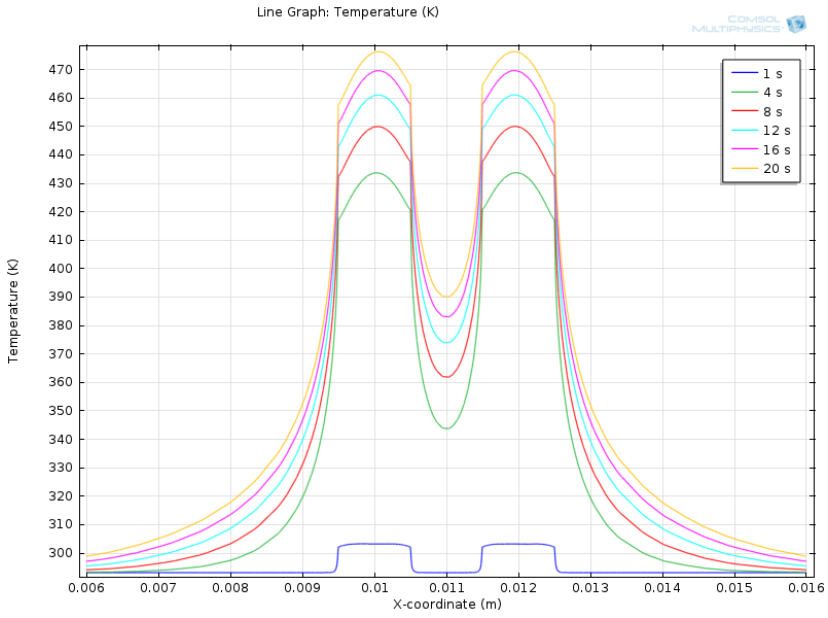

Figure 5.14: Temperature distribution of the interface between PMMA and PMMA substrates.

In order to study the effect of the ceramic plate, the simulation work is repeated at the

ceramic plate is removed from the setup as shown in Figure 5.9. In this case the PMMA substrate assembly is placed on the steel platform. Figure 5.15 shows the temperature distributions. Although the highest temperature can rise to 450 K (157 ℃), it is lower than the corresponding temperature of 500 K in Figure 5.14. This is because that thermal dissipation is faster when the bottom PMMA substrate is in direct contact with the steel plate since the thermal conductivity of the steel plate is two orders of magnitude higher than that of the ceramic plate. The results are in agreement with the experimental work described in section 3.5.3 which showed that a higher power by ~10% is necessary for laser microwelding of PMMA substrates when the ceramic plate was not used. Figure 5.16 shows the temperature distribution for the bonding setup shown in Figure 5.9.

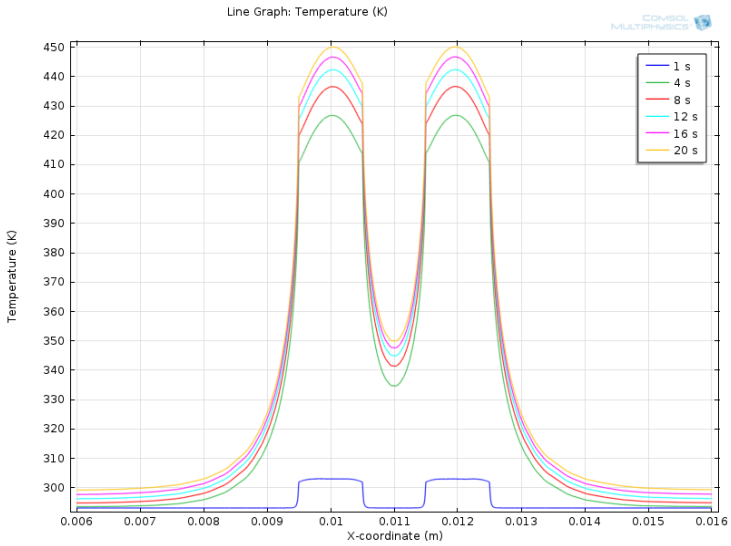

Figure 5.15: Temperature distribution of PMMA substrates bonding with a steel plate placed on the bottom.

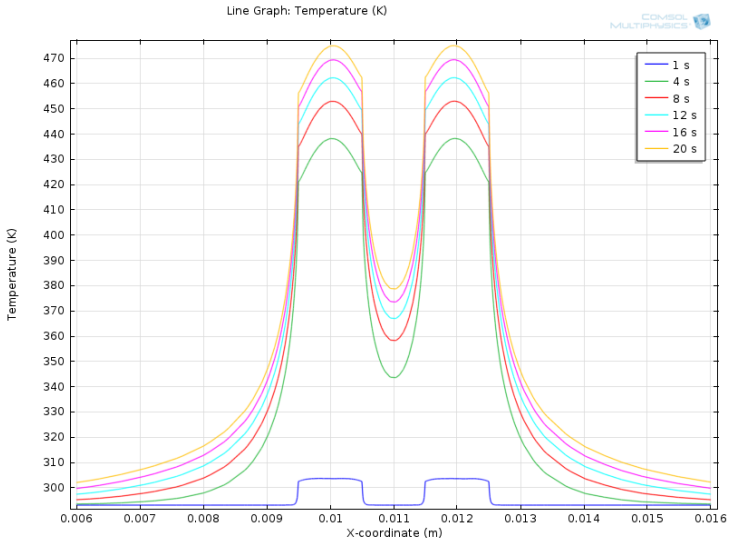

Figure 5.16: Temperature distribution of PMMA substrates bonding with glass cap and ceramic at bottom.

In order to understand more details of PMMA to PMMA substrate bonding, it is necessary to analyze the temperature distribution in the Z direction across the substrate assembly. Figure 5.17 shows the temperature distribution across the PMMA substrates, it is assumed that the PMMA substrate assembly is free standing without the rest of the experimental setup shown in Figure 5.9. The highest temperature at the interface between the two PMMA substrates is approximate 475 K (182 ℃) after 20 s. The temperature in the top and bottom PMMA substrates decreases away from their interface. The temperature distribution is symmetric with respect to the interface as expected since the substrate arrangement is a symmetric configuration.

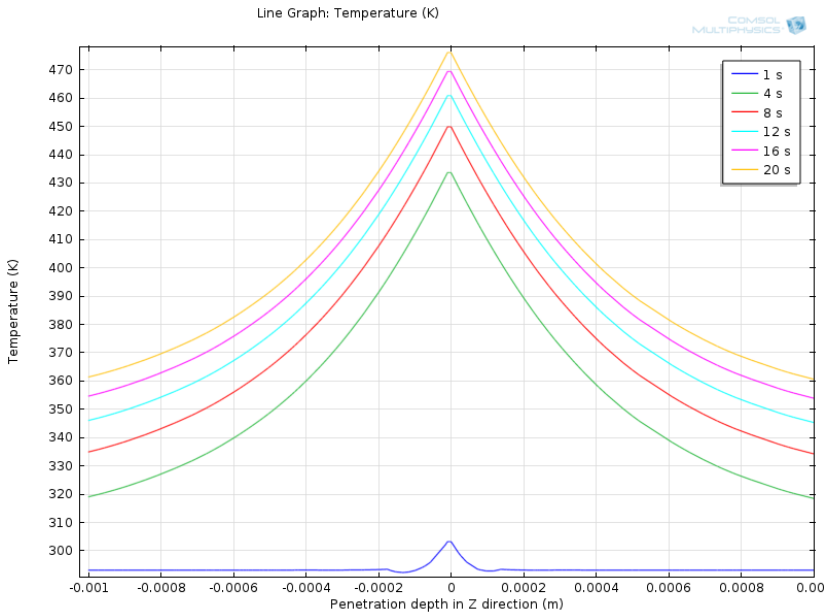

Figure 5.17: Temperature distribution from the top PMMA substrate to bottom PMMA substrate in Z direction.

Figure 5.18 shows the results for the bonding setup shown in Figure 5.9 but without the ceramic plate. From Figure 5.18, it can be seen that the temperature distribution in the top PMMA and bottom PMMA substrate is different since the steel plate with high thermal conductivity removes the heat faster from the bottom PMMA substrate. Therefore, when the steel plate is placed under the PMMA substrates, the temperature in the bottom PMMA substrate decreases faster towards the steel plate. Another phenomenon is that the temperature distribution in the bottom steel plate is close to the initial temperature (293 K) since much faster conduction of heat away from the interface. In this case, it is useful for assembly of microfluidic devices if the bottom substrate with channel structures which are more sensitive to temperature. But in this case a higher laser power would be necessary in order to produce the required

temperature since the bonding interface to achieve joining of the substrates.

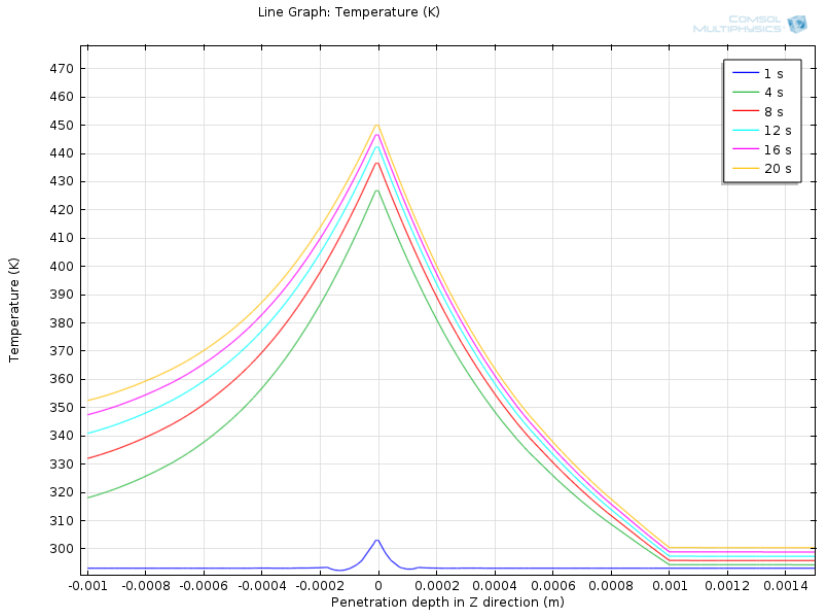

Figure 5.18: Temperature distribution from top glass cap to bottom steel plate in Z direction.

Figure 5.19 shows the temperature distribution in the vertical (Z) direction for the bonding setup in Figure 5.9. As expected the temperature profile is in between those shown in Figure 5.17 and Figure 5.18. The peak temperature at the interface is lower than that of the free standing PMMA-PMMA assembly, but higher than the case without the ceramic plate. The transition of the temperature across the interface with the ceramic plate is not as sharp as shown in Figure 5.18 across the interface between the bottom PMMA substrate and the steel plate. Based on the results of simulation and the experimental results, the setup shown in Figure 5.9 is the best configuration for laser microwelding of the PMMA substrate.

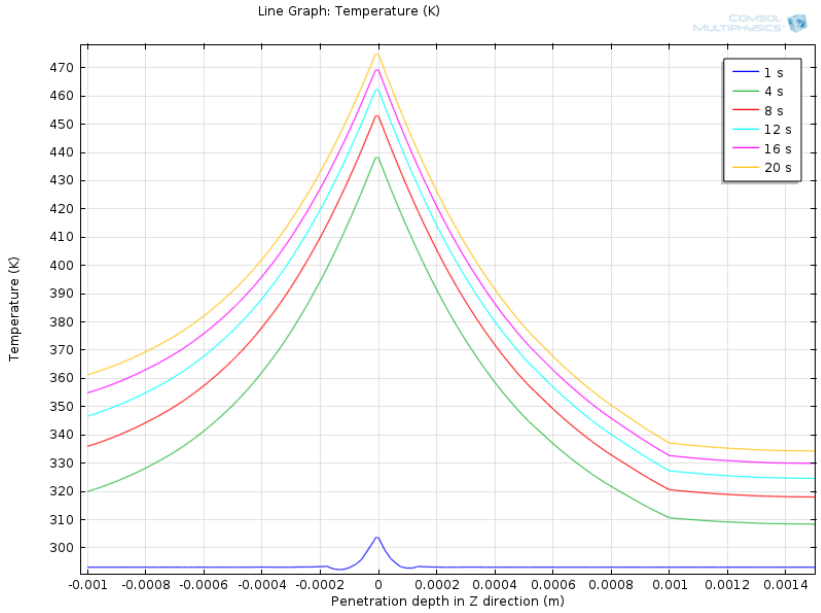

Figure 5.19: Temperature distribution from top glass cap to bottom ceramic in Z direction.

5.6 Modelling of Laser Bonding for MEMS Packaging

Optical and sensor packages are often made from several materials. Since the diverse properties of these materials, the thermal conductivities are important in modelling and simulation work. The COMSOL finite element model is an efficient approach for calculation of the effective thermal conductivity of the package assembly. Therefore, a three-dimensional finite element model of the MEMS packaging process is developed in this section. In the model for MEMS applications, the thickness of the package assembly ranges from 2.65 mm to 3.65 mm, including glass to glass substrate bonding, silicon to silicon bonding, silicon cap to glass substrate bonding and silicon cap to LCP package bonding, all based on an intermediate LCP layer. Similar to the model for laser transmission welding of the PMMA substrates, the heat source is a diode laser system at the wavelength of 970 nm. In this simulation, it is assumed that 30% of the laser intensity is reflected. In the three-dimension model for the top silicon substrate, it is also necessary to sweep the mesh in different layers in the Z direction so that the mesh size is compatible with the mesh definitions in X and Y directions.

The material properties which are used in the modelling and simulation work are shown in Table 5.3 [187].

Table 5.3: Property of materials used in the model [187].

	K (W/m K)	Cp (J/kg K)	ρ (kg/m^3)
Glass	1.1	480	2200
Titanium	21.9	522	4506
Silicon	130	700	2329
LCP	0.2	1600	1760
Al_2O_3	30	730	3965

5.6.1 Laser Assisted Glass to Glass Bonding

The laser assisted glass to glass bonding is similar to the PMMA to PMMA welding configuration in which a titanium layer was used as the absorber. But in this case an intermediate LCP layer is used as the bonding material. It is assumed that the titanium film absorbs all of the transmitted laser radiation through the top glass substrate [189]. An independent measurement using a 633 nm He-Ne laser showed negligible reflection from the titanium film deposited on the LCP layer. The cross-sectional view of the model is shown in Figure 5.20.

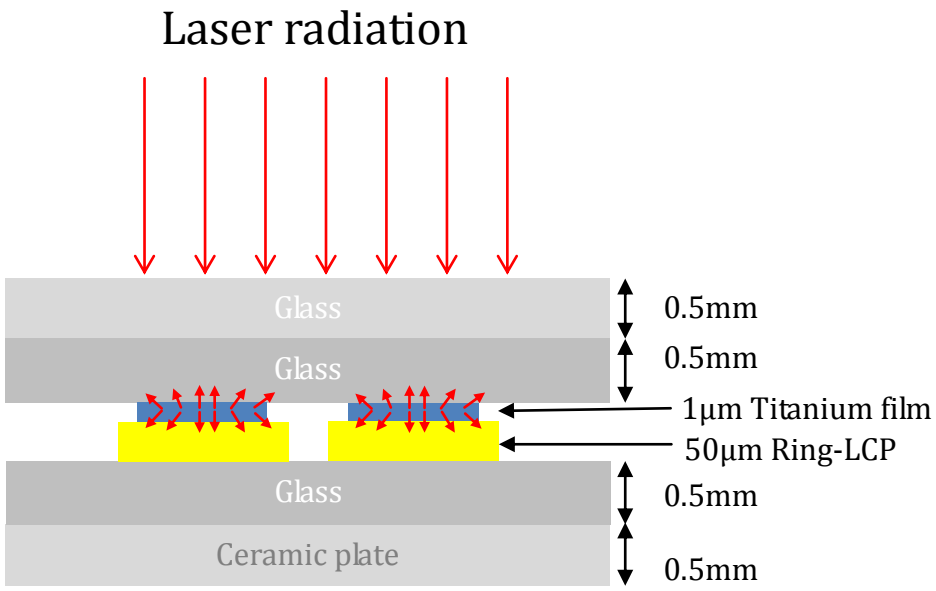

Figure 5.20: Schematic of laser bonding glass to glass substrates.

In this model, an average heat transfer coefficient of $h = 2\ W/m^2\ K$ is used which has been discussed before and the ambient temperature is 293.15 K. The ceramic plate is included as it was the case in the experiment work. Figure 5.21 shows the mesh configuration of the model, it can be seen that the intermediate titanium film is finely meshed to ensure the simulation accuracy. Since the thickness of the titanium film layer is very small between the two glass substrates, therefore, the mesh number generated in the thin layer is much higher.

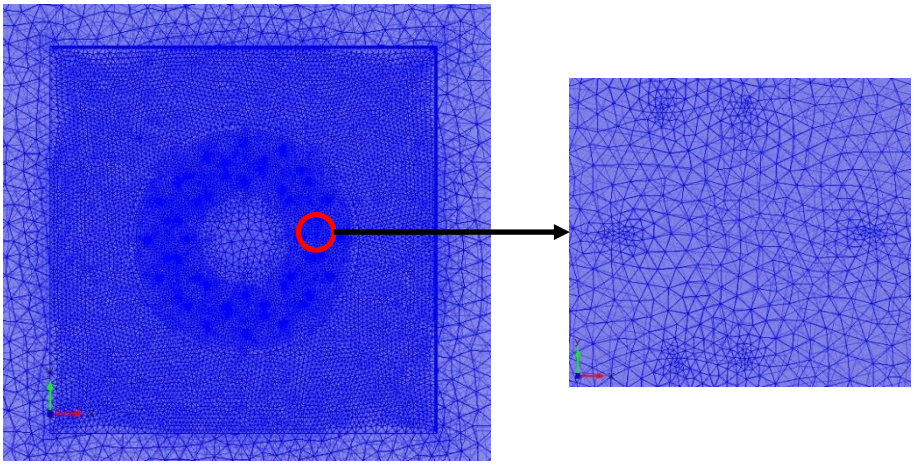

Figure 5.21: The mesh configuration of glass to glass bonding.

Figure 5.22 shows the results of temperature distribution at the interface between two glass substrates. After 80 s, the temperature in titanium layer reaches to 580 K (287 ℃) which is just above the melting temperature (285 ℃) of LCP film. It is found that the values of temperature at the inner and outer edges of the LCP film are different. The temperature at the inner edge is 10 ℃ higher than at the external edge due to the small area within the LCP ring. The heat dissipation is less efficient in the inner area. In the external area, the heat dissipation is faster since the heat can spread into a much larger surrounding area.

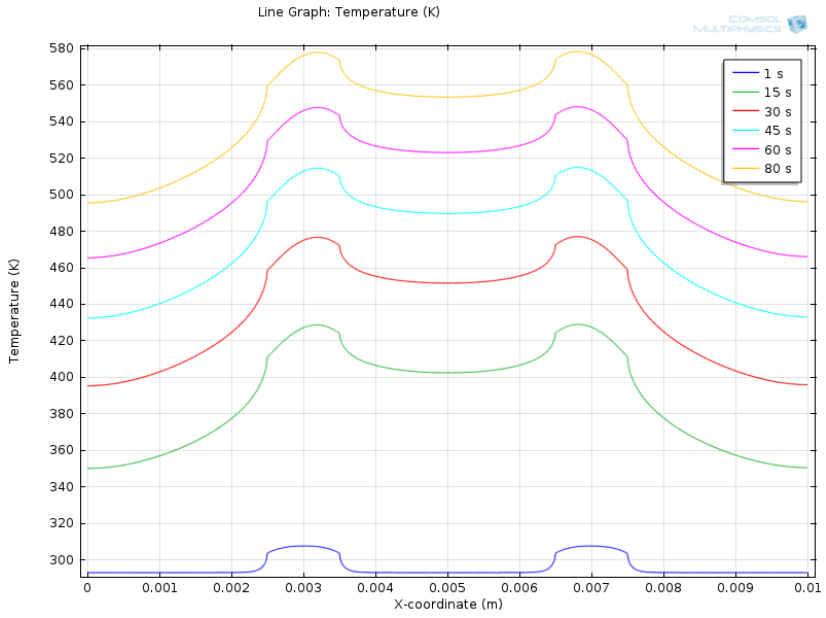

Figure 5.22: Temperature distribution across the glass substrates in X direction.

Figure 5.23 shows the temperature distribution in the Z direction across LCP layer in glass to glass bonding. The laser power is 48 W. It is can be seen that the temperature of the top glass substrate is 20 ℃ higher than the temperature of the bottom glass substrate.

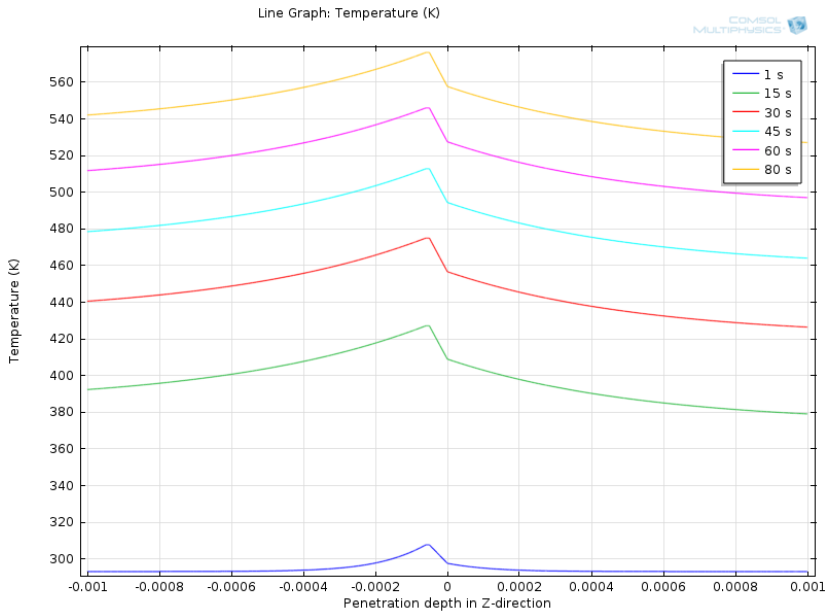

Figure 5.23: Temperature distribution across the top glass to bottom glass substrate.

5.6.2 Laser Assisted Silicon to Glass/Silicon Bonding

In silicon to glass/silicon bonding, there is no additional intermediate absorber layer since the upper silicon cap acts as the absorbing substrate at the wavelength of the laser beam. As has been shown in previous discussion, all of the laser radiation apart from reflection (~30%) can be absorbed by the 0.5 mm thick silicon substrate. The cross-sectional design configuration for modelling of silicon to glass/silicon bonding is shown in Figure 5.24.

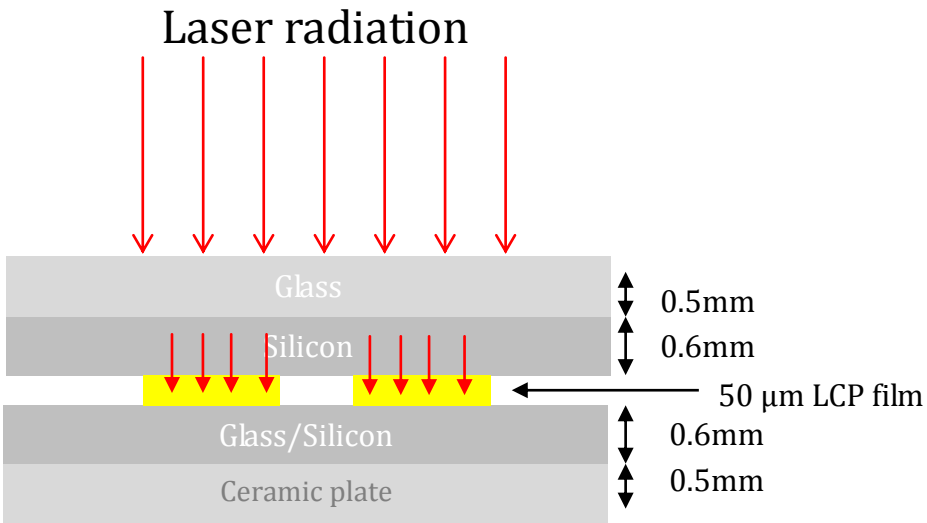

Figure 5.24: A schematic of laser bonding of silicon to glass/silicon.

Figure 5.25 (a) and (b) show the mesh configurations of the silicon to glass/silicon bonding model, the silicon substrate is finely meshed to achieve precision and efficiency in simulation work. The thickness of the LCP film layer is very small and it is between the silicon and glass substrates, therefore, the generated mesh is finer in the thin layer. The mesh is also linearly graded from fine to coarse elements, based on the expected reduction in temperature gradient moving away from the heat source.

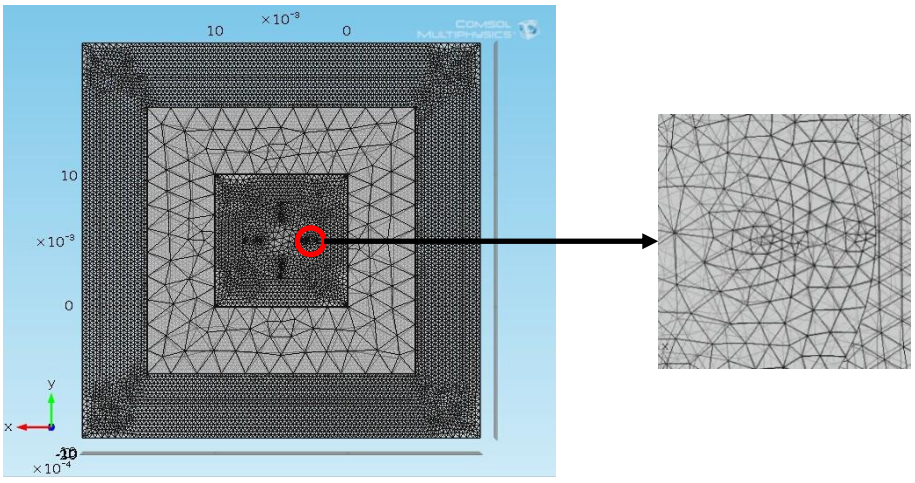

(a)

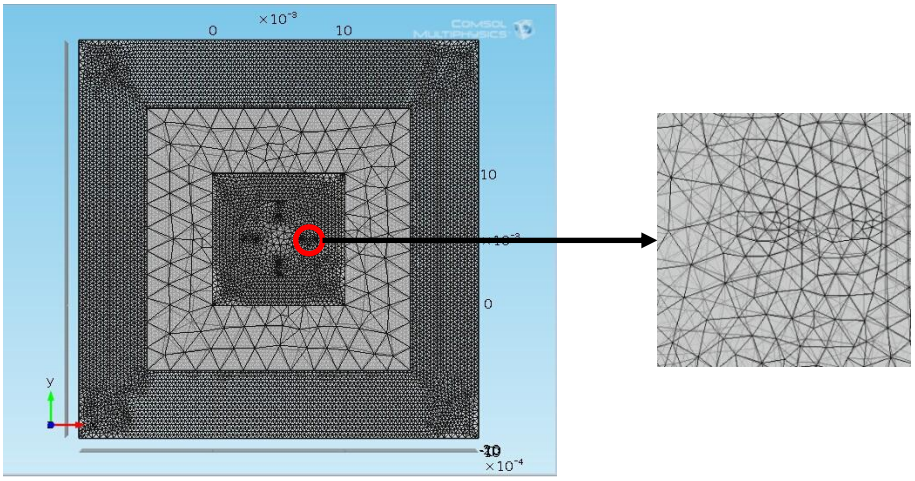

(b)

Figure 5.25: The mesh configuration of (a) silicon to glass bonding, and (b) silicon to silicon bonding.

According to the studies by Glassbrenner *el* [190], the thermal conductivity of silicon is a function of temperature which is shown in Figure 5.26. Since the maximum laser heating temperature is around 300 ℃, it is assumed that the thermal conductivity of silicon is constant and it is the value of 1.1 *W/m K* at 300 K. The rest of the parameters including heat capacity and density is also concluded in Table 5.3.

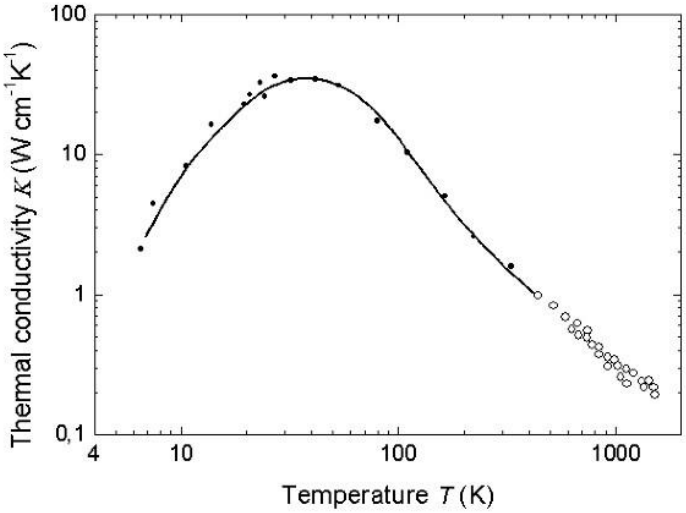

Figure 5.26: Thermal conductivity of silicon as a function of temperature [190].

Figure 5.27 shows the temperature distribution of silicon to glass substrate bonding using an intermediate LCP layer. The laser power is 23 W. Since the melting temperature of the LCP material used in this thesis is roughly 285 ℃ (578 K), it takes about 30 s for the LCP material to reach the melting point and to begin to change from the solid state to the liquid state. After the laser beam is terminated, the liquid state LCP immediately returns to the solid state and produces a strong bond between the silicon and glass substrate. According to the simulation, the LCP layer bonding could be completed within 40 s. If the bonding time is over 40 s, the LCP film will be deformed. In the study the LCP material is a circular ring, therefore the temperature in the middle of the LCP ring is higher than at the external edge because the thermal diffusion process is slow towards the center as discussed in section 3.6.3.

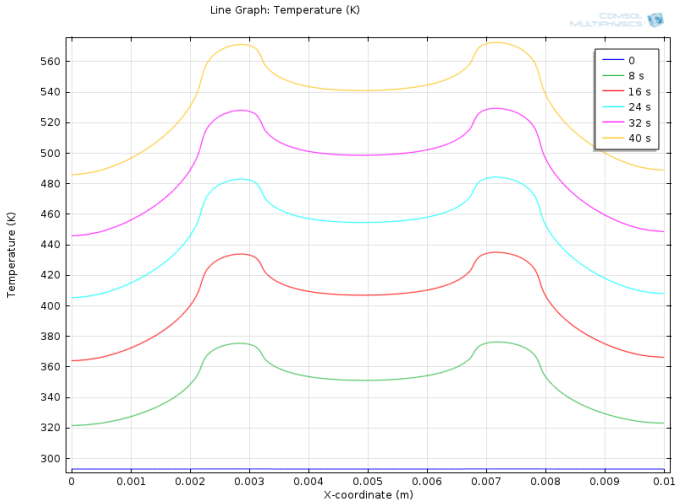

Figure 5.27: Temperature distribution of silicon to glass bonding.

Figure 5.28 shows the temperature distribution of silicon to silicon substrate bonding. The laser power is 35 W. Similar to the effect in silicon to glass bonding, the LCP film melts at 285 ℃ (578 K). However, there are several differences between silicon to glass bonding and silicon to silicon bonding. Because the silicon substrate has higher thermal conductivity than glass, the input laser power for silicon to silicon bonding is also higher than silicon to glass processing. In this model, the input laser power for silicon to silicon bonding is nearly 60% higher than that for silicon to glass bonding. Comparing the results in Figure 5.28 with Figure 5.27, it can be observed that the temperatures both inside and outside the LCP ring are higher in silicon to silicon bonding and in silicon to glass bonding. Besides the temperature difference the inner and outer edges of the LCP ring in silicon to silicon bonding is 20 ℃ higher than that of silicon to glass bonding.

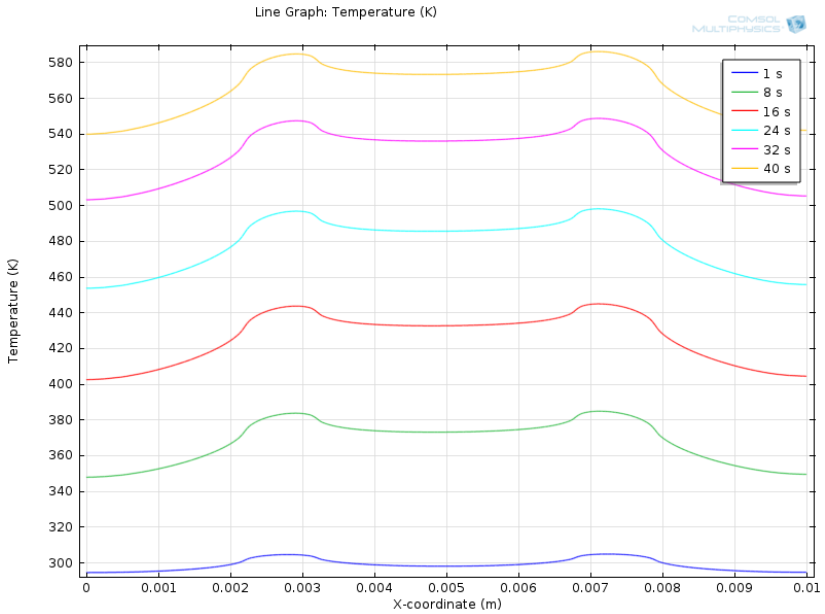

Figure 5.28: Temperature distribution of silicon to silicon bonding.

Figure 5.29 and Figure 5.30 show the temperature distribution in the Z direction across the layers in silicon to glass and silicon to silicon bonding respectively. Although silicon to silicon bonding method achieves higher temperature in the top substrate, it requires much more laser power than that of silicon to glass bonding. In both figures, the temperature decreases from the LCP layer to the bottom substrate because the thermal conductivity of the LCP is low. Therefore, there is a sharp drop in temperature across the LCP layer. The temperature gradient across the LCP layer is higher in bonding silicon to glass bonding because thermal conductivity of the bottom substrate is larger when it is silicon than it is for glass.

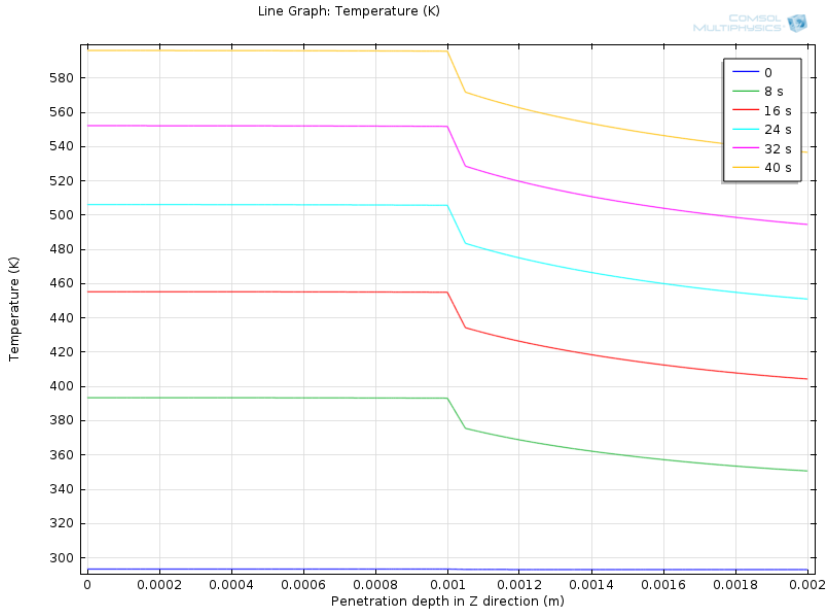

Figure 5.29: Temperature distribution along the top silicon to bottom glass substrate.

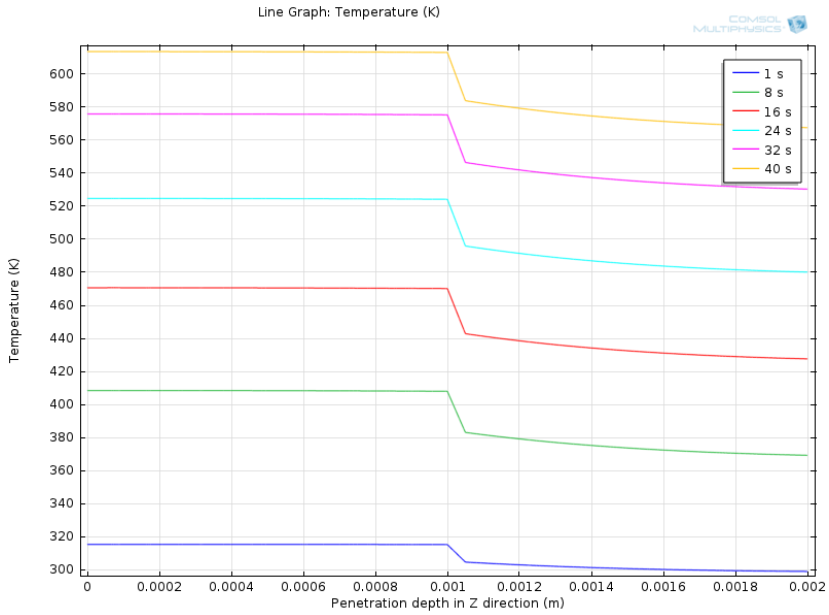

Figure 5.30: Temperature distribution along the top silicon to bottom silicon substrate.

5.6.3 Laser Assisted Silicon to LCP Package Bonding

In silicon to LCP package bonding, the silicon substrate acts as an effective absorber of the laser radiation. As discussed in the previous section, most of the laser radiation is absorbed by the 0.5 mm thick silicon substrate. The cross-sectional design configuration of laser bonding of silicon to the LCP package is shown in Figure 5.31.

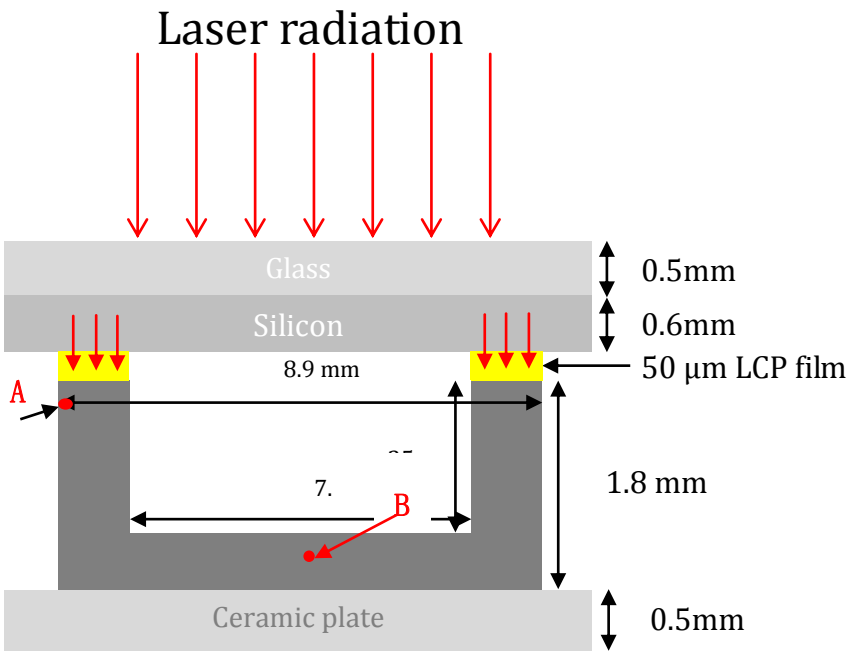

Figure 5.31: The schematic of laser bonding silicon to LCP package.

Figure 5.32 shows the mesh configuration of the model for bonding of silicon to LCP package. The laser power is 30 W. The silicon substrate is finely meshed. According to the expected reduction in temperature gradient moving away from the heat source, the mesh is linearly graded from fine to coarse by definition.

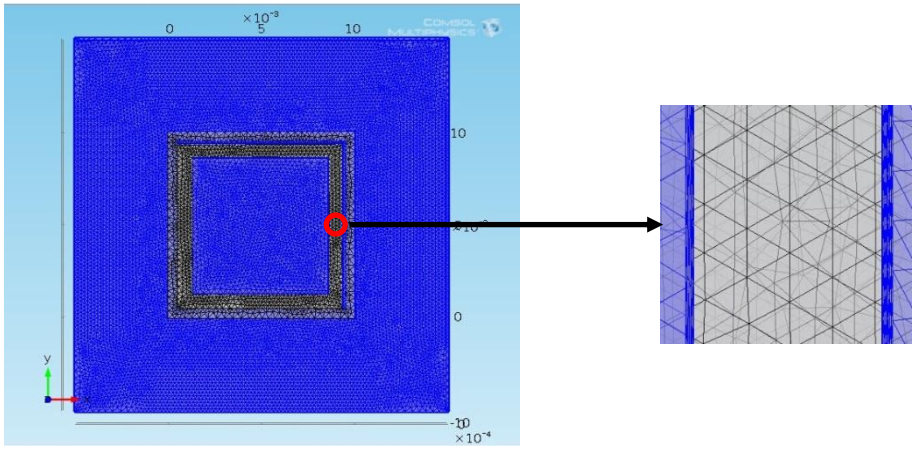

Figure 5.32: Mesh configuration of silicon to LCP package bonding.

The numerical simulations are determined in continuous time and the results are shown in Figure 5.33. It illustrates the evolution of temperature distribution in 2D profile. It is found that the temperature at the interface of the silicon cap and the LCP package increases to 580 K (287 ℃) in 120 s, however the temperature at middle bottom frame of package is 520 K (227 ℃). Moreover after laser heating the temperature distribution

at point “B” in the bottom surface of the package is only 480 K (187 ℃) which is useful for real MEMS bonding applications since the inner area has a lower temperature (140 ℃ lower than bonding temperature).

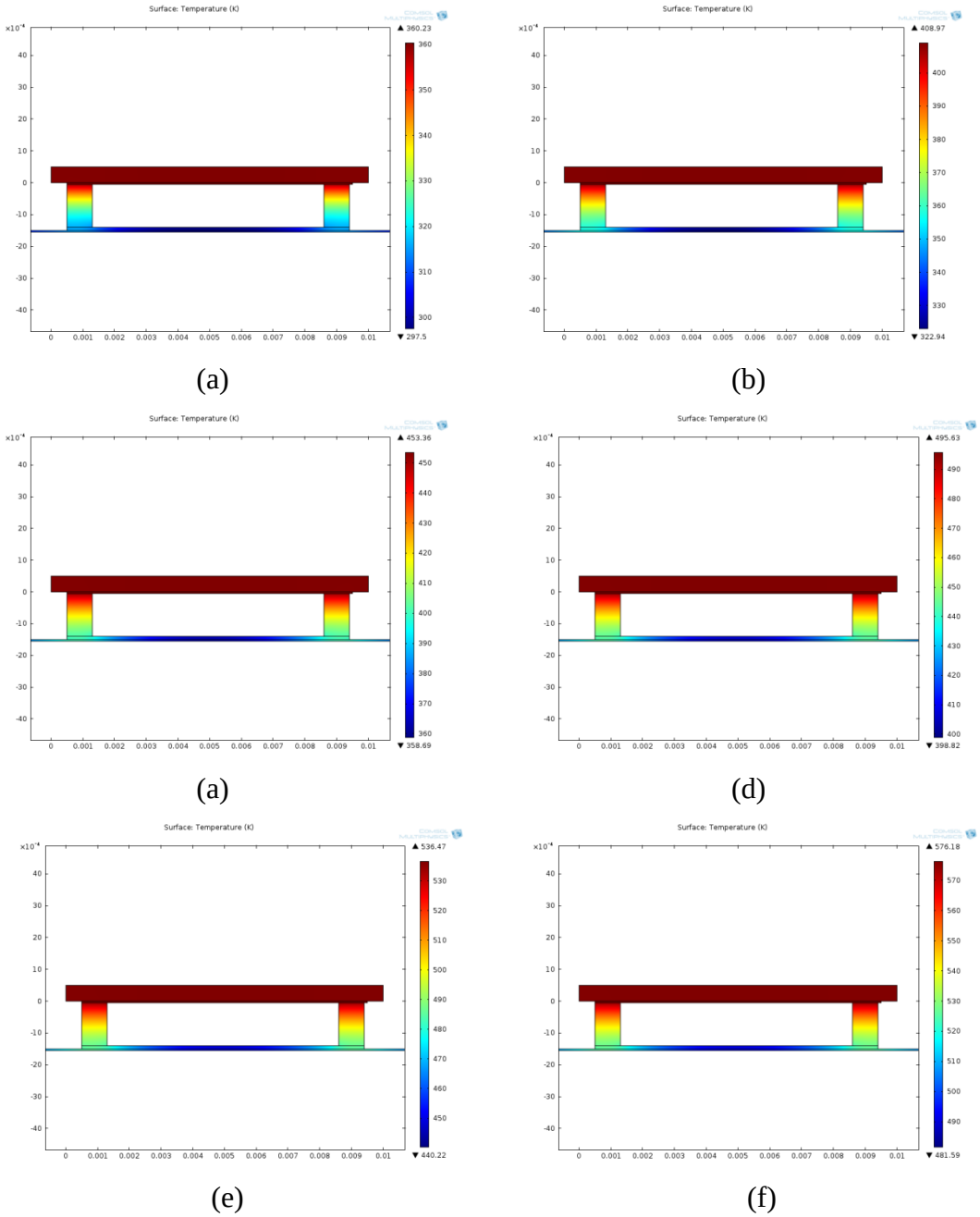

Figure 5.33: The evolution temperature distribution in 2D profile.

In order to understand the heat transfer from the silicon substrate to the LCP package, the temperature distribution of the package in Z direction is simulated and shown in Figure 5.34. The silicon substrate is assumed to be the heat source absorbing the laser power and transfers the heat to the LCP film and the LCP package. It is expected the heat transfer in the LCP package is slow due to the low thermal conductivity of the LCP

material.

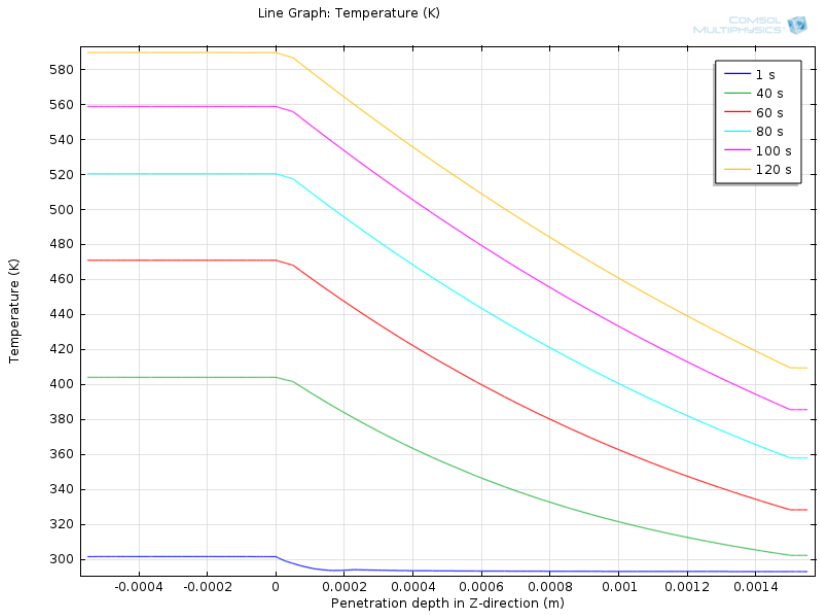

Figure 5.34: Temperature distribution of laser processing silicon to LCP package in Z direction.

In addition, the profiles of temperature dependence on time at the two points "A" and "B" (shown in Figure 5.31) are shown in Figure 5.35 along with the measured results from Fig. 4.14. A reasonable agreement is obtained between the simulation and measured results. Disagreement is possible due to the changeability of thermal conductivity and heat flow.

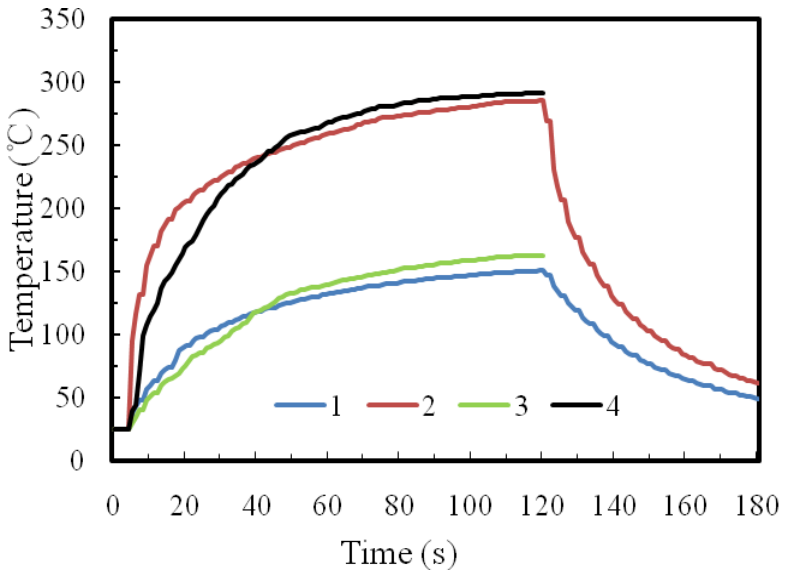

Figure 5.35: The comparison of measured temperature and simulated temperature. 1): the measured temperature in point 'A', 2): the measured temperature in point 'B', 3): the simulated temperature in point 'A', 4): the simulated temperature in point 'B'.

5.7 Conclusions

The main aim of this chapter was to determine the temperature distribution based on the finite element modeling of the laser based PMMA to PMMA bonding and LCP bonding. The principle of heat transfer was discussed including the heat transfer mechanisms. The COMSOL Multiphysics software tool was used to carry out the modelling and simulation work. A model of laser transmission welding of PMMA substrates was developed including the layout design and material properties. The results were shown in 2D temperature distribution for a given constant laser power as a function of time at the interface of the PMMA substrates. Three different set-ups for PMMA bonding were simulated including the cases of no platform below the PMMA substrates, on the stainless steel platform and on the ceramic plate as used in bonding experiments described in chapter 4. Numerical models for laser based LCP bonding for MEMS packaging were also developed and studied, including glass to glass bonding, silicon to glass/silicon bonding and silicon to LCP package bonding. For glass to glass bonding and silicon to glass bonding, the temperature distributions along the interface and z direction were simulated. The results show that the numerical models are suitable for prediction of temperature distribution in laser bonding of the substrates. For silicon to LCP package bonding, a 2D profile of the cross-sectional bonding setup was created. The simulation results are in broad agreement with the measurements of the temperature profiles from the temperature monitoring experiments described in Chapter 4. Compared the simulation results with measured results, a reasonable agreement is obtained.

Chapter 6 Conclusions and Future Work

6.1 Conclusions

A novel laser microwelding method for assembly and packaging of PMMA based microfluidic devices has been studied. A titanium thin film spot pattern was used as the intermediate absorber for sealing microfluidic devices in the laser microwelding method. A laser assisted bonding method using an LCP film has also been investigated for MEMS packaging. Modelling and simulations of the laser assembly methods was carried out using the COMSOL Multiphysics software tool.

For sealing microfluidic device, a novel method of bonding PMMA substrates using an intermediate titanium thin film bonding has been studied. The dependence of the melted zone and the heat affected zone on laser power and exposure time has been investigated. It has been found that a laser power of 25 W with processing time of 15 s can produce a good bond between the two PMMA substrates. A continuous weld between the adjacent titanium film spots can be obtained by controlling the separation between the titanium film spots. These results show that for large area substrate joining the spot array design is better than a large thin film patch. In order to view the bonded interface, cross-sectional studies were carried out using optical microscopy. From the results of tensile strength measurements, the tensile strength is as high as 6 MPa. The laser microwelding method has been successfully applied in encapsulation of a microchannel device exhibiting leak free performance.

For MEMS packaging, a laser assisted bonding method using an LCP film for cavity based packaging applications has been studied. Laser based LCP bonding of both planar silicon and glass substrates and also a molded LCP package has been successfully developed and also near-hermetic bonding has been achieved. A laser machining method was developed to use a CO_2 laser system to cut bonding rings from an LCP sheet. For glass to glass bonding, it has been shown that a thin film titanium material can be used as an effective optical absorber in the laser based LCP bonding technique. Successful bonding processes have been developed for reliable bonding in all of the cavity combinations based on glass and silicon substrates. Laser bonding of a silicon cap to a molded LCP package has been demonstrated successfully. A temperature monitoring method has been developed using embedded miniature thermocouple elements. The results show that the temperature at the base of the LCP package (~130 ℃)

is substantially lower than the bonding temperature (~280 ℃). This demonstrates the unique advantage of the laser based approach in encapsulation of molded LCP cavity packages for packaging of temperature sensitive devices. A strong bond strength has been obtained ranging from 7.7 MPa to 11.6 MPa in shear test experiments. Hermetic tests have been conducted and most of the samples passed the gross leak test and fine leak test. The colour liquid based leak testing has been carried out to show the long-term stability of the bond. SEM micrographs of the cross sections of the bonded samples have been obtained and the pictures show that good bonds were achieved at the interface without any voids.

In the modelling study, simulation was carried out to predict the temperature in the welding area from the laser generated heat at the interface. A commercial software tool (COMSOL Multiphysics) was used to perform the simulation work. Models for both of the laser bonding processes, PMMA-PMMA bonding and LCP bonding, have been developed. It is shown that a good agreement is obtained between the simulation results and the measurements from the temperature monitoring experiments.

In summary, the main conclusions can be described as follows:

- A new laser assembly method for fabrication of polymer based microfluidic devices using a localised absorber.
- Using an intermediate layer absorber design consisting of thin film metal spots for laser assembly. The use of discrete metal film spots allows continuous homogenous bonding between two polymer substrates. The bond strength is enhanced compared to that of a large area metal film based absorber.
- Successful demonstration of the method in leak-free encapsulation of a microfluidic channel.
- Successful temperature monitoring in laser bonding of silicon cap to an LCP package.
- Laser bonding of near-hermetic microcavities between glass and glass, silicon to glass/silicon, and silicon to LCP package.
- Development of mechanical and leak measurement method for assessment of bond strength and hermeticity.
- Modelling and simulation using the COMSOL Multiphysics software tool for laser microwelding of PMMA substrates and laser bonding of glass and silicon

substrates, and silicon to LCP packages.

6.2 Future Work

In this thesis, new laser assembly methods have been studied for applications in manufacturing of microfluidic devices and MEMS packaging. Modelling and simulation of temperature distribution in the laser packaging process have also been studied.

In the future work more detailed modelling work can be carried out. In this thesis work the material properties have been assumed to be independent of temperature. However this is not the case, for example the thermal properties of the PMMA material will change as the material changes from its solid state to become a viscous form.

In laser assembly of microfluidic devices, alternative thermo plastic polymers such as cyclic olefin copolymer (COC) can be studied. The COC material can be processed at lower temperature than PMMA and it also has low water absorption (0.01%) property for microfluidic applications. Although a simple microfluidic channel has been successfully sealed, multilayer microchannels can be designed for advanced applications. In the thesis work, attachment of the two PMMA cover to the microchannel substrate was carried out by a section based bonding method, 5 mm at each step. In future a contour based approach can be developed using a suitable motion control system. More advanced alignment methods are necessary in order to improve alignment accuracy to replace the manual approach.

In development of the laser based method for MEMS packaging using an LCP film, application of surface modifications before bonding may improve the bond strength between the two substrates. For example plasma based methods can be used to activate the chemical bonds at the surfaces of the LCP film to enhance the interface adhesion between the LCP film and the laser bonding partners. It is necessary to further investigate the bonding method using actual MEMS devices or other sensors to validate its potential application in manufacturing of commercial devices.

References

[1] Adams, Thomas M., Layton, *Richard A., Introductory MEMS- Fabrication and Applications*, Springer US, 2010.

[2] Tian, W. and Finehout, E., *Microfluidics for biological applications*. Springer, 2010. New York, USA.

[3] Tsao, C. and DeVoe, D. L., *Bonding of thermoplastic polymer microfluidics.* Microfluid Nanofluid, 2009. **6**(1): p. 1-16.

[4] Piruska, A., Nikcevic, I., Lee, S.H., Ahn C., Heineman, W.R., Limbach, P.A., Seliskar, C.J., *The autofluorescence of plastic materials and chips measured under laser irradiation.* Lab chip,2005. **5**(12): p. 1348-1354.

[5] Strong, A.B., *Plastics: Materials and Processing.* Prentice-Hall, 2000, Upper Saddle River, USA.

[6] Jackman, R., Floyd, T., Ghodssi, R., Schmidt, M., Jensen, K., *Microfluidic System with on-line UV detection fabricated in photodefinable epoxy.* Journal of Micromechanics and Microengineering, 2001. **11**(1): p. 703-705.

[7] Niklaus, F., Enoksson, P., Kalvesten, E., Stemme, G., *Low-temperature full wafer adhesive bonding.* Journal of Micromechanics and Microengineering, 2001. **11**(2): p. 100-107.

[8] Dang, F., Shinohara, S., Tabata, O., Yamaoka, Y., Kurokawa, M., Shinohara, Y., Ishikawa, M., Baba, Y., *Replica multichannel polymer chips with a network of sacrificial sealed by adhesive printing method.* Lab Chip, 2005. **5**(4): p. 472-478.

[9] Wu, H., Huang, B., Zare, R., *Construction of microfluidic chips using polydimethylsiloxane for adhesive bonding.* Lab Chip, 2005. **5**(12): p. 1393-1398.

[10] Kentsch, J., Breisch, S., Stelzle, M., *Low temperature adhesion bonding for BioMEMS.* Journal of Micromechanics and Microengineering, 2006. **16**(4): p. 802-807.

[11] Becker, H., Gartner, C., *Polymer microfabrication methods for microfluidic analytical applications*. Electrophoresis, 2000. 21(1): p. 12-26.

[12] Rotting, O., Ropke, W., Becker, H., Gartner C., *Polymer microfabrication technologies*. Microsystem Technologies, 2002. **23**(6): p. 858-867.

[13] Paul, D., Pallandre, A., Miserere, S., Weber, J., Viovy, J., *Lamination-based rapid*

prototyping of microfluidic devices using flexible thermoplastic substrates. Electrophoresis, 2007. **28**(7): p. 1115-1122.

[14] Abgrall, P., Lattes, C., Conederal, V., Dollat, X., Colin, S., Gue, A.M., *A novel fabrication method of flexible and monolithic 3D microfluidic structures using lamination of SU-8 films*. Journal of Micromechanics and Microengineering, 2006. **16**(1): p. 113-121.

[15] Li, Y, Buch, J.S., Rosenberger, F., DeVoe, D.L., Lee, C.S., *Integration of isoelectric focusing with parallel sodium dodecyl sulfate gelel ectrophoresis for multidimensional protein separations in a plastic microfludic network.* Analytical Chemistry, 2004. **76**(3): p. 742–748.

[16] Buch, J.S., Kimball, C., Rosenberger, F., Highsmith, W.E., DeVoe, D.L., Lee, C.S., *DNA mutation detection in a polymer microfluidic network using temperature gradient gel electrophoresis*. Analytical Chemistry, 2004. 76(4): p. 874–881.

[17] Wang, Y.X., Zhou, Y., Balgley, B.M., Cooper, J.W., Lee, C.S., DeVoe, D.L., *Electrospray interfacing of polymer microfluidics to MALDI-MS*. Electrophoresis, 2005. **26**(19): p. 3631–3640.

[18] Wang, Y.R., Chen, H.W., He, Q.H., Soper, S.A., *A high-performance polycarbonate electrophoresis microchip with integrated threeelectrode system for end-channel amperometric detection*. Electrophoresis, 2008. 29(9):1881–1888.

[19] Park, D.S.W., Hupert, M.L., Witek, M.A., You, B.H., Datta, P., Guy, J., Lee, J.B., Soper, S.A., Nikitopoulos, D.E., Murphy, M.C., *A titer platebased polymer microfluidic platform for high throughput nucleic acid purification*. Biomed Microdevices, 2008. **10**(1): p. 21–33.

[20] Chen, Z.F., Gao, Y.H., Su, R.G., Li, C.W., Lin, J.M., *Fabrication and characterization of poly(methyl methacrylate) microchannels by in situ polymerization with a novel metal template*. Electrophoresis, 2003. **24**(18): p. 3246–3252.

[21] Yao, L.Y., Liu, B., Chen, T., Liu, S.B., Zuo, T.C., *Micro flow-through PCR in a PMMA chip fabricated by KrF excimer laser*. Biomed Microdevices, 2005. **7**(3): p. 253–257.

[22] Sun, Y., Kwok, Y.C., Nguyen, N.T., *Low-pressure, high-temperature thermal bonding of polymeric microfluidic devices and their applications for electrophoretic separation*. Journal of Micromechanics and Microengineering,

2006. **16**(8): p. 1681–1688.

[23] Nikcevic, I., Lee, S.H., Piruska, A., Ahn, C.H., Ridgway, T.H., Limbach, P.A., Wehmeyer, K.R., Heineman, W.R., Seliskar, C.J., *Characterization and performance of injection molded poly(methylmethacrylate) microchips for capillary electrophoresis*. Journal of Chromatography A, 2007. **1154**(1–2): p. 444–453.

[24] Arroyo, M.T., Fernandez, L.J., Agirregabiria, M., Ibanez, N., Aurrekoetxea, J., Blanco, F.J., *Novel all-polymer microfluidic devices monolithically integrated within metallic electrodes for SDSCGE of proteins*. Journal of Micromechanics and Microengineering, 2007. **17**(7): p. 1289–1298.

[25] Nie, Z., Fung, Y.S., *Microchip capillary electrophoresis for frontal analysis of free bilirubin and study of its interaction with human serum albumin*. Electrophoresis, 2008. **29**(9): p. 1924–1931.

[26] Ahn, C.H., Choi, J.W., Beaucage, G., Nevin, J.H., Lee, J.B., Puntambekar, A., Lee, J.Y., *Disposable Smart lab on a chip for point-of-care clinical diagnostics*. Proceedings of the IEEE, 2004.**92**(1): p. 154–173.

[27] Fredrickson, C.K., Xia, Z., Das, C., Ferguson, R., Tavares, F.T., Fan, Z.H., *Effects of fabrication process parameters on the properties of cyclic olefin copolymer microfluidic devices*. Journal of Microelectromechanical Systems, 2006. **15**(5): p. 1060–1068.

[28] Riegger, L., Grumann, M., Steigert, J., Lutz, S., Steinert, C.P., Mueller, C., Viertel, J., Prucker, O., Ruhe, J., Zengerle, R., Ducree, J., *Single-step centrifugal hematocrit determination on a 10-$ processing device*. Biomed Microdevices, 2007. **9**(6): p. 795–799.

[29] Tsao, C.W., Liu, J., DeVoe, D.L., *Droplet formation from hydrodynamically coupled capillaries for parallel microfluidic contact spotting*. Journal of Micromechanics and Microengineering, 2008. **18(2)**:025013.

[30] Olivero, D., Fan, Z.H., *lamination of plastic microfluidic devices*. Lab Chip: Chips & Tips, 2008. http://www.rsc.org/Publishing/Journals/lc/Chips_and_Tips/lamination.asp

[31] Shadpour, H., Musyimi, H., Chen, J.F., Soper, S.A., *Physiochemical properties of various polymer substrates and their effects on microchip electrophoresis performance*. Journal of Chromatography A, 2006. **1111**(2): p. 238–251.

[32] Locascio, L.E., Perso, C.E., Lee, C.S., *Measurement of electroosmotic flow in plastic imprinted microfluid devices and the effect of protein adsorption on flow*

rate. Journal of Chromatography A, 1999. **857**(1– 2): p. 275–284.

[33] Hromada, L.P., Nablo, B.J., Kasianowicz, J.J., Gaitan, M.A., DeVoe, D.L., *Single molecule measurements within individual membrane bound ion channels using a polymer-based bilayer lipid membrane chip*. Lab Chip, 2008. **8**(4): p. 602–608.

[34] Bhattacharyya, A., Klapperich, C.M., *Thermoplastic microfluidic device for on-chip purification of nucleic acids for disposable diagnostics*. Analytical Chemistry, 2006. **78**(3): p. 788–792.

[35] Liu, J., Yang, S., Lee, C.S., DeVoe, D.L., *Polyacrylamide gel plugs enabling 2-D microfluidic protein separations via isoelectric focusing and multiplexed sodium dodecyl sulfate gel electrophoresis*. Electrophoresis, 2008. **29**(11): p. 2241–2250.

[36] Klank, H., Kutter, J.P., Geschke, O., *CO2-laser micromachining and back-end processing for rapid production of PMMA-based microfluidic systems*. Lab on a Chip, 2002. **2**(4): p. 242–246.

[37] Hsu, Y.C., Chen, T.Y., *Applying Taguchi methods for solventassisted PMMA bonding technique for static and dynamic mu-TAS devices*. Biomed Microdevices, 2007. **9**(4): p. 513–522.

[38] Kelly, R.T., Pan, T.,Woolley, A.T., *Phase-changing sacrificialmaterials for solvent bonding of high-performance polymeric capillary electrophoresis microchips*. Analytical Chemistry, 2005. **77**(11): p. 3536–3541.

[39] Koesdjojo, M.T., Tennico, Y.H., Reincho, V.T., *Fabrication of a microfluidic system for capillary electrophoresis using a two stage embossing technique and solvent welding on poly(methyl methacrylate) with water as a sacrificial layer*. Analytical Chemistry, 2008. **80**(7): p. 2311–2318.

[40] Truckenmuller, R., Ahrens, R., Cheng, Y., Fischer, G., Saile, V., *An ultrasonic welding based process for building up a new class of inert fluidic microsensors and actuators from polymers*. Sensors and Actuators A Physical, 2006a. **132**(1): p. 385–392.

[41] Knauf, B. J., Webb, D. P., Liu, C. Q., Conway, P. P., *Plastic packaging using low frequency induction heating for microsytems*. Proceedings of the 10th International IEEE Electronics Packaging Technology Conference (EPTC 2008), Singapore, 2008, ISBN 9781424421183, p. 172-180.

[42] Yussuf, A.A., Sbarski, I., Solomon, M., Tran, N., Hayes, J.P., *Sealing of polymeric-microfluidic devices by using high frequency electromagnetic field and screen printing technique*. Journal of Materials Processing Technology, 2007. **189**(1–3): p. 401–408.

[43] Wallis, G. and D.I. Pomerantz, *Field Assisted Glass-Metal Sealing.* Journal of Applied Physics, 1969. **40**(10): p. 3946-3949.

[44] Lee, T.M.H., I.M. Hsing, and C.Y.N. Liaw, *An improved anodic bonding process using pulsed voltage technique.* Journal of Microelectromechanical Systems, 2000. **9**(4): p. 469-473.

[45] Rogers, T. and J. Kowal, *Selection of glass, anodic bonding conditions and material compatibility for silicon-glass capacitive sensors.* Sensors and Actuators A: Physical, 1995. **46**(1-3): p. 113-120.

[46] Schmidt, M.A., *Wafer-to-wafer bonding for microstructure formation.* Proceedings of the IEEE, 1998. **86**(8): p. 1575-1585.

[47] Wei, J., *Wafer bonding techniques for microsystem packaging.* Journal of Physics: Conference Series, 2006. **34**(1): p. 943.

[48] Wei, J. and et al., *Low temperature wafer anodic bonding.* Journal of Micromechanics and Microengineering, 2003. **13**(2): p. 217.

[49] Younger, P.R., *Hermetic glass sealing by electrostatic bonding.* Journal of Non-Crystalline Solids, 1980. **38-39**(Part 2): p. 909-914.

[50] Yu, P., C. Pan, and J. Xue, *The anodic bonding between K4 glass and Si.* Materials Letters, 2005. **59**(19-20): p. 2492-2495.

[51] Madou, M.J., *Fundamentals of Microfabrication - The Science of Miniaturization.* 2nd ed. 2002, Florida, USA: CRC PRESS.

[52] Lin, Y.C., M. Baum, M. Haubold, J. Fromel, M. Wiemer, T. Gessner, and M. Esashi. *Development and evaluation of AuSi eutectic wafer bonding.* in The 15th International Conference on Solid-State Sensors, Actuators and Microsystems, TRANSDUCERS 2009. 2009. Denver, US.

[53] Wolffenbuttel, R.F. and K.D. Wise, *Low-temperature silicon wafer-to-wafer bonding using gold at eutectic temperature.* Sensors and Actuators A: Physical, 1994. **43**(1-3): p. 223-229.

[54] Khalil, N. *Micropackaging Technologies for Integrated Microsystems: Applications to MEMS and MOEMS.* 2003: SPIE.

[55] Tan, A.W.Y. and F.E.H. Tay, *Localized laser assisted eutectic bonding of quartz and silicon by Nd : YAG pulsed-laser.* Sensors and Actuators A: Physical, 2005. **120**(2): p. 550-561.

[56] Wolffenbuttel, R.F., *Low-temperature intermediate Au-Si wafer bonding; eutectic or silicide bond.* Sensors and Actuators A: Physical, 1997. **62**(1-3): p. 680-686.

[57] Wang, Q., S.-H. Choa, W. Kim, J. Hwang, S. Ham, and C. Moon, *Application of*

Au-Sn eutectic bonding in hermetic radio-frequency microelectromechanical system wafer level packaging. Journal of Electronic Materials, 2006. **35**(3): p. 425-432.

[58] Kim, W., Q. Wang, K. Jung, J. Hwang, and C. Moon. *Application of Au-Sn eutectic bonding in hermetic RF MEMS wafer level packaging.* in 9th International Symposium on Advanced Packaging Materials: Processes, Properties and Interfaces. 2004. Atlanta, Georgia, US.

[59] Tiensuu, A.L., J.A. Schweitz, and S. Johansson. *In situ investigation of precise high strength micro assembly using Au-Si eutectic bonding.* in The 8th International Conference on Solid-State Sensors and Actuators and Eurosensors IX, TRANSDUCERS '95. 1995.

[60] Lee, C., W.-F. Huang, and J.-S. Shie, *Wafer bonding by low-temperature soldering. Sensors and Actuators A: Physical*, 2000. **85**(1-3): p. 330-334.

[61] Ham, S.J., B.G. Jeong, J.H. Lim, K.D. Jung, K.D. Baek, W.B. Kim, and C.Y. Moon, *Characterization and reliability verification of wafer-level hermetic package with nano-liter cavity for RF-MEMS applications,* in Proceedings of 57th Electronic Components & Technology Conference. 2007, IEEE: New York. p. 1127-1134.

[62] Sohn, Y.C., Q. Wang, S.J. Ham, B.G. Jeong, K.D. Jung, M.S. Choi, W.B. Kim, and C.Y. Moon, *Wafer-level low temperature bonding with Au-In system,* in Proceedings of 57th Electronic Components & Technology Conference. 2007, IEEE: New York. p. 633-637.

[63] Chong, S.C., X.L. Zhang, S. Mohanraj, C.S. Premachandran, and N. Ranganathan. *Effect of passivation on frit glass bonding method for wafer level hermetic sealing on MEMS devices.* in Proceedings of 5th Electronics Packaging Technology Conference. 2003. New York: IEEE.

[64] Dresbach, C., A. Krombbolz, M. Ebert, and J. Bagdahn, *Mechanical properties of glass frit bonded micro packages.* Microsystem Technologies, 2006. 12(5): p. 473-480.

[65] Ebert, M. and J. Bagdahn, *Determination of residual stress in glass frit bonded MEMS by Finite Element Analysis,* in Thermal and Mechanical Simulation and Experiments in Microelectronics and Microsystems, L.J. Ernst, et al., Editors. 2004, IEEE: New York. p. 407-412.

[66] Fujii, M., I. Kimura, T. Satoh, and K. Imanaka, *RF MEMS Switch with Wafer Level Package Utilizing Frit Glass Bonding.* in 32nd European Microwave

Conference. 2002. Milan, Italy.

[67] Knechtel, R., *Glass frit bonding: an universal technology for wafer level encapsulation and packaging.* Microsystem Technologies, 2005. **12**(1-2): p. 63-68.

[68] Knechtel, R., M. Wiemer, and J. Fromel, *Wafer level encapsulation of microsystems using glass frit bonding.* Microsystem Technologies, 2006. **12**(5): p. 468-472.

[69] Petzold, M., C. Dresbach, M. Ebert, J. Bagdahn, M. Wiemer, K. Glien, J. Graf, R. Muller-Fiedler, and H. Hofer, *Fracture mechanical life-time investigation of glass frit-bonded MEMS sensors,* in 2006 Proceedings 10th Intersociety Conference on Thermal and Thermomechanical Phenomena in Electronics Systems, Vols 1 and 2. 2006, IEEE: New York. p. 1343-1348.

[70] Seki, T., *Recent progress in packaging of RF MEMS.* in IEEE Compound Semiconductor Integrated Circuit Symposium. 2004. Monterey, US.

[71] Sparks, D., S. Massoud-Ansari, and N. Najafi, *Long-term evaluation of hermetically glass frit sealed silicon to Pyrex wafers with feedthroughs.* Journal of Micromechanics and Microengineering, 2005. **15**(8): p. 1560-1564.

[72] Sparks, D., S. Massoud-Ansari, and N. Najafi, *Reliable vacuum packaging using NanoGetters (TM) and glass frit bonding,* in Reliability, Testing and Characterization of MEMS/MOEMS III, D.M. Tanner and R. Ramesham, Editors. 2004, SPIE-Int Society Optical Engineering: Bellingham. p. 70-78.

[73] Sparks, D.R., S. Massoud-Ansari, and N. Najafi, *Chip-level vacuum packaging of micromachines using NanoGetters.* IEEE Transactions on Advanced Packaging, 2003. **26**(3): p. 277-282.

[74] Audet, S.A. and K.M. Edenfeld, *Integrated sensor wafer-level packaging,* in The 9th International Conference on Solid-State Sensors and Actuators, TRANSDUCERS '97. 1997. Chicago, US.

[75] http://www.agc.com/english/products/products_01.html (Date:05/03/2015)

[76] http://www.diemat.com/docs/products/glass/DM2700P-H848%202011-06-2.pdf (Date:05/03/2015)

[77] Sparks, D.R. and et al., *An all-glass chip-scale MEMS package with variable cavity pressure.* Journal of Micromechanics and Microengineering, 2006. **16**(11): p. 2488.

[78] Olowinsky, A. and H. Kind, *Laser glass frit bonding for hermetic sealing of glass substrates and sensors.* in Proceedings of LPM2010 - the 11th International

Symposium on Laser Precision Microfabrication. 2010. Stuttgart, Germany.

[79] Choi, Y.S., J.S. Park, H.D. Park, Y.H. Song, J.S. Jung, and S.G. Kang, *Effects of temperatures on microstructures and bonding strengths of Si-Si bonding using bisbenzocyclobutene.* Sensors and Actuators A: Physical, 2003. **108**(1-3): p. 201-205.

[80] Niklaus, F., G. Stemme, J.Q. Lu, and R.J. Gutmann, *Adhesive wafer bonding.* Journal of Applied Physics, 2006. **99**(3).

[81] Jourdain, A., P. De Moor, K. Baert, I. De Wolf, and H.A.C. Tilmans, *Mechanical and electrical characterization of BCB as a bond and seal material for cavities housing (RF-)MEMS devices.* Journal of Micromechanics and Microengineering, 2005. **15**(7): p. S89-S96.

[82] Jourdain, A., P. De Moor, S. Pamdighantam, and H.A.C. Tilmans, *Investigation of the hermeticity of BCB-sealed cavities for housing (RF-)MEMS devices*, in *Fifteenth IEEE International Conference on Micro Electro Mechinical Systems, Technical Digest*. 2002, IEEE: New York. p. 677-680.

[83] Jourdain, A., H. Ziad, P. De Moor, and H.A.C. Tilmans, *Wafer-scale 0-level packaging of (RF-)MEMS devices using BCB*, in *DTIP 2003: Design, Test, Integration and Packaging of MEMS/MOEMS 2003*, K. Bergman, et al., Editors. 2003, IEEE: New York. p. 239-244.

[84] Kim, Y.K., E.K. Kim, S.W. Kim, and B.K. Ju, *Low temperature epoxy bonding for wafer level MEMS packaging.* Sensors and Actuators A: Physical, 2008. **143**(2): p. 323-328.

[85] Liming, Y. and et al., *Adhesive bonding with SU-8 at wafer level for microfluidic devices.* Journal of Physics: Conference Series, 2006. **34**(1): p. 776.

[86] Lou, X., Z.H. Li, and Y.F. Jin, *Plastic-silicon bonding for MEMS packaging application*, in *Proceedings of 7th International Conference on Electronics Packaging Technology (ICEPT)*, B. Kenyun, Editor. 2006, IEEE: New York. p. 524-526.

[87] Na, K.H., I.H. Kim, E.S. Lee, H.C. Kim, Y.H. Lee, and K. Chun, *Wafer level package using polymer bonding of thick SU-8 photoresist*, in *Proceedings of International Conference on MEMS, Nano and Smart Systems*, W. Badawy and A. Salem, Editors. 2006, IEEE: New York. p. 31-34.

[88] Niklaus, F., P. Enoksson, E. Kalvesten, and G. Stemme, *Low-temperature full wafer adhesive bonding.* Journal of Micromechanics and Microengineering, 2001. **11**(2): p. 100-107.

[89] Noh, H.S., K.S. Moon, A. Cannon, P.J. Hesketh, and C.P. Wong, *Wafer bonding using microwave heating of parylene for MEMS packaging*, in *54th Electronic Components & Technology Conference, Vols 1 and 2, Proceedings*. 2004, IEEE: New York. p. 924-930.

[90] Oberhammer, J., E. Niklaus, and G. Stemme, *Selective wafer-level adhesive bonding with benzocyclobutene for fabrication of cavities.* Sensors and Actuators A: Physical, 2003. **105**(3): p. 297-304.

[91] Oberhammer, J., F. Niklaus, and G. Stemme, *Sealing of adhesive bonded devices on wafer level.* Sensors and Actuators A: Physical, 2004. **110**(1-3): p. 407-412.

[92] Oberhammer, J. and G. Stemme, *BCB contact printing for patterned adhesive full-wafer bonded 0-level packages.* Journal of Microelectromechanical Systems, 2005. **14**(2): p. 419-425.

[93] Pan, C.T., P.J. Cheng, M.F. Chen, and C.K. Yen, *Intermediate wafer level bonding and interface behavior.* Microelectronics and Reliability, 2004. **45**(3-4): p. 657-663.

[94] Pan, C.T. and et al., *A low-temperature wafer bonding technique using patternable materials.* Journal of Micromechanics and Microengineering, 2002. **12**(5): p. 611.

[95] Polyakov, A., M. Bartek, and J.N. Burghartz, *Area-Selective Adhesive Bonding Using Photosensitive BCB for WL CSP Applications.* Journal of Electronic Packaging, 2005. **127**(1): p. 7-11.

[96] Seok, S., N. Rolland, and P.A. Rolland, *Design, fabrication, and measurement of benzocyclobutene polymer zero-level packaging for millimeter-wave applications.* IEEE Transactions on Microwave Theory and Techniques, 2007. **55**(5): p. 1040-1045.

[97] Seok, S., N. Rolland, and P.A. Rolland, *Mechanical and electrical characterization of Benzocyclobutene membrane packaging*, in *57th Electronic Components & Technology Conference, Proceedings*. 2007, IEEE: New York. p. 1685-1689.

[98] Seok, S., N. Rolland, and P.A. Rolland, *A new BCB film zero-level packaging for RF devices*, in *2006 European Microwave Conference, Vols 1-4*. 2006, IEEE: New York. p. 13-16.

[99] Tai, A., H. Karagozoglu, and K.L. Chuan, *Organic sealant materials for quasi-hermetic sealing of MEMS sensor packages*. In *EPTC 2006: 8th Electronic Packaging Technology Conference, Vols 1 and 2*, J.H.L. Pang, et al.,

Editors. 2006, IEEE: New York. p. 462-471.

[100] Tian, J. and M. Bartek. *Low Temperature Wafer-Level Packaging of RF-MEMS using SU-8 Printing*. In *STW Annual Workshop on Semiconductor Advances for Future Electronics and Sensors (SAFE 2005)*. 2005. Veldhoven, the Netherlands.

[101] Tilmans, H.A.C., H. Ziad, H. Jansen, O. Di Monaco, A. Jourdain, W. De Raedt, E. Rottenberg, E. De Backer, A. Decaussemaeker, and K. Baert. *Wafer-level packaged RF-MEMS switches fabricated in a CMOS fab*, in *Technical Digest on International Electron Devices Meeting (IEDM)*. 2001. Washington, DC, USA.

[102] Wiemer, M., C. Jia, M. Toepper, and K. Hauck. *Wafer Bonding with BCB and SU-8 for MEMS Packaging*, in *1st Electronics Systemintegration Technology Conference*. 2006. Dresden, Germany.

[103] K. Jayaraj, T. E. Noll, and D. R. Singh, *RF characterization of a low cost multichip packaging technology for monolithic microwave and millimeter wave integrated circuits,* in *URSI* Int. Signals, Systems, and Electronics Symp., 1995, pp. 443–446.

[104] G. Zou, H. Gronqvist, P. Starski, and J. Liu, *High frequency characteristics of liquid crystal polymer for system in a package application*, in IEEE 8th International Symposium on Advanced Packaging Materials, 2002, pp. 337–341.

[105] G. Zou, H. Gronqvist, J. P. Starski, and J. Liu, *Characterization of liquid crystal polymer for high frequency system-in-a-package applications*. IEEE Transactions on Advanced Packaging, 2002. **25**(4): p. 503-508.

[106] B. Farrell and M. S. Lawrence, *The processing of liquid crystalline polymer printed circuits*, in IEEE Electronic Components and Technology Conference, 2002. pp. 667–671.

[107] D. Thompson, *Characterization and design of liquid crystal polymer (LCP) based multilayer RF components and packages.* Ph.D thesis, 2006. Georgia Institute of Technology, USA.

[108] http://www.rogerscorp.com/documents/822/acm/Fabrication-Guidelines-ULT RALAM-3000-LCP-Materials.pdf

[109] X. Wang, J. Engel, and C. Liu, *Liquid crystal polymer (LCP) for MEMS: processes and applications.* Journal of Micromechical Microengineering, 2002. **13**(5): p. 628-633.

[110] A. Kottapalli, C. Tan, M. Olfatnia, J. Miao, G. Barbastathis, and M. Triantafyllou, *A liquid crystal polymer membrane MEMS sensor for flow rate and flow direction sensing applications.* Journal of Micromechical Microengineering,

2011, **21**(8): 085006.

[111] A. Kottapalli, C. Tan, M. Olfatnia, J. Miao, G. Barbastathis, and M. Triantafyllou, *A flexible liquid crystal polymer MEMS pressure sensor array for fish-like underwater sensing.* Smart Materials and Structures, 2012. **21**(11): 115030.

[112] K. Aihara, M. Chen, and A. Pham, *Development of thin film liquid crystalpolymer surface mount packages for Ka- band applications.* IEEE Transactions on Microwave Theory and Techniques, 2008. **56**(9): p. 2111-2117.

[113] K. Aihara, M. Chen and C. Chen, *Reliability of liquid crystal polymer air cavity packaging,* IEEE Transactions on Components, Packaging and Manufacturing Technology, 2012. **2**(2): P. 224- 230.

[114] M. P. Mcgrath, K. Aihara, A. Pham and S.R. Nelson, *Development of LCP surface mount package with a bandpass feed through at K-band,* Proc. IEEE MTT-S International Microwave Symposium Digest, 2008. pp. 93-96.

[115] A. C. Chen, M. J. Chen and A. V. Pham, *Design and fabrication of ultra-wideband baluns embedded in multilayer liquid crystal polymer flex.* IEEE Transaction on Advanced Packaging, 2007. **30**(3): p. 533-540.

[116] M. Chen, A. Pham, N. Evers, C. Kapusta, J. Iannotti, W. Kornrumpf, J. Maciel, and N. Karabudak, *Design and development of a package using LCP for RF/microwave MEMS switches,* IEEE Transactions on Microwave Theory and Techniques, 2006. **54**(11): p. 4009-4015,

[117] J.M. Köhler, U. Dillner, A. Mokansky, S. Poser and T. Schulz, *Micro channel reactors for fast thermocycling.* 2nd International Conference on Microreaction Technology, 1998. pp.241-247.

[118] TREFFERT company online. Online, Date accessed: Mar. 2014. Available: http://www.treffert.org/engl/bLaser7.html

[119] Fox, M., *Optical Properties of Solids.* Oxford University Press, 2001. Oxford, UK.

[120] M. Sieffert, *Farbstoffe und Pigmente- von Schwarz bis weiß zu kunterbunt.* Aachener Laser Seminare: Aachen, 2003

[121] J. Van de Ven, and A. Erdman, *Simultaneous Measurement of Laser Reflection and Transmission of Poly(Vinyl Chloride).* Optical Engineering. 2006. **45**(9): 094301.

[122] I. Jones, *Laser welding for plastic components. Assembly Automation.* Assembly Automation, 2002. **22**(2): p. 129-35.

[123] M. J. Troughton, *Handbook of plastics joining: a practical guide (2nd ed).*

William Andrew, 2008. UK: The welding institute.

[124] Y. Chung, M. Kamal, *Morphology of PA-6 vibration welded joints and its effects on weld strength*. Polymer Engineering and Science, 2008. **48**(2): 240– 248.

[125] D. Valladares, M. Cakmak, *Initiation and development of the heat-affected zone in the vibration welding of polyvinylidene fluoride and its copolymers.* Journal of Applied Polymer Science, 2002. **86**(13): p. 3377–88.

[126] J. Kim, X. Xu, *Excimer laser fabrication of polymer microfluidic devices.* Journal of Laser Applications, 2003. **15**(4): p. 255–260.

[127] H. Potente, F. Becker, G. Fiegler, J. Korte, *Investigations towards application of a new technique on laser transmission welding*. Welding in the World, 2001. **45**(5-6): p. 15–20.

[128] B. Acherjee,D. Misra, D. Bose, K. Venkadeshwaran, *Prediction of weld strength and seam width for laser transmission welding of thermoplastic using response surface methodology.* Optics and Laser Technology, 2009. **41**(8): p. 956–67.

[129] G. Georgiev, R. Baird, E. McCullen, G. Newaz, G. Auner, R. Patwa, et al, *Chemical bond formation during laser bonding of Teflon FEP and titanium.* Applied Surface Science, 2009, **255**(15): p. 7078–83.

[130] F. Bundgaard, G. Perozziello, O. Geschke, *Rapid prototyping tools and methods for all-Topas® cyclic olefin copolymer fluidic microsystems.* In: Proceedings for the 1st International Conference on Multi-material Micro Manufacture (4M), 2006. **220**(11): p. 405-407.

[131] T. Ussing, L.V. Petersen, C.B. Helbo, L. HØjslet, *Micro laser welding of polymer microstructures using low power laser diodes*, The international Journal of Advanced Manufacturing Technology, 2007. 33(1-2): p. 198-205.

[132] W. Pfleging, O. Baldus, *Laser patterning and welding of transparent polymers for microfluidic device fabrication.* Proceedings of SPIE, 2006. **6107**: p. 610705.

[133] Sun, L., A. Malshe, S. Cunningham, and A. Morris, *Investigation of localized laser bonding process for ceramic MEMS packaging*, in *56th Electronic Components & Technology Conference 2006, Vol 1 and 2, Proceedings*. 2006, IEEE: New York. p. 1740-1744.

[134] Bosse, L., A. Schildecker, A. Gillner, and R. Poprawe, *High quality laser beam soldering.* Microsystem Technologies, 2002. **7**(5-6): p. 215-219.

[135] Chaminade, C., A. Olowinsky, and H. Kind. *Laser-based glass soldering for MEMS packaging*. in *ICALEO 2007 Congress Proceedings*. 2007. Orlando, FL, USA.

[136] Gillner, A., J. Holtkamp, C. Hartmann, A. Olowinsky, J. Gedicke, K. Klages, L. Bosse, and A. Bayer, *Laser applications in microtechnology.* Journal of Materials Processing Technology, 2005. **167**(2-3): p. 494-498.

[137] Gillner, A., M. Wild, and R. Poprawe, *Laser bonding of micro optical components*, in *Laser Micromachining for Optoelectronic Device Fabrication*, A. Ostendorf, Editor. 2003, SPIE-Int Society Optical Engineering: Bellingham. p. 112-120.

[138] Haberstroh, E., W.M. Hoffmann, R. Poprawe, and F. Sari, *3 Laser transmission joining in microtechnology.* Microsystem Technologies, 2006. **12**(7): p. 632-639.

[139] Joseph, P.J., P. Monajemi, F. Ayazi, and P.A. Kohl, *Wafer-level packaging of micromechanical resonators.* IEEE Transactions on Advanced Packaging, 2007. **30**(1): p. 19-26.

[140] Luo, C. and L.W. Lin, *The application of nanosecond-pulsed laser welding technology in MEMS packaging with a shadow mask.* Sensors and Actuators A: Physical, 2002. **97-8**: p. 398-404.

[141] Mescheder, U.M., M. Alavi, K. Hiltmann, C. Lietzau, C. Nachtigall, and H. Sandmaier, *Local laser bonding for low temperature budget.* Sensors and Actuators A: Physical, 2002. **97-8**: p. 422-427.

[142] Mohan, A., C.B. O'Neal, A.P. Malshe, and R.B. Foster, *A wafer-level packaging approach for MEMS & related microsystems using selective laser-assisted bonding (LAB).* Proceedings of 55th Electronic Components & Technology Conference, 2005. **1&2**: p. 1099-1102.

[143] Sun, L., A.P. Malshe, S. Cunningham, and A. Morris, *Localized CO2 laser bonding process for MEMS packaging.* Transactions of Nonferrous Metals Society of China, 2006. **16**: p. S577-S581.

[144] Tan, A.W.Y., F.E.H. Tay, and J. Zhang, *Characterization of localized laser assisted eutectic bonds.* Sensors and Actuators A: Physical, 2006. **125**(2): p. 573-585.

[145] Tao, Y., A.P. Malshe, and W.D. Brown, *Selective bonding and encapsulation for wafer-level vacuum packaging of MEMS and related micro systems.* Microelectronics Reliability, 2004. **44**(2): p. 251-258.

[146] Tao, Y., A.P. Malshe, W.D. Brown, D.R. DeReus, and S. Cunningham, *Laser-assisted sealing and testing for ceramic packaging of MEMS devices.* IEEE Transactions on Advanced Packaging, 2003. **26**(3): p. 283-288.

[147] Theppakuttai, S., D.B. Shao, and S.C. Chen, *Localized laser transmission bonding for microsystem fabrication and packaging.* Journal of Manufacturing Processes, 2004. **6**(1): p. 1-8.

[148] Wild, M.J., A. Gillner, and R. Poprawe, *Advances in silicon to glass bonding with laser.* MEMS Design, Fabrication, Characterization, and Packaging, 2001. **4407**: p. 135-141.

[149] Wild, M.J., A. Gillner, and R. Poprawe, *Locally selective bonding of silicon and glass with laser.* Sensors and Actuators A: Physical, 2001. **93**(1): p. 63-69.

[150] Wu, Q., N. Lorenz, K.M. Cannon, and D.P. Hand, *Glass frit as a hermetic joining layer in laser based joining of miniature devices.* IEEE Transactions on Components and Packaging Technologies, 2010. **33**(2): p. 470-477.

[151] Lorenz, N., S. Millar, M. Desmulliez, and D.P. Hand, *Hermetic glass frit packaging in air and vacuum with localized laser joining.* Journal of Micromechanics and Microengineering, 2011. **21**(4): p. 045039

[152] R. Cruz, J. A. Da Cruz, J. Macaira, F. Ribeiro, A. M. Batista, J.M. Oliveira, M. H. F. V. Fernandes, H. Aguilar, J. G. Mendes, and A. Menes, *Glass-glass laser-assisted glass frit bonding.* IEEE Transactions on Components and Packaging Technologies, 2012. **2**(12): p. 1949-1956.

[153] Bardin, F., S. Kloss, C.H. Wang, A.J. Moore, A. Jourdain, I. De Wolf, and D.P. Hand, *Laser bonding of glass to silicon using polymer for microsystems packaging.* Journal of Microelectromechanical Systems, 2007. **16**(3): p. 571-580.

[154] Liu, Y.F., J. Zeng, and C.H. Wang, *Temperature monitoring in laser assisted polymer bonding for MEMS packaging using a thin film sensor array,* in Proceedings of IEEE Sensors Applications Symposium (SAS 2009). 2009, IEEE: New York. p. 52-55.

[155] Wang, C., J. Zeng, and Y. Liu, *Recent advances in laser assisted polymer intermediate layer bonding for MEMS packaging,* in International Conference on Electronic Packaging Technology & High Density Packaging (ICEPT-HDP '09). 2009. Beijing, China.

[156] Liu, Y.F., J. Zeng, and C.H. Wang, *Accurate Temperature Monitoring in Laser-Assisted Polymer Bonding for MEMS Packaging Using an Embedded Microsensor Array.* Journal of Microelectromechanical Systems, 2010. **19**(4): p. 903-910.

[157] Wu, Q., N. Lorenz, K.M. Cannon, and D.P. Hand, *Glass frit as a hermetic joining layer in laser based joining of miniature devices.* IEEE Transactions on Components and Packaging Technologies, 2010. **33**(2): p. 470-477.

[158] Lorenz, N., M.D. Smith, and D.P. Hand, *Wafer-level packaging of silicon to glass with a BCB intermediate layer using localised laser heating.* Microelectronics Reliability, 2011, **21**(4): p. 2257-2262.

[159] http://www.chemistry2011.org/ResourceFiles/10.pdf (Date: 05/03/2015)

[160] http://uk.rs-online.com/web/p/solid-plastic-sheets/0824632 (Date: 05/03/2015)

[161] W. M. Steen, K. Watkins, *Laser Material Processing*. 2003. Springer: New York.

[162] Hong, T. F., Ju, W. J., Tsai, C. H., Wang, Y. N., and Fu, L. M., *An integrated microfluidic chip for rapid methanol detection*. International Journal of Automation and Smart Technology. 2012. **2**(1).

[163] Belic, I., and Stanic, J., *Optical & Laser Technology*. 1987. 19: p. 309-311.

[164] Flynn, D., *The manufacture and characterization of microscale magnetic components*. Phd thesis. 2007.

[165] Kim, J. and Xu, X.F., *Excimer laser fabrication of polymer microfluidic devices*. Journal of Laser Application. 2003. **15**: p. 255-260.

[166] http://www.engineeringarchives.com/les_mom_tensiletest.html (Date: 05/02/2015)

[167] Pfleging, W., Baldus, O., *Laser-assisted welding of transparent polymers for microchemical engineering and life science*. SPIE, 2005. **5713**: p. 479-488.

[168] Van de Ven, J. D., Erdman, A. G., *Laser transmission welding of thermo plastics–PartII: experimental model validation*. J. Manuf Sci Eng., 2007. **129**: p. 859–67.

[169] Donald, A., Windle, A., Hanna, S., *Liquid Crystalline Polymers*. 2nd edition, Cambridge University Press, 2006.

[170] Pham, A., Chen, M., Aihara, K., *LCP for Microwave Packages and Modules*. 1st edition, Cambridge University Press, 2012.

[171] http://www.rogerscorp.com/documents/731/acm/ULTRALAM-3000-LCP-Prepreg-ULTRALAM-3908.pdf (Date: 05/03/2015)

[172] MIL-STD-883H T.M. 1014.13, '*Seal*'. United States of America Department of Defence. Test method standards. Microcircuits, 2010. pp. 81-99.

[173] http://onrese.nerim.net/hermleak_0.php?s=m (Date: 05/03/2015)

[174] Cheng, Y. T., Lin, L., and Najafi, K., *Localized silicon fusion and eutectic bonding for MEMS fabrication and packaging*. IEEE/ASME J. Microelectromech. Syst , 2000. **9**: pp. 3-8.

[175] Yang, H., Wu, M., and Fang, W., *Localized induction heating solder bonding for wafer level MEMS packaging.* J. Micromech. Microeng., 2004. **15**(2): pp. 394-399.

[176] Nellis, G. and Klein, S., *Heat Transfer*, Cambridge University Press, New York, 2009.

[177] Burmeister, L. C., (1993) *Convective Heat Transfer*, 2nd ed. Publisher Wiley-Interscience, 1993. Google Book Search.

[178] Planck, M., *Über eine Verbesserung der Wienschen Spektralgleichung*, Verhandlungen der Deutschen Physikalischen Gesellschaft, 1900. **2**: pp. 202–204. Translated in Ter Haar, D., *On an Improvement of Wien's Equation for the Spectrum*, The Old Quantum Theory. 1967. pp. 79–81.

[179] Narimanov. E. E., and Smolyaninov, I. I., *Beyond Stefan-Boltzmann Law: Thermal Hyper-Conductivity,* Quantum Electronics and Laser Science Conference, 2012, OSA technical Digest (Optical Society of America).

[180] Sands, D., *Pulsed Laser Heating and Melting*, Heat Transfer - Engineering Applications, 2011. pp. 47-70.

[181] http://en.wikipedia.org/wiki/Poly(methyl_methacrylate) (Date: 05/03/2015)

[182] http://www.britannica.com/EBchecked/topic/597135/titanium-Ti (Date：05/03/2015)

[183] Van Krevelen, D. W., *Properties of Polymers*, Elsevier Science Publishers, 1990.

[184] Bicerano, J., *Prediction of Polymer Properties*, Marecl Dekker Inc., 1993.

[185] Prabhakaran, R., *Laser transmission Welding of PA6*, MSc Thesis, Chemical Engineering Department, Queen's University. 2003.

[186] http://www.comsol.com/model/download/142935/IntroductionToHeatTransferModule.pdf (Date: 05/03/2015)

[187] http://pveducation.org/pvcdrom/materials/optical-properties-of-silicon (Date: 05/03/2015)

[188] https://www.thorlabs.us/newgrouppage9.cfm?objectgroup_id=6138 (Date: 05/03/2015)

[189] http://fp.optics.arizona.edu/optomech/references/glass/Schott/tie-35_transmittance_us.pdf (Date:05/03/2015)

[190] Glassbrenner, C. J. and Slack, G. A., *Thermal Conductivity of Silicon and Germanium from 3^{o}K to Melting Point*, Physical Review Letters, 1964. **134**(4A): pp. A1058-A1069.